Role of charge and spin fluctuations and their interplay in solids

A Green's function approach

Sjöstrand, Tor

2022

Role of charge and spin fluctuations and their interplay in solids

A Green's function approach

TOR SJÖSTRAND
DEPARTMENT OF PHYSICS | FACULTY OF SCIENCE | LUND UNIVERSITY

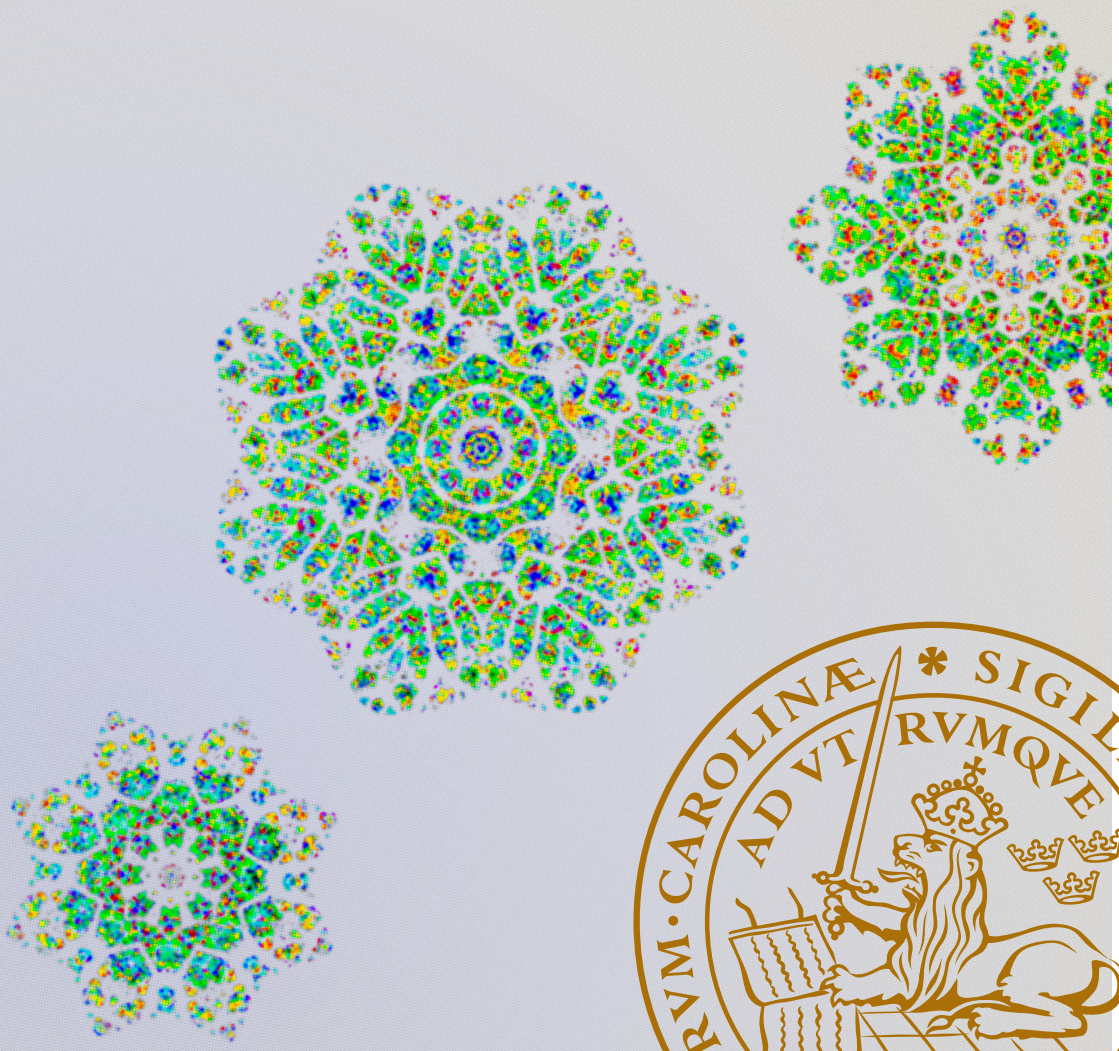

Role of charge and spin fluctuations and their interplay in solids

Role of charge and spin fluctuations and their interplay in solids

A Green's function approach

by Tor Sjöstrand

LUND
UNIVERSITY

Thesis for the degree of Doctor of Philosophy
Thesis advisors: Prof. Ferdi Aryasetiawan, Prof. Claudio Verdozzi
Faculty opponent: Prof. Lucia Reining

To be presented, with the permission of the Faculty of Science of Lund University, for public criticism in the Rydberg lecture hall (Rydbergsalen) at the Department of Physics on Monday, the 12th of December 2022 at 13:00.

Organization	Document name
LUND UNIVERSITY Department of Physics Box 118 SE–221 00 LUND Sweden	**DOCTORAL DISSERTATION** Date of disputation 2022-12-12 Sponsoring organization
Author Tor Sjöstrand	

Title and subtitle

Role of charge and spin fluctuations and their interplay in solids: A Green's function approach

Abstract

Due to the large number of electrons, solid state physics boils down to many-body approximations in which only selected types of collective excitations are taken into account, guided by the emergent properties of the material under study. In this thesis, the collective excitations of primary interest are electronic charge and spin fluctuations (plasmons and magnons) and nuclear charge fluctuations (phonons). Part I introduces the many-electron problem and provides a background theory for charge and spin fluctuations. Part II introduces the papers and summarizes their key results. These are appended in their published form in Part III.

In Paper I, electronic charge fluctuation effects are studied within the random-phase approximation through the spatiotemporal behavior of Hedin's screened interaction W (and the partially screened analog U) in two cuprates (La_2CuO_4 and $HgBa_2CuO_4$) and in $SrVO_3$, from initial local density calculations. The 1- and 3-band models for the cuprates produce, respectively, stable and short-lived regions with a negative effective interaction U.

In Paper II, the effect of electronic charge fluctuations on the orbital magnetization is studied in the spin-1/2 Haldane-Hubbard model by computing it using the one-shot GW Green's function. The major finding is that, for a small local repulsion U, interband charge fluctuations boost the orbital magnetization if the inversion symmetry breaking staggered potential Δ_{AB} is larger than the nearest-neighbor hopping t_1.

In Paper III, which comprises the major work of this thesis, a microscopic Green's function formula for the exchange-mediated contribution to the magnon-phonon interaction is derived from the underlying electronic structure. Despite the absence of spin-orbit induced magnon-phonon interconversion, the room-temperature renormalized magnon spectra acquire splittings due to phonon absorption in a minimal three-dimensional model.

In Paper IV, a new formalism for the Green's function [1], which relies on neither self-energy nor Dyson's equation and is based on a time delay-extended exchange-correlation potential V_{xc}, is applied to the half-filled 1-band Hubbard chain. V_{xc} is approximated by that of the Hubbard dimer, which is accessible analytically. The one-shot analytic spectra agree well with the density-matrix renormalization group method, and the U-dependent band gap is very close to the exact solution.

Key words

Green's function, correlations, collective excitations, screened interaction, electric polarization, orbital and spin magnetization, magnon-phonon interaction, Fierz ambiguity, time-dependent exchange-correlation potential

Classification system and/or index terms (if any)

Supplementary bibliographical information	Language
	English
ISSN and key title	ISBN
	978-91-8039-355-3 (print) 978-91-8039-356-0 (pdf)
Recipient's notes	Number of pages: 89 / Price
	Security classification

Signature _____ Date 2022-11-01

Role of charge and spin fluctuations and their interplay in solids

A Green's function approach

by Tor Sjöstrand

LUND
UNIVERSITY

This thesis consists of three parts. Part I gives the necessary introduction and background theory to be able to describe charge and spin fluctuations and Part II introduces the papers and summarizes their key results. These papers are appended in their published form in Part III together with a description of the author's individual contributions.

Cover illustration: Artistic rendition of a collective excitation of unknown floating objects on the surface of a pond. Made by the author.

Funding information: Financial support by The Swedish Research Council (VR).

Faculty of Science, Department of Physics

ISBN: 978-91-8039-355-3 (print)
ISBN: 978-91-8039-356-0 (pdf)

Printed in Sweden by Media-Tryck, Lund University, Lund 2022

We really do not know anything about life
U.G. Krishnamurti

Acknowledgements

I would like to start by thanking my excellent thesis advisors Ferdi Aryasetiawan and Claudio Verdozzi for your vast knowledge and your friendly support throughout my thesis work, as well as Fredrik Nilsson, Krister Karlsson and Christoph Friedrich for the nice collaborations and your many brilliant ideas. I am also grateful to Silke Biermann for stimulating and helpful conversations. I would like to give special thanks to my better half Lila, my parents Åsa and Per, my sister Linn, my nephews Felix and Malte and my old friend Ted for simply being awesome and helping me distance myself from the thesis work. Lastly, I would like to thank all the fun and unique PhD students and professors who enriched my time at the division, Katarina for your help in matters I know little about and Cecilia for your wisdom and inspiring passion for physics. I dedicate this thesis to my parents and to the birds living in their chimney.

Popular summary (in swedish)

Kvantmekaniken säger att energi och vågvibrationer är intimt relaterade. Det finns två typer av energi: strålningsenergi (till exempel ljus) och bunden energi (materia). Den första typen beskrivs av kraftbärande partiklar med heltalsspinn (bosoner) och den andra av partiklar med halvtalsspinn (fermioner). Spinnet refererar till partiklarnas inre snurr. Två identiska fermioner med samma spinnriktning kan inte befinna sig på samma plats (Pauliprincipen), vilket ligger till grund för materians stabilitet mot självkollaps. Det finns många typer av bosoner och fermioner, men tack vare att vågfenomenen de beskriver har vitt skiljda storleksordningar och tidsskalor går det ofta att studera ett begränsat urval i taget.

Elektrodynamik begränsas till en typ av fundamentala bosoner vid namnet fotoner, och till elektriskt laddade fermioner, vilka innefattar negativt laddade elektroner (fundamentala fermioner) samt positivt laddade protoner (kompositа fermioner) inuti atomkärnor. Atomkärnors massor, vilka är mycket större än elektronernas, påverkas även av laddningsneutrala neutroner, vilka indirekt påverkar elektrodynamiken när atomkärnornas vibrationer är oförsumbara. En beskrivning baserad på elektroner och atomkärnor räcker för att förstå de fyra makroskopiska tillstånden av materia: fast, flytande, gas och plasma. Fasta tillståndets fysik fokuserar på den förstnämnda kategorin och kännetecknas av tätt packade kristaller av joner[1] i vilka mer eller mindre bundna elektroner befinner sig, så att materialet i sin helhet är laddningsneutralt. Trots att ett material är i sitt fasta tillstånd behöver inte elektronerna i sig vara det. I isolatorer betér sig elektronerna, likt jonkristallen, som ett eget fast tillstånd, medan de i metaller betér sig som en gas. Däremellan finns de flesta komplicerade material, där elektronerna betér sig som en vätska. För att förstå makroskopiska egenskaper och fenomenen i material krävs en mikroskopisk kvantmekanisk beskrivning. Anledningen är att elektronernas och kristallvibrationernas tillåtna energinivåer förekommer i band åtskilda med gap, vilket följer från den ovannämnda relationen mellan energi och vågvibrationer, vilka är begränsade till en diskret uppsättning fundamentala vibrationsmoder.

Varje elektron i ett material har en laddning, ett spinn samt en hastighet relativt materialet som helhet,[2] och dessa bidrar alla till att generera elektriska och magnetiska fält, i enlighet med Maxwells fältekvationer. De genererade fälten från en elektron resulterar i en kraft agerande på de andra elektronerna, och vice versa. Detta betyder att alla elektroner i materialet växelverkar, vilket leder till ett olösbart stort matematiskt problem. Exempelvis finns det circa femtio miljoner miljarder miljarder kolatomer i ett kilogram kol, och fyra gånger fler valenselektroner (aktiva elektroner). För att kringgå problemet krävs kunskap om materialets kollektiva och emergenta makroskopiska egenskaper och fenomen, vilka förvisso är konsekvenser av den komplicerade växelverkan men som kan vägleda en approximativ beskrivning. Mer specifikt gäller det att, baserat på empiri, göra antaganden kring vilka typer

[1] Jonerna består av atomkärnor tillsammans med de hårdast bundna elektronerna.

[2] Elektronen kan liknas vid en laddad liten stavmagnet.

av kollektiva excitationer som är viktiga för olika material, och därmed försumma de mindre viktiga. I denna avhandling studeras två viktiga kollektiva excitationer for elektronerna i en kristall, nämligen laddnings- och spinnfluktuationer, med hjälp av Hedins ekvationer för elektronernas så kallade Greensfunktion. Greensfunktionen ger den materialberoende sannolikheten för en adderad elektrons samt borttagen elektrons (adderat hål) möjliga rörelser, och kan användas för att beräkna de kollektiva excitationerna i materialet. Den adderade partikeln är på grund av sin laddning, sitt spinn samt sin hastighet tvingad att dra med sig ett moln (aggregat) av laddning, spinn och hastighet från materialets elektroner. Molnet leder till en skärmad effektiv växelverkan med elektronerna i materialet, och partikeln tillsammans med sitt moln kallas för en kvasipartikel.

I Artikel I studeras rums- och tidsberoendet av laddningsfluktuationers skärmningseffekt i kupraterna La_2CuO_4 och $HgBa_2CuO_4$[3] samt i den korrelerade metallen $SrVO_3$. Den fullt skärmade växelverkan jämförs med en delvis skärmad som agerar som effektiv växelverkan vid låg energi. Stabila områden med negativ effektiv växelverkan finnes i kupraterna, vilket är kännetecknande för bundna tillstånd och således kan ha en koppling till supraledning. Dock krävs framtida studier som går bortom de antagna approximationerna och som inkluderar spinnfluktuationer. I Artikel II studeras elektronrörelsens bidrag till magnetism med hjälp av Greensfunktionen för interagerande elektroner i en spinn-opolariserade tvådimensionell modell. För en svag lokal repulsion mellan elektronerna visar sig laddningsfluktuationer inom den kända GW approximationen leda till en ökning av magnetiseringen, givet att energipotentialskillnaden mellan modellmaterialets två distinkta atomer dominerar över den kinetiska energin härstammande från elektronhopp mellan grannatomer. I Artikel III härleds en mikroskopisk formel för ett bidrag till kopplingen mellan spinnfluktuationer och kristallvibrationer som hittills varit dåligt förstått. Detta bidrag härstammar från den ovan nämnda Pauliprincipen. I Artikel IV används en ny Greensfunktionsmetod på en endimensionell kedja av atomer, med en elektron per atom (halvfyllda Hubbardkedjan). Genom att utnyttja den exakta lösningen för ett tvåatomsystem erhålls analytiska energispektra för den oändliga kedjan som överensstämmer väl med de baserade på mer sofistikerade metoder. Bandgapets växelverkansberoende visar sig dessutom vara väldigt likt det exakta resultatet. I Artikel V generaliseras den så kallade Fierzambiguiteten, vilken har att göra med Pauliprincipen, till växelverkan med lång räckvidd. Ett spelfall i formalismen är en Greensfunktionsmetod som behandlar fysiken vid kort och lång räckvidd olika. Detta specialfall, som i sin enklaste form beror på en parameter α, är studerat för ett tvåatomsystem. Det visar sig fördelaktigt att låta α avvika från sitt trivialvärde inom GW approximationen.

[3]När La_2CuO_4 och $HgBa_2CuO_4$ dopas med elektroner blir de supraledande upp till relativt höga temperaturer. Dessa temperaturer betraktas dock inte som höga av livsformer.

List of publications and author's contributions

This thesis is based on the following publications, referred to by their Roman numerals. All papers are reproduced with permission of the publisher.

I **Position representation of effective electron-electron interactions in solids**
T. J. Sjöstrand, F. Nilsson, C. Friedrich and F. Aryasetiawan
Phys. Rev. B **99**, 195136 (2019)
The screened interaction W and its partially screened analog U enter into Hedin's equations and low-energy models, respectively. In Paper I, a formula is derived for obtaining the position representation of W (U) from matrix elements of the linear density response R (R^{r}) in a Bloch product basis. The causal interaction in time domain due to the insertion of an impurity at time $\tau = 0$ is also derived. As a test, W (U) is computed within the (constrained) random-phase approximation for the cuprate parent compounds La_2CuO_4 and $HgBa_2CuO_4$ and the correlated metal $SrVO_3$, based on the spin-unpolarized local density approximation. The major finding is the presence of spatial regions with a strong negative U in the cuprates, which are short-lived in the 3-band model but stable in the 1-band model.
Contributions: I derived the formulas needed to obtain the spatial representations when working with a mixed product basis, wrote the necessary extension to the existing codes, produced the figures and plots and wrote most of the article.

II **Influence of correlations on the orbital magnetization of the spin-1/2 Haldane-Hubbard model**
T. J. Sjöstrand, K. Karlsson and F. Aryasetiawan
Phys. Rev. B **100**, 054427 (2019)
The orbital magnetization has been accessible in the mean-field approximation for general solids for less than two decades. In Paper II, the recent extension to correlated electron systems is used to study the effect of charge fluctuations on the orbital magnetization, by applying it to the spin-1/2 Haldane-Hubbard model within the one-shot GW approximation. For a small local repulsion U, the charge fluctuations are shown to boost the orbital magnetization if the staggered potential Δ_{AB} of the model is larger than the nearest-neighbor hopping t_1. This boost stems from interband correlations and occurs for all time-reversal symmetry-breaking phases φ of the next-nearest neighbor hopping t_2.
Contributions: I wrote the majority of the code, ran the calculations, produced the plots and wrote most of the article, except the introduction.

III **Magnon-phonon interaction and the underlying role of the Pauli exclusion principle**
T. J. Sjöstrand and F. Aryasetiawan
Phys. Rev. B **105**, 014433 (2022)

The magnon-phonon interaction $\mathcal{A}$ is crucial in many solid-state devices and technologies. It enters spin caloritronics since it affects the interplay between heat and spin currents and acoustic spintronics since it can be used for spin pumping. It also yields phononic spin and a mechanism for the thermal Hall effect. The non-relativistic exchange contribution is less understood than the spin-orbit contribution and therefore derived in Paper III from the underlying electronic structure. First, the finite-temperature interaction Δ between reference (Hartree-Fock) magnons is derived by utilizing the Fierz ambiguity and Schwinger's functional derivative method. After a Hubbard approximation, Δ is iterated, contracted to a two-point quantity and extended to account for phonons. The result indirectly yields a microscopic formula for $\mathcal{A}$ and is applied to a three-dimensional model with isotropic magnon dispersion and a dispersion-free optical phonon. Increasing $\mathcal{A}$ from zero induces a magnon band splitting at finite temperatures by phonon absorption, which increases the low-energy magnon density of states and thus decreases the Curie temperature.

Contributions: I came up with most crucial steps for deriving the magnon-phonon interaction, like the Fierz ambiguity, to work with a crossing-symmetric extension of Hedin's W, to use an iterative scheme and to contract the four-point Δ at the end. I also constructed the model, produced the results and wrote most of the article.

IV **Spectral functions of the half-filled one-dimensional Hubbard chain within the exchange-correlation potential formalism**
F. Aryasetiawan and T. J. Sjöstrand
Phys. Rev. B **106**, 045123 (2022)

The Green's function G is a useful tool to determine, among other things, the Fermi surface in conductors and band gap in semiconductors and insulators. Unlike the wavefunction, it depends on only two spatial (and spin) coordinates in many-electron systems. Since the emergence of Green's function theory in the 1950s, self-energy methods based on Dyson's equation have been the standard for computing G. It was recently shown [1] that the equation of motion for G is naturally reformulated so as to replace the convolution term ΣG by a multiplicative term $V_{\mathrm{xc}}G$, where V_{xc} is the *time-dependent* exchange-correlation potential, caused by the exchange-correlation hole density n_{xc}. In Paper IV, the formalism is applied to the spectral function of the half-filled 1-band Hubbard chain, using the exact V_{xc} of the Hubbard dimer. At the one-shot level, analytic spectra are available and found to be close to those of the more sophisticated dynamic density-matrix renormalization group method, and the U-dependent band gap is similar to the exact one, found using the Bethe ansatz.

Contributions: I contributed with initial ideas, made connections to the standard self-energy approach, performed some calculations and helped writing the article.

Contents

Part I

Introduction & background theory

1

Introduction

The plurality and complexity of natural phenomena makes it quite remarkable that theories about nature have been established which stand the test of time. Yet, the reason for this is rather simple. Science does not ask unanswerable questions about the ultimate origin of things or why the world looks the way it does. Physics, for example, was developed from the marriage between observation and the use of mathematical language to express dynamical equations, and can easily explain how a ball moves when thrown, without having to relate it to events that took place before. The throwing of the ball is the cause, and the trajectory is the effect. Physics can thus get away with quite few equations since specifics of a certain system is not described by the dynamical equations, but by initial and boundary conditions determined from observations.

1.1 The many-electron problem

Condensed matter physics is the study of the macroscopic properties of systems with many strongly interacting particles, i.e. essentially solids and liquids. It does not explain how the particles came together in the first place. Rather, it describes the physical processes allowed by the geometric conditions set by the particular system. Solid state physics, which is a subdivision of condensed matter physics, is primarily concerned with the electronic properties in crystals described by a periodic lattice of atomic nuclei, which are assumed fixed (unless lattice vibrations are important) due to their large mass and point-like due to their small size. The electrons repel each other since they are all negatively charged but are attracted by the nuclei, which are positively charged. The smallest repeating unit is called the unit cell, and the geometric condition in solids is specified by the coordinates and species of the atomic nuclei in the unit cell.

The dynamical equations which govern the motion of the electrons are known and the geometric conditions can easily be imposed. The difficulty of solid state physics is thus computational rather than theoretical, and stems from the exponential growth of possible many-body configurations as a function of the particle number N. A simple example is the case when each particle only has two possible states, say $\uparrow$ and $\downarrow$. This results in 2^N many-body configurations, and since the calculations are based on quantum mechanics, they require the summing over all paths.[1] Plugging in $N = 10^{24}$ (approximately a mole) particles yields $2^{10^{24}}$ many-body configurations. An insane number. In fact, the number of configurations of this simple example reaches the number of atoms in the observable universe for only $N = 260$, which shows that the many-body problem quickly becomes too large to solve exactly, even on a supercomputer. The major task of modern solid-state physics thus boils down to finding approximations to the many-body problem.

Many-body approximations are often guided by knowledge of the collective behavior of a system, i.e. the emergent macroscopic properties caused by the interactions. A plasma, for example, which is a minimal model for simple metals, is a dense gas of interacting charges, both positive and negative. Due to interactions, however, it is not accurately viewed as being comprised of individual particles, but as a whole, with the characteristic tendency of striving for local charge neutrality. When adding an external electric field, the free charges immediately strive to screen it. Collective behavior like this is described quantitatively by specifying and calculating the collective excitations of the system. In this thesis, the most important collective excitations are electronic charge and spin fluctuations (plasmons and magnons) and nuclear charge fluctuations (phonons). Due to the charge screening, spin screening[2] and spin twisting effects of these fluctuations, the particles are forced to carry around a cloud (or aggregate) of charge and spin stemming from collective rearrangements of the other particles. Such a particle together with its cloud is called a quasiparticle. Unfortunately, the collective one-particle excitations, which are described by the linear spin-density response, are typically not sufficient to describe the electronic structure accurately in strongly correlated systems, unless it is renormalized by many-particle excitations, i.e. the non-linear spin-density response.

Due to the fundamental role of charge and spin fluctuations in solid state physics, the common thread of this thesis is to investigate them through the use of Hedin's Green's function formalism [2] (or tailored reformulations of it), based on Schwinger's functional derivative technique. These fluctuations will be studied either through their spectra, their role in screening or other phenomena (such as orbital magnetization), or through their interplay, at different levels of approximation.

[1] A quantum mechanical particle is essentially described by its average motion, together with fluctuations around it. This is a consequence of the necessity, for whatever reason, to describe particles probabilistically.

[2] The notion of spin screening is a bit misleading in ferromagnets, which favour alignment of spins, as arguably would be better termed as antiscreening. Also, the absence of magnetic charges (monopoles) also makes the notion of magnetic field screening fundamentally distinct from electric field screening.

1.2 Thesis outline

This thesis consists of three parts. Part I gives the necessary introduction and background theory to be able to describe charge and spin fluctuations and Part II introduces the papers and summarizes their key results. These papers are appended in their published form in Part III together with a description of the author's individual contributions. The latter is also included in the 'List of publications and author's contributions' in the thesis preamble, together with an overview of the papers.

In Paper I, electronic charge fluctuation effects are studied within the random-phase approximation through the spatiotemporal behavior of Hedin's screened interaction W (and the partially screened analog U) in two cuprates (La_2CuO_4 and $HgBa_2CuO_4$) and in $SrVO_3$, from initial local density calculations. The 1- and 3-band models for the cuprates produce, respectively, stable and short-lived regions with a negative effective interaction U. In Paper II, the effect of electronic charge fluctuations on the orbital magnetization is studied in the spin-1/2 Haldane-Hubbard model by computing it using the one-shot GW Green's function. The major finding is that, for a small local repulsion U, interband charge fluctuations boost the orbital magnetization if the inversion symmetry breaking staggered potential Δ_{AB} is larger than the nearest-neighbor hopping t_1. In Paper III, which comprises the major work of this thesis, a microscopic Green's function formula for the exchange-mediated contribution to the magnon-phonon interaction is derived from the underlying electronic structure. Despite the absence of spin-orbit induced magnon-phonon interconversion, the room-temperature renormalized magnon spectra acquire splittings due to phonon absorption in a minimal three-dimensional model. In Paper IV, a new formalism for the Green's function [1], which relies on neither self-energy nor Dyson's equation and is based on a time delay-extended exchange-correlation potential V_{xc}, is applied to the half-filled 1-band Hubbard chain. V_{xc} is approximated by that of the Hubbard dimer, which is accessible analytically. The one-shot analytic spectra agree well with the density-matrix renormalization group method, and the U-dependent band gap is very close to the exact solution.

2

Electromagnetic field in a medium

In order to find the classical interaction between two particles it is necessary to know how the charge, spin and motion of a particle generate electric and magnetic fields, through Maxwell's equations. This is the theme of this chapter. In vacuum, these fields propagate with the speed of light c, and are quickly "felt" by surrounding particles. More precisely, the fields caused by the charge, spin and motion of one particle translate into a (Lorentz-Stern-Gerlach) force[1] acting on other particles, owing to the charge, spin and motion of the latter. One particle thus affects another particle at a distance, and vice versa, i.e. they behave collectively and are said to interact. This is discussed in more detail in Chap. 3. Central to this thesis is the fact that only a fraction of the electronic spin-orbitals are typically of interest. The remaining ones are then treated as a background medium, through which the field propagation, and thereby the effective force and interaction, is altered.

2.1 Maxwell's equations

$$\nabla \cdot \mathbf{E}(\mathbf{r},t) = 4\pi\rho(\mathbf{r},t), \quad (2.1) \qquad \nabla \cdot \mathbf{B}(\mathbf{r},t) = 0, \quad (2.3)$$

$$\nabla \times \mathbf{E}(\mathbf{r},t) = -\frac{1}{c}\frac{\partial \mathbf{B}(\mathbf{r},t)}{\partial t}, \quad (2.2) \qquad \nabla \times \mathbf{B}(\mathbf{r},t) = \frac{4\pi}{c}\mathbf{J}(\mathbf{r},t) + \frac{1}{c}\frac{\partial \mathbf{E}(\mathbf{r},t)}{\partial t}, \quad (2.4)$$

constitute Maxwell's equations in Gaussian units.[2] $\mathbf{E}$ and $\mathbf{B}$ are the electric and magnetic fields and ρ and $\mathbf{J}$ the charge and current densities, all functions of space $\mathbf{r}$ and time t. ρ

[1] The fields also translate into a torque acting on magnetic moments.

[2] In SI units, Maxwell's vacuum is specified by the speed of light $c = 1/\sqrt{\epsilon_0\mu_0}$ and wave impedance $Z = \sqrt{\mu_0/\epsilon_0}$, where the latter is hidden by the Gaussian units in Eqs. (2.1)-(2.4). The recently updated SI units allow for Z to vary in the vicinity of particles. However, Eqs. (2.1)-(2.4) assume that it does not.

and $\mathbf{J}$ are often treated as known sources to $\mathbf{E}$ and $\mathbf{B}$, but in practice they are unknown and Maxwell's equations have to be combined with dynamical equations for the sources.

2.2 Polarization and magnetization

By decomposing the sources into free and bound components,[3] i.e. $\rho = \rho_{\rm b} + \rho_{\rm f}$ and $\mathbf{J} = \mathbf{J}_{\rm b} + \mathbf{J}_{\rm f}$, it is often advantageous to interpret the bound components as stemming from a medium with polarization $\mathbf{P}$ and magnetization $\mathbf{M}$, so that

$$\rho_{\rm b}(\mathbf{r},t) = -\nabla\cdot\mathbf{P}(\mathbf{r},t), \qquad (2.5) \qquad \mathbf{J}_{\rm b}(\mathbf{r},t) = c\nabla\times\mathbf{M}(\mathbf{r},t) + \frac{\partial\mathbf{P}(\mathbf{r},t)}{\partial t}. \qquad (2.6)$$

These yield Maxwell's macroscopic equations for the free sources when plugged into Eqs. (2.1)-(2.4). $\rho_{\rm b}$ is identified as the polarization charge density whereas $\mathbf{J}_{\rm b}$ is the sum of a magnetization current density and a polarization current density. While the external fields $\mathbf{E}_{\rm ext} = \mathbf{E} + 4\pi\mathbf{P}$ and $\mathbf{B}_{\rm ext} = \mathbf{B} - 4\pi\mathbf{M}$ are the bare fields due to the free sources, $\mathbf{E}$ and $\mathbf{B}$ are the total (screened) fields [3]. The terminology of screening, which usually refers to the reduction of $|\mathbf{E}|$ compared to $|\mathbf{E}_{\rm ext}|$ in a materials, is in this thesis used rather broadly to also include field twisting and antiscreening effects due to $\mathbf{M}$ and $\mathbf{P}$. The latter is important in ferromagnets, where $|\mathbf{B}| = 4\pi|\mathbf{M}|$ is finite despite an absent $|\mathbf{B}_{\rm ext}|$.[4]

2.3 Susceptibilities

The (non-linear) susceptibility tensors $\overleftrightarrow{\chi}_{\rm e}$, $\overleftrightarrow{\chi}_{\rm em}$, $\overleftrightarrow{\chi}_{\rm me}$ and $\overleftrightarrow{\chi}_{\rm m}$ are defined as memory functions by the constitutive relations

$$\begin{bmatrix}\mathbf{P}(x)\\ \mathbf{M}(x)\end{bmatrix} = \int dx' \begin{bmatrix}\overleftrightarrow{\chi}_{\rm e}(x,x';\mathbf{E},\mathbf{B}) & \overleftrightarrow{\chi}_{\rm em}(x,x';\mathbf{E},\mathbf{B})\\ \overleftrightarrow{\chi}_{\rm me}(x,x';\mathbf{E},\mathbf{B}) & \overleftrightarrow{\chi}_{\rm m}(x,x';\mathbf{E},\mathbf{B})\end{bmatrix}\begin{bmatrix}\mathbf{E}(x')\\ \mathbf{B}(x')\end{bmatrix}, \qquad (2.7)$$

where $x = (\mathbf{r},t)$. The susceptibility tensors are causal and thus vanish unless x' is in the past light cone of x. If the particles in the medium move slowly, the non-relativistic causality condition $t' < t$ suffices. The (tensorial) expansion coefficients in $\mathbf{E}$ and $\mathbf{B}$ of the susceptibility tensors are intrinsic to the medium. In linear media, the susceptibility tensors of Eq. (2.7) are independent of the fields, and thus given by the functional derivatives $\overleftrightarrow{\chi}_{\rm e}(x,x') = \delta\mathbf{P}(x)/\delta\mathbf{E}(x')$, $\overleftrightarrow{\chi}_{\rm m}(x,x') = \delta\mathbf{M}(x)/\delta\mathbf{B}(x')$, and similarly for the off-diagonal components. Hysteresis [4] and spontaneous polarization [5] and magnetization [6, 7] are thus absent in linear media. The linear approximation fails in ferromagnets,

[3] All electrons in a solid, and the nuclei if necessary, should in principle be treated as bound, whereas the free sources are the ones responsible for external fields.

[4] More precisely, $\mathbf{M}$ actually depends on $\mathbf{B}_{\rm ext}$ in the past.

but works in plasmas as well as in para- and diamagnets.[5] In multiferroics, which can have a strong magnetoelectric coupling, $\overleftrightarrow{\chi}_{\rm em}$ and $\overleftrightarrow{\chi}_{\rm me}$ are important. In isotropic materials, $\overleftrightarrow{\chi}_{\rm e} = \chi_e \mathbb{I}$, and likewise for the other componens, where $\mathbb{I}$ is the 3-by-3 identity matrix. The spatio-temporal dependencies of the linear susceptibilities are related to dispersion, i.e. how the angular frequency ω of a (low-intensity) collective mode of excitation depends on its wave vector $\mathbf{q}$. The dispersion thus dictates the transmission and absorption properties of the medium. For long-wavelength excitations, the discrete translational symmetry of the periodic lattice can be replaced by a continuous symmetry. Consequently, the spatio-temporal dependencies of the susceptibility tensors become independent of the centre-of-mass $\frac{1}{2}(x + x')$ [6] and thus simple functions of $x - x'$. By Fourier transforming[7] to wave vector $\mathbf{q}$ and angular frequency ω, the constitutive relation of Eq. (2.7) becomes multiplicative, i.e.

$$\begin{bmatrix} \mathbf{P}(\mathbf{q},\omega) \\ \mathbf{M}(\mathbf{q},\omega) \end{bmatrix} = \begin{bmatrix} \overleftrightarrow{\chi}_{\rm e}(\mathbf{q},\omega) & \overleftrightarrow{\chi}_{\rm em}(\mathbf{q},\omega) \\ \overleftrightarrow{\chi}_{\rm me}(\mathbf{q},\omega) & \overleftrightarrow{\chi}_{\rm m}(\mathbf{q},\omega) \end{bmatrix} \begin{bmatrix} \mathbf{E}(\mathbf{q},\omega) \\ \mathbf{B}(\mathbf{q},\omega) \end{bmatrix}. \tag{2.8}$$

One could say that material science revolves around determining the susceptibility tensors. In electric and magnetic insulators, for example, the bound sources are confined to their respective unit cells, which makes the susceptibility tensors independent of $\mathbf{q}$.

2.4 Screening: A spatial view

The electric and magnetic fields are related to the electric scalar potential ϕ and the magnetic vector potential $\mathbf{A}$, through the relations

$$\mathbf{E}(\mathbf{r},t) = -\nabla\phi(\mathbf{r},t) - \frac{1}{c}\frac{\partial \mathbf{A}(\mathbf{r},t)}{\partial t}, \tag{2.9}$$

$$\mathbf{B}(\mathbf{r},t) = \nabla \times \mathbf{A}(\mathbf{r},t), \tag{2.10}$$

A physical system described by the pair $(\phi, \mathbf{A})$ can also be described by $(\phi', \mathbf{A}')$, where $\phi' = \phi - \frac{1}{c}\frac{\partial \lambda}{\partial t}$ and $\mathbf{A}' = \mathbf{A} + \nabla\lambda$ for an arbitrary scalar field $\lambda(\mathbf{r},t)$. This is called gauge freedom. When describing static field screening, the Coulomb gauge is convenient, where $\nabla \cdot \mathbf{A} = 0$. The static limit of the Maxwell theory is obtained by removing all time-derivatives. Dropping the time-variables, Eqs. (2.1)-(2.4) reduce to

$$-\nabla^2\phi(\mathbf{r}) = 4\pi\rho(\mathbf{r}) = 4\pi\rho_{\rm f}(\mathbf{r}) - 4\pi\nabla\cdot\mathbf{P}(\mathbf{r}), \tag{2.11}$$

$$-\nabla^2\mathbf{A}(\mathbf{r}) = \frac{4\pi}{c}\mathbf{J}(\mathbf{r}) = \frac{4\pi}{c}\mathbf{J}_{\rm f}(\mathbf{r}) + 4\pi\nabla\times\mathbf{M}(\mathbf{r}), \tag{2.12}$$

[5] Paramagnets (diamagnets) have an average positive (negative) $\chi_{\rm m}$, but no spontaneous magnetic order.

[6] This also requires the absence of external fields.

[7] Fourier transform: $f(\mathbf{q},\omega) = \int d\mathbf{r}dt e^{-i(\mathbf{q}\cdot\mathbf{r}-\omega t)} f(\mathbf{r},t)$. Inverse: $f(\mathbf{r},t) = \int \frac{d\mathbf{q}d\omega}{(2\pi)^4} e^{i(\mathbf{q}\cdot\mathbf{r}-\omega t)} f(\mathbf{q},\omega)$. The Fourier transform maps the operators ∇ and $\partial/\partial t$ to $i\mathbf{q}$ and $-i\omega$, respectively.

where Eqs. (2.5)-(2.6) have been utilized. If the polarization and magnetization are neglected, the external fields generated by the free source(s) in vacuum are obtained. If the free source is a single impurity at the origin with charge q and spin magnetic moment $\boldsymbol{\mu}^{\mathrm{S}}$, it follows that $\rho_{\mathrm{f}}(\mathbf{r}) = q\delta(\mathbf{r})$ and $\mathbf{J}_{\mathrm{f}}(\mathbf{r}) = c\nabla \times [\boldsymbol{\mu}^{\mathrm{S}}\delta(\mathbf{r})]$, where δ denotes the Dirac delta function. It is then easy to solve for the external potentials and fields, with the result

$$\phi_{\mathrm{ext}}(\mathbf{r}) = \frac{q}{r}, \qquad (2.13) \qquad \mathbf{E}_{\mathrm{ext}}(\mathbf{r}) = q\frac{\hat{\mathbf{r}}}{r^2}, \qquad (2.15)$$

$$\mathbf{A}_{\mathrm{ext}}(\mathbf{r}) = \frac{\boldsymbol{\mu}^{\mathrm{S}} \times \mathbf{r}}{r^3}, \qquad (2.14) \qquad \mathbf{B}_{\mathrm{ext}}(\mathbf{r}) = \frac{8\pi}{3}\boldsymbol{\mu}^{\mathrm{S}}\delta(\mathbf{r}) + \frac{3\hat{\mathbf{r}}(\hat{\mathbf{r}} \cdot \boldsymbol{\mu}^{\mathrm{S}}) - \boldsymbol{\mu}^{\mathrm{S}}}{r^3}, \qquad (2.16)$$

where $\hat{\mathbf{r}} = \mathbf{r}/r$. When the polarizable and magnetizable medium is taken into account, the potentials and fields get modified. The simplest is to consider a non-magnetic system. In this case, the effect of $\mathbf{P}(\mathbf{r})$ in Eq. (2.11) is to screen the external electric potential and field. A minimal description of insulators (Eq. (2.17)) and conductors (i.e. metals and thermally excited semiconductors; Eq. (2.18)) is to take

$$\rho_{\mathrm{b}}(\mathbf{r}) = -4\pi\chi_{\mathrm{e}}\rho(\mathbf{r}), \qquad (2.17) \qquad \rho_{\mathrm{b}}(\mathbf{r}) = -\frac{\phi(\mathbf{r})}{4\pi r_0^2}, \qquad (2.18)$$

where $\chi_{\mathrm{e}} > 0$ and $r_0 > 0$. Eq. (2.17) for simple insulators is obtained by taking the divergence of the minimal constitutive relation $\mathbf{P}(\mathbf{r}) = \chi_{\mathrm{e}}\mathbf{E}(\mathbf{r})$, whereas the argument behind Eq. (2.18) for simple conductors in the long-wavelength limit is described in the footnote.[8] The scalar potentials from the impurity at the origin then take the form

$$\phi(\mathbf{r}) = \frac{q}{(1 + 4\pi\chi_{\mathrm{e}})r}, \qquad (2.20) \qquad \phi(\mathbf{r}) = \frac{qe^{-r/r_0}}{r}, \qquad (2.21)$$

where Eq. (2.20) and Eq. (2.21) describe insulators and conductors, respectively. While the screening in insulators results in a simple rescaling of the external potential, the screening in conductors is characterized by a finite screening length r_0. It can be shown that

[8] The bound charge density is thought of as the induced charge density due to ϕ, i.e.

$$\rho_{\mathrm{b}}(\mathbf{r}) = -e\int dE\, D(E)\big(n_{\mathrm{F}}(E - \mu_0 - e\phi(\mathbf{r})) - n_{\mathrm{F}}(E - \mu_0)\big), \qquad (2.19)$$

where $-e$ is the electron charge, $n_{\mathrm{F}}(x) = 1/(e^{x\beta}+1)$ the Fermi occupation, $\beta = 1/k_{\mathrm{B}}T$ the inverse thermal energy and μ_0 the chemical potential in the absence of ϕ. The density of states $D(E)$ is defined so that $D(E)dE$ is the number of states per unit volume with energy between E and $E + dE$.

In metals, the change in occupation (which appears in Eq. (2.19)) can be expanded in ϕ to linear order, and since thermal effects are typically negligible T can be put to zero. Since μ_0 equals the Fermi energy E_{F} in metals, it follows from the Fermi statistics that $\rho_{\mathrm{b}} = -e^2 D(E_{\mathrm{F}})\phi$, which leads to the Thomas-Fermi screening length $r_0 = 1/(4\pi e^2 D(E_{\mathrm{F}}))^{1/2}$. Since metals are characterized by $D(E_{\mathrm{F}}) \neq 0$ they acquire a finite screening length. In a free-electron gas with density n, $D(E_{\mathrm{F}}) \propto n^{1/3}$ and consequently $r_0 \propto 1/n^{1/6}$.

In non-degenerate semiconductors, the conduction electrons can be described by classical Boltzmann occupations. To linear order in ϕ, it follows that $\rho_{\mathrm{b}} = -e^2 n\beta\phi$, where $n = \int dE D(E) e^{-(E-\mu_0)\beta}$. This yields the Debye screening length $r_0 = (k_{\mathrm{B}}T/4\pi e^2 n)^{1/2}$.

aggregates larger than r_0 display organized behavior. The potential in Eq. (2.21) is known as the Yukawa potential, and can be thought of as being mediated by massive photons,[9] where the mass is acquired from the medium. This is understood by the continuous absorption and re-emission of light throughout the medium, which effectively slows it down below its vacuum speed c. In real metals, the decaying Yukawa potential of Eq. (2.21) is modulated by radial Friedel oscillations [8] with a length scale determined by the Fermi surface.[10] The reason for this is that the static impurity implies that electronic scattering is elastic. Since electrons cannot occupy the same state, only electrons on the Fermi surface can scatter elastically. The argument is similar for semiconductors at finite temperature.

2.5 Screening: A temporal view

Apart from the spatial characteristics of field screening, which was discussed quite generally in Sec. 2.4 for non-magnetic systems, there are also temporal characteristics. The discussion of the latter will be restricted to non-magnetic insulators, for which the Lorentz model is suitable,[11] but the extension necessary for conductors is mentioned as a comment. The Lorentz model assumes a driven electric field $\mathbf{E}(t)$ which is homogeneous but time-varying, and thus the opposite of the electric field caused by the impurity in Sec. 2.4. Owing to the homogeneity, the polarization can in a minimal description be takes as the total electric dipole moment divided by the volume V of the system, i.e. $\mathbf{P}(t) = -ne\mathbf{r}(t)$, where $n = N/V$ is the valence electron density and $\mathbf{r}(t)$ the displacement, which is assumed the same for all valence electrons. Newton's force law for an arbitrary valence electron then implies that $m\frac{\partial^2}{\partial t^2}\mathbf{r}(t) = \mathbf{F}(t)$, where $\mathbf{F}(t)$ is the Force acting on it. By including a spring force $-k\mathbf{r}(t)$ (k: material-specific spring constant), a friction force $-m\Gamma\frac{\partial}{\partial t}\mathbf{r}(t)$ (Γ: material-specific friction coefficient) and the electric force $-e\mathbf{E}(t)$ (the first term in Eq. (3.4) of Sec. 3.1), Newton's force law implies the Lorentz polarization dynamics

$$\frac{\partial^2}{\partial t^2}\mathbf{P}(t) + \Gamma\frac{\partial}{\partial t}\mathbf{P}(t) + \omega_0^2\mathbf{P}(t) = \frac{\omega_{\mathrm{P}}^2}{4\pi}\mathbf{E}(t), \tag{2.22}$$

where $\omega_0 = \sqrt{k/m}$ is the stiffness and $\omega_{\mathrm{P}} = \sqrt{4\pi ne^2/m}$ the plasma frequency. Fourier transforming to frequency domain yields

$$\mathbf{P}(\omega) = \chi_{\mathrm{e}}(\omega)\mathbf{E}(\omega), \tag{2.23}$$

$$\chi_{\mathrm{e}}(\omega) = \frac{1}{4\pi}\frac{-\omega_{\mathrm{P}}^2}{\omega^2 + i\Gamma\omega - \omega_0^2}. \tag{2.24}$$

Since the external field is defined as $\mathbf{E}_{\mathrm{ext}} = \mathbf{E} + 4\pi\mathbf{P}$, it takes the form

[9] Photons are the (bosonic) particles of electromagnetic radiation.

[10] The Fermi surface is the set of wave vectors for which the energy dispersion crosses the Fermi energy E_F.

[11] The Lorentz model is not applicable to conductors, since assuming electron conservation in each unit cell.

$$\mathbf{E}_{\rm ext}(\omega) = \epsilon_{\rm r}(\omega)\mathbf{E}(\omega), \qquad (2.25) \qquad\qquad \epsilon_{\rm r}(\omega) = 1 + \frac{-\omega_{\rm P}^2}{\omega^2 + i\Gamma\omega - \omega_0^2}, \qquad (2.26)$$

where $\epsilon_{\rm r} = 1 + 4\pi\chi_{\rm e}$ is the relative permittivity.[12] By writing $\mathbf{E}_{\rm ext}(\omega) = E_{\rm ext}(\omega)\mathbf{e}_x$ and $\mathbf{E}(\omega) = E(\omega)\mathbf{e}_x$, it follows that the field strength is reduced in the material by the factor

$$\epsilon_{\rm r}^{-1}(\omega) = \frac{E(\omega)}{E_{\rm ext}(\omega)} = 1 + \frac{\omega_{\rm P}^2}{\omega^2 + i\Gamma\omega - \omega_0^2 - \omega_{\rm P}^2}, \qquad (2.32)$$

which in the static limit $\omega \to 0$ becomes $\omega_0^2/(\omega_0^2 + \omega_{\rm P}^2)$. This means that when there are no valence electrons, i.e. when $\omega_{\rm P} = 0$, the static field is not screened. On the other hand, if the spring constant is small, i.e. if $\omega_0 \ll \omega_{\rm P}$, the field is screened very efficiently. In general, Eq. (2.32) has to be extended to account for occupation factors, quantum mechanical transition rates and disparities in the effective oscillator parameters for different valence states. Despite the breakdown of the oscillator model for conduction electrons in metals, $\epsilon_{\rm r}^{-1}$ for a given crystal momentum $\mathbf{k}$ still has the form of Eq. (2.32).[13]

[12] The relative permittivity is formally introduced through the relation

$$\mathbf{E}_{\rm ext}(x) = \int dx' \overleftrightarrow{\epsilon}_{\rm r}(x, x'; \mathbf{E})\mathbf{E}(x'), \qquad (2.27)$$

in the absence of magnetoelectric coupling. Eq. (2.7) and the definition $\mathbf{E}_{\rm ext} = \mathbf{E} + 4\pi\mathbf{P}$ then implies that

$$\overleftrightarrow{\epsilon}_{\rm r}(x, x'; \mathbf{E}) = \delta(x - x')\mathbb{I} + 4\pi\overleftrightarrow{\chi}_{\rm e}(x, x'; \mathbf{E}) \qquad (2.28)$$

Similarly, the inverse relative permeability is formally introduced through the relation

$$\mathbf{B}_{\rm ext}(x) = \int dx' \overleftrightarrow{\mu}_{\rm r}^{-1}(x, x'; \mathbf{B})\mathbf{B}(x'), \qquad (2.29)$$

in the absence of magnetoelectric coupling. Eq. (2.7) and the definition $\mathbf{B}_{\rm ext} = \mathbf{B} - 4\pi\mathbf{M}$ then implies that

$$\overleftrightarrow{\mu}_{\rm r}^{-1}(x, x'; \mathbf{B}) = \delta(x - x')\mathbb{I} - 4\pi\overleftrightarrow{\chi}_{\rm m}(x, x'; \mathbf{B}). \qquad (2.30)$$

Eq. (2.30) differs from Eq. (2.28) in that the relative permeability enters through its inverse, and the magnetic susceptibility with a minus sign. This is simply a matter of definition and a historical coincidence. Nonetheless, for small magnetic susceptibilities, a form is obtained which agrees with Eq. (2.28):

$$\overleftrightarrow{\mu}_{\rm r}(x, x'; \mathbf{B}) \approx \delta(x - x')\mathbb{I} + 4\pi\overleftrightarrow{\chi}_{\rm m}(x, x'; \mathbf{B}). \qquad (2.31)$$

[13] The magnetization dynamics not discussed here requires the use of the famous Landau–Lifshitz equation, or extensions to it. The most general extension is the Landau–Lifshitz–Gilbert–Slonczewski equation [9].

3

Classical force and Hamiltonian

In this chapter, the force that acts on a moving classical point particle with charge and spin magnetic moment is briefly reviewed along with the associated Hamiltonian. The latter is used to derive the classical interaction between two particles, which carries over to the second quantized formalism of Sec. 4.2.

3.1 The force acting on charges and magnetic moments

For a non-relativistic point particle i, the Lorentz force density reads

$$\boldsymbol{\mathcal{F}}_i(\mathbf{r},t) = \rho_i(\mathbf{r},t)\mathbf{E}_i(\mathbf{r},t) + \frac{1}{c}\mathbf{J}_i(\mathbf{r},t)\times\mathbf{B}_i(\mathbf{r},t), \tag{3.1}$$

with (bound) charge and current densities[1]

$$\rho_i(\mathbf{r},t) = q_i\delta(\mathbf{r}-\mathbf{r}_i(t)), \tag{3.2}$$

$$\mathbf{J}_i(\mathbf{r},t) = q_i\mathbf{v}_i(t)\delta(\mathbf{r}-\mathbf{r}_i(t)) + c\nabla\times\big(\boldsymbol{\mu}_i^{\mathrm{S}}(t)\delta(\mathbf{r}-\mathbf{r}_i(t))\big) \tag{3.3}$$

in terms of the charge q_i, spin magnetic moment $\boldsymbol{\mu}_i^{\mathrm{S}}(t)$, position $\mathbf{r}_i(t)$ and velocity $\mathbf{v}_i(t)$. The fields $\mathbf{E}_i$ and $\mathbf{B}_i$ in Eq. (3.1) depend on i since they exclude the self-induced field of particle i. The force acting on particle i is obtained by integrating $\boldsymbol{\mathcal{F}}_i$ over $\mathbf{r}$, yielding (the missing steps are presented in App. A)

$$\mathbf{F}_i(t) = q_i\Big(\mathbf{E}_i(t) + \frac{1}{c}\mathbf{v}_i(t)\times\mathbf{B}_i(t)\Big) + \nabla\Big(\boldsymbol{\mu}_i^{\mathrm{S}}(t)\cdot\mathbf{B}_i(\mathbf{r},t)\Big)\Big|_{\mathbf{r}=\mathbf{r}_i(t)}, \tag{3.4}$$

[1] Eqs. (3.2)-(3.3) can be thought of as describing a moving and rotating charge distribution with total charge q_i in the zero-volume limit.

where $\mathbf{E}_i(t)$ is brief for $\mathbf{E}_i(\mathbf{r}=\mathbf{r}_i(t),t)$ and $\mathbf{B}_i(t)$ is defined analogously. The first term is the usual Lorentz force for particles without local magnetic moments and the second term is the Stern-Gerlach force named after the Stern-Gerlach experiment, where particles are accelerated in different directions in the presence of magnetic field gradients depending on the orientation of the intrinsic magnetic moment. It is also possible to derive the famous Zeeman torque, whose spin contribution[2] is $\boldsymbol{\tau}_i(t) = \boldsymbol{\mu}_i^{\mathrm{S}}(t)\times\mathbf{B}_i(t)$, and which leads to precession of the magnetic moment around the direction of the magnetic field.

The intrinsic spin magnetic moment of fundamental particles (fermions) stems from Dirac's relativistic quantum mechanics, and the contribution to the current density may be thought of as a macroscopic consequence of that theory. The theory up until Sec. 4.1 is thus referred to as classical, which is true in the sense that the coherent phase information in the quantum mechanical wavefunction is neglected but false in the sense that it relies on a purely quantum relativistic (zero-point) contribution to angular momentum. The total magnetization is a sum of the spin magnetization and the orbital magnetization, where the latter stems from Amperian loops of the velocity current (first term of Eq. (3.3)) caused by electronic orbits around the ions in the medium. Both the orbital and spin magnetization require quantum mechanics to be understood properly.

3.2 Hamiltonian formulation

The classical minimal coupling Hamiltonian for a nonrelativistic particle i with mass m_i, charge q_i, position $\mathbf{r}_i(t)$ and canonical momentum $\mathbf{p}_i(t)$ reads

$$H_i(t) = \frac{m_i v_i(t)^2}{2} + q_i\phi_i(t), \tag{3.5}$$

with kinematic velocity

$$\mathbf{v}_i(t) = \frac{\mathbf{p}_i(t)}{m_i} - \frac{q_i\mathbf{A}_i(t)}{m_i c}. \tag{3.6}$$

The total Hamiltonian is obtained by summing over i. As explained in Sec. 3.1, the potentials depend on i not only through $\mathbf{r}_i(t)$ but also explicitly because particle i cannot experience its self-induced field. This explains the difficulty of dealing with many-body systems and why mean-field treatments are not exact. "Minimal coupling" means the inclusion of charge q_i but not spin magnetic moment $\boldsymbol{\mu}_i^{\mathrm{S}}(t)$. Using one of Hamilton's two equations, Eq. (3.5) leads to the Lorentz force, i.e. the first term of Eq. (3.4). The second "Stern-Gerlach" term is not captured, as should not be surprising since the presence of spin stems from Dirac's theory of relativistic quantum particles. Yet, with a simple intuitive

[2]It also has an orbital contribution.

trick, spin can be sneaked into the Hamiltonian. The particle is simply allowed to fluctuate around $\mathbf{r}_i$ with probability $P_i(\mathbf{r},t)$. Eq. (3.5) then extends to

$$H_i(t) = \frac{m_i}{2q_i}\int d\mathbf{r}\,\mathbf{J}_i(\mathbf{r},t)\cdot\mathbf{v}_i(\mathbf{r},t) + \int d\mathbf{r}\,\rho_i(\mathbf{r},t)\phi_i(\mathbf{r},t), \tag{3.7}$$

where $\rho_i(\mathbf{r},t) = q_iP_i(\mathbf{r},t)$ and $\mathbf{J}_i(\mathbf{r},t) = q_iP_i(\mathbf{r},t)\mathbf{v}_i(\mathbf{r},t)$. By replacing ρ_i and $\mathbf{J}_i$ by Eqs. (3.2)-(3.3), the spin moment $\boldsymbol{\mu}_i^{\mathrm{S}}(t)$ is assimilated. In fact, this should enter into Eq. (3.7) with a factor of two since also the velocity acquires a contribution. The result is the Pauli coupling Hamiltonian (the missing steps are presented in App. B)

$$H_i(t) = \frac{m_i}{2}v_i(t)^2 + q_i\phi_i(t) - \boldsymbol{\mu}_i^{\mathrm{S}}(t)\cdot\mathbf{B}_i(t), \tag{3.8}$$

which reproduces the full Lorentz-Stern-Gerlach force of Eq. (3.4). If the particles move quickly, relativistic corrections are necessary, such as the spin-orbit effect. The terms involving the vector potential $\mathbf{A}_i$ when expanding out the square are necessary for describing orbital magnetization. The total magnetic moment is the sum of the orbital and the spin moments, i.e.[3]

$$\boldsymbol{\mu}_i^{\mathrm{tot}}(t) = \frac{1}{2c}\int d\mathbf{r}\,\mathbf{r}\times\mathbf{J}_i(\mathbf{r},t) = \frac{q_i}{2m_ic}\big(\mathbf{L}_i(t) + g_i\mathbf{S}_i(t)\big), \tag{3.9}$$

where Eq. (3.3) for $\mathbf{J}_i$ has been used. $\mathbf{L}_i(t) = m_i\mathbf{r}_i(t)\times\mathbf{v}_i(t)$ is the orbital angular momentum of particle i and the associated term the orbital magnetic moment, which contains a paramagnetic contribution (the $\mathbf{p}_i$-term) due to partially filled electronic subshells and diamagnetic contribution (the $\mathbf{A}_i$-term) which is always present yet typically small. The last term follows from the relation $\boldsymbol{\mu}_i^{\mathrm{S}}(t) = \gamma_i\mathbf{S}_i(t)$, where $\mathbf{S}_i(t)$ is the intrinsic spin angular momentum, $\gamma_i = g_iq_i/2m_ic$ the gyromagnetic ratio and g_i the g-factor, which is 1 for a classical Amperian loop and approximately 2 for electrons. Classically, the magnetization is obtained by summing up Eq. (3.9) for all particles i together with factors of $\delta(\mathbf{r}-\mathbf{r}_i(t))$. In para- and diamagnets, the thermally fluctuating orientations of the magnetic moments are independent in the absence of an external magnetic field, which yields a vanishing magnetization. However, in permanent magnets, the energy gained by aligning the moments is too high for thermal fluctuations to uncorrelate their orientations, yielding a net magnetization even without an external magnetic field.

In most magnetic solids without 4f rare earth ions, the orbital magnetization is quenched and thus small compared to the spin magnetization [11]. For such materials, the vector potential in the Pauli Hamiltonian of Eq. (3.8) can be ignored, so that

$$H_i(t) = \frac{p_i^2(t)}{2m_i} + q_i\phi_i(t) - \boldsymbol{\mu}_i^{\mathrm{S}}(t)\cdot\mathbf{B}_i(t), \tag{3.10}$$

[3]The first equality is not general since, just like ρ_i cannot generally specify the polarization $\mathbf{P}_i$, $\mathbf{J}_i$ cannot generally specify the magnetization $\mathbf{M}_i$ [10]. Nonetheless, $\boldsymbol{\mu}_i^{\mathrm{tot}}(t) = \frac{q_i}{2m_ic}\big(\mathbf{L}_i(t)+g_i\mathbf{S}_i(t)\big)$ holds generally.

which corresponds to the Lorentz-Stern-Gerlach force of Eq. (3.4) but without the velocity term. This is the Hamiltonian of interest in the following, but the orbital magnetic moment will be revisited in Chap. 7.

3.3 Interacting point charges and magnetic moments

Eqs. (2.13) and (2.16), i.e. the Coulomb gauge scalar potential and magnetic field generated in quasi-steady state by a point particle in vacuum, can be plugged into Eq. (3.10). Adding up the contributions from all particles $j \neq i$ yields

$$\phi_i(t) = \phi_i^{\text{ext}}(t) + \sum_{j\neq i} \frac{q_j}{r_{ij}(t)}, \tag{3.11}$$

$$\mathbf{B}_i(t) = \mathbf{B}_i^{\text{ext}}(t) + \sum_{j\neq i} \left(\frac{8\pi}{3}\delta\big(\mathbf{r}_{ij}(t)\big)\mathbb{I} + \frac{3\hat{\mathbf{r}}_{ij}(t)\hat{\mathbf{r}}_{ij}(t) - \mathbb{I}}{r_{ij}(t)^3} \right) \cdot \boldsymbol{\mu}_j^{\text{S}}(t), \tag{3.12}$$

where $\mathbf{r}_{ij}(t) = \mathbf{r}_i - \mathbf{r}_j$, and $\hat{\mathbf{r}}_{ij}(t) = \mathbf{r}_{ij}(t)/r_{ij}(t)$. The Hamiltonian for particle i (Eq. (3.10)) thus takes the form

$$H_i(t) = \frac{p_i^2(t)}{2m_i} + q_i\phi_i^{\text{ext}}(t) - \boldsymbol{\mu}_i^{\text{S}}(t)\cdot\mathbf{B}_i^{\text{ext}}(t) + \frac{1}{2}\sum_{j\neq i} H_{ij}^{\text{int}}(t), \tag{3.13}$$

$$H_{ij}^{\text{int}}(t) = \frac{q_iq_j}{r_{ij}(t)} - \boldsymbol{\mu}_i^{\text{S}}(t)\cdot\left(\frac{8\pi}{3}\delta\big(\mathbf{r}_{ij}(t)\big)\mathbb{I} + \frac{3\hat{\mathbf{r}}_{ij}(t)\hat{\mathbf{r}}_{ij}(t) - \mathbb{I}}{r_{ij}(t)^3} \right) \cdot \boldsymbol{\mu}_j^{\text{S}}(t), \tag{3.14}$$

where H_{ij}^{int} is the pairwise interaction between particles i and j, and the factor of $1/2$ in Eq. (3.13) is needed to not count particle pairs twice.[4] The first term of (3.14) is the Coulomb interaction and the second is the short-range dipole-dipole interaction. In most solids, both the electronic and nuclear dipole-dipole interaction energies are small so that the pair-wise interaction of Eq. (3.14) can be approximated as

$$H_{ij}^{\text{int}}(t) \approx \frac{q_iq_j}{r_{ij}(t)}. \tag{3.15}$$

In this classical theory, the neglect of the dipole-dipole interaction uncorrelates the magnetic moments. By transitioning to a quantum formulation, this correlation is recovered through the exchange interaction, which is a consequence of the Pauli exclusion principle. The exchange interaction is typically several orders of magnitude larger than the dipole-dipole interaction. For this reason, the Coulomb interaction of Eq. (3.15) is responsible for essentially all collective properties in solids, as long as the spin-orbit effect is negligible.

[4] More precisely, the factor of $1/2$ is only needed after summing over i. Since the last term in Eq. (3.13) is only half of the actual potential felt by particle i, $H_i(t)$ should be thought of as demanding a sum over i rather than being the Hamiltonian for particle i.

4

Quantization for identical particles

Quantum mechanics is needed to explain the discrete spectra of atoms. A proper description of solids, which are comprised of atoms, thus requires quantum mechanics. This chapter starts with a brief summary of first and second quantization for one and many identical particles and continues by making connections to the charge, magnetization and current densities introduced in Chap. 2. It also introduces the orbital representation used later in this thesis and ends by reviewing the Fierz ambiguity, which stems from the quantum mechanical indistinguishability of two identical (fermionic) particles.

4.1 First quantization for a single particle

The Liouville equation[1] describes the classical phase-space evolution of a system. For a single particle in an external field the phase-space distribution can be written as $n = n(\mathbf{r}, \mathbf{p}, t)$, and the Liouville equation reads

$$\left(\frac{\partial}{\partial t} + \frac{d\mathbf{r}}{dt} \cdot \frac{\partial}{\partial \mathbf{r}} + \frac{d\mathbf{p}}{dt} \cdot \frac{\partial}{\partial \mathbf{p}} \right) n(\mathbf{r}, \mathbf{p}, t) = 0. \tag{4.1}$$

Since the magnetic vector potential is neglected in the classical Hamiltonian of Eq. (3.13), Hamilton's equations yield that $d\mathbf{r}/dt = \mathbf{p}/m$ and $d\mathbf{p}/dt = \mathbf{F}(\mathbf{r}, t) = -q\nabla\phi(\mathbf{r}, t) + \gamma\nabla_1\big(\mathbf{S}(\mathbf{r}, t) \cdot \mathbf{B}(\mathbf{r}_1, t)\big)\big|_{\mathbf{r}_1 = \mathbf{r}}$, where $\nabla_1 = \partial/\partial\mathbf{r}_1$. The quantization procedure, which has

[1] The Liouville equation is based on Liouville's theorem, which states that the phase-space distribution function is constant along particle trajectories. This assumption is violated in systems with non-zero Berry phase [12], which stems from what can be thought of as a generalization of the Aharonov-Bohm effect to an extended parameter space. A vanishing Berry phase will be assumed throughout this thesis, except in Chap. 7.

Eq. (4.1) as its starting point, is outlined in App. C. It results in the famous Schrödinger-Pauli equation ($\sigma_i = \uparrow$ or $\downarrow$)

$$i\hbar \frac{\partial \Psi_{\sigma_1}(\mathbf{r},t)}{\partial t} = \sum_{\sigma_2} \hat{H}_{\sigma_1\sigma_2}(\mathbf{r},t)\Psi_{\sigma_2}(\mathbf{r},t), \tag{4.2}$$

where Ψ_{σ_i} is the σ_i-component of the spinor wavefunction and[2]

$$\hat{H}_{\sigma_1\sigma_2}(\mathbf{r},t) = \delta_{\sigma_1\sigma_2}\left(-\frac{\hbar^2\nabla^2}{2m} + q\phi(\mathbf{r},t)\right) - \gamma \mathbf{S}_{\sigma_1\sigma_2}\cdot\mathbf{B}(\mathbf{r},t) \tag{4.3}$$

the $\sigma_1\sigma_2$-component of the Hamiltonian operator $\hat{H}$. $\hbar$ is Planck's constant and $\mathbf{S}$ the spin operator, defined in Eq. (C5) of App. C. The quantized theory is seen to be obtained by the prescription $H \mapsto \hat{H} = i\hbar\partial/\partial t$, $\mathbf{r} \mapsto \hat{\mathbf{r}} = \mathbf{r}$ and $\mathbf{p} \mapsto \hat{\mathbf{p}} = -i\hbar\nabla$, where classical observables O are replaced by hermitean operators $\hat{O} = \hat{O}^\dagger$.[3] Hermiticity ensures real-valued eigenvalues, as is necessary since these comprise the possible measurement outcomes. Eq. (4.2) is a one-body equation since it depends on a single spin index σ and spatial coordinate $\mathbf{r}$, and can be used in many-body systems (in solids) only when interactions can be modelled by mean fields $\phi_{\mathrm{MF}}(\mathbf{r},t)$ and $\mathbf{B}_{\mathrm{MF}}(\mathbf{r},t)$, but this comes with the penalty of turning the effective mass m in Eq. 4.3 into a tensor field [13], so that $\nabla^2/m \mapsto \nabla\cdot\overleftrightarrow{m}^{-1}_{\sigma_1\sigma_2}(\mathbf{r},t)\nabla$. Also the gyromagnetic ratio γ, which depends on m, becomes a tensor field.[4] These fields have to be computed from a more fundamental theory, as provided by a many-body extension of Eqs. (4.2)-(4.3). In the following, Dirac's bra-ket notation is used, where state vectors $|\Psi\rangle$ are used instead of wavefunctions $\Psi_\sigma(\mathbf{r}) = \langle \mathbf{r},\sigma|\Psi\rangle$.

4.2 Second quantization for identical particles

An N-body state vector depends on N spin indices σ_i and spatial coordinates $\mathbf{r}_i$. The discussion here is restricted to indistinguishable particles, like electrons, which means that they have equal mass, charge and gyromagnetic ratio.[5] It follows from causality (spin statistics theorem) that a many-body eigenfunction to the Hamiltonian is either symmetric or antisymmetric under permutation of two coordinates, $\mathbf{r}_i,\sigma_i$ and $\mathbf{r}_j,\sigma_j$. It is symmetric for integer spin particles (bosons) and antisymmetric for half-integer spin particles (fermions). The antisymmetry of the fermionic wavefunction leads to the Pauli exclusion principle, which forbids two identical fermions to occupy the same one-body state. The exclusion

[2] "Hat-symbols" denote quantum mechanical operators.

[3] Generally, one-body operators are written $\hat{O} = \sum_{ij} |i\rangle O_{ij}\langle j|$. Thus, $\hat{O}^\dagger = \sum_{ij} |i\rangle O^*_{ji}\langle j|$.

[4] The Koster equation is an additional non-linear extension to Eq. (4.3) for Brownian particles in a medium, which due to friction couple to their own phase fluctuations (Eq. (32) in Ref. [14]).

[5] Zero temperature ($T = 0$) is also assumed. The imaginary time formalism for $T > 0$ is used in Chap. 8.

principle plays a central role in Chaps. 8. Since electrons are spin-$1/2$ fermions, antisymmetry is assumed in the following. For the purpose of generality, however, the electron charge $q = -e$, mass $m = m_\mathrm{e}$ and g-factor $g \approx 2$ are not assumed. Beyond adding up the one-body Hamiltonians of the form of Eq. (4.3) for the N fermions, Coulomb interaction (classically given by Eq. (3.15)) also has to be included. Since the interaction is permutation-symmetric, the Hamiltonian commutes with permutation, so that the antisymmetry of the fermionic N-body state is preserved under time-evolution.

In second quantization, creation and annihilation operators are used to represent state vectors in Hilbert spaces of different particle numbers N. In position representation, the annihilation operator is called a field operator, $\hat{\psi}_\sigma(\mathbf{r})$. When acting on an N-body state vector, $\hat{\psi}_{\sigma_i}(\mathbf{r}_i)$ and $\hat{\psi}^\dagger_{\sigma_i}(\mathbf{r}_i)$ respectively remove or add a particle at position $\mathbf{r}_i$ with spin σ_i. Annihilating the vacuum state $|0\rangle$, defined as the normalized zero-body state, yields a state with zero norm; $\hat{\psi}_\sigma(\mathbf{r})|0\rangle = |\,\mathrm{null}\rangle$, where $\langle \mathrm{null}\,|\,\mathrm{null}\rangle = 0$. The N-body state with one-body occupations $n_i = n_i(t)$ (0 for unoccupied and 1 for occupied) can be written as

$$|n_1, n_2, ...\rangle = \prod_i^{n_i \neq 0} \hat{\psi}^\dagger_{\sigma_i}(\mathbf{r}_i)|0\rangle, \tag{4.4}$$

where $N = \sum_i n_i$ and the product is ordered so that $\hat{\psi}^\dagger_{\sigma_i}(\mathbf{r}_i)$ with $i < j$ ends up to the left of $\hat{\psi}^\dagger_{\sigma_j}(\mathbf{r}_j)$. Skipping details, Eq. (4.4) allows for the expression of the antisymmetry of the fermionic N-body state in terms of the anticommutation relations[6]

$$\{\hat{\psi}_{\sigma_i}(\mathbf{r}_i), \hat{\psi}_{\sigma_j}(\mathbf{r}_j)\} = \{\hat{\psi}^\dagger_{\sigma_i}(\mathbf{r}_i), \hat{\psi}^\dagger_{\sigma_j}(\mathbf{r}_j)\} = 0, \tag{4.5}$$

$$\{\hat{\psi}_{\sigma_i}(\mathbf{r}_i), \hat{\psi}^\dagger_{\sigma_j}(\mathbf{r}_j)\} = \delta_{ij} = \delta_{\sigma_i\sigma_j}\delta(\mathbf{r}_i - \mathbf{r}_j). \tag{4.6}$$

From Eq. (4.5) it follows that $\hat{\psi}_{\sigma_i}(\mathbf{r}_i)^2 = 0$ and $\hat{\psi}^\dagger_{\sigma_i}(\mathbf{r}_i)^2 = 0$, where the first relation states that a particle can only be removed once from an N-body state and the second that a one-body state cannot be occupied by several identical particles (the Pauli principle). The field operators can be used to represent the many-body Hamiltonian. Using the first quantized Hamiltonian of Eq. (4.3) and the classical Coulomb interaction of Eq. (3.15), the second quantized Hamiltonian $\hat{H}$ is defined by requiring that

$$\hat{H}(t)|n_1, n_2, ...\rangle = \sum_i n_i \left(-\frac{\hbar^2\nabla_i^2}{2m} + \hat{V}_i^\mathrm{ext}(t) + \frac{1}{2}\sum_{j\neq i} \frac{n_j q^2}{|\mathbf{r}_i - \mathbf{r}_j|} \right) |n_1, n_2, ...\rangle, \tag{4.7}$$

where $\hat{V}_i^\mathrm{ext}(t) = q\phi_i^\mathrm{ext}(t) - \gamma \mathbf{S}_i(t)\cdot\mathbf{B}_i^\mathrm{ext}(t)$. By defining $\hat{\psi} = [\hat{\psi}_\uparrow\, \hat{\psi}_\downarrow]^T$, the Hamiltonian that fulfils this is expressed by field operators as

$$\hat{H}(t) = \int d\mathbf{r}\, \hat{\psi}^\dagger(\mathbf{r}) \left(\hat{T} + \hat{V}_\mathrm{ext}(\mathbf{r}, t) + \frac{1}{2}\int d\mathbf{r}' \hat{\psi}^\dagger(\mathbf{r}') \frac{q^2}{|\mathbf{r} - \mathbf{r}'|} \hat{\psi}(\mathbf{r}') \right) \hat{\psi}(\mathbf{r}), \tag{4.8}$$

[6] $\{\hat{A}, \hat{B}\} = \hat{A}\hat{B} + \hat{A}\hat{B}$.

where $\hat{T} = -\hbar^2\nabla^2/2m$ is the kinetic energy operator and

$$\hat{V}_{\text{ext}}(\mathbf{r},t) = q\phi_{\text{ext}}(\mathbf{r},t) - \gamma\mathbf{S}\cdot\mathbf{B}_{\text{ext}}(\mathbf{r},t) \tag{4.9}$$

is the external potential operator. ϕ_{ext} includes the ionic (lattice) potential. Lattice vibrations (phonons), which are discussed in Sec. 5.7, enter the description through ϕ_{ext}.

4.3 Charge, magnetization and current densities

In the following, $\langle\hat{A}\rangle_t$ is short notation for the expectation value $\langle\Psi(t)|\hat{A}|\Psi(t)\rangle$ of an operator $\hat{A}$ in the time-dependent N-body state $|\Psi(t)\rangle$ of the system.[7] The (bound) charge and spin magnetization densities due to the indistinguishable fermions then read[8]

$$\rho_{\text{b}}(\mathbf{r},t) = q\big\langle\hat{\psi}^\dagger(\mathbf{r})\hat{\psi}(\mathbf{r})\big\rangle_t, \tag{4.10}$$

$$\mathbf{M}(\mathbf{r},t) = \gamma\big\langle\hat{\psi}^\dagger(\mathbf{r})\mathbf{S}\hat{\psi}(\mathbf{r})\big\rangle_t, \tag{4.11}$$

and the (bound) Pauli current density reads

$$\mathbf{J}_{\text{b}}(\mathbf{r},t) = \tfrac{iq\hbar}{2m}\big\langle\nabla\hat{\psi}^\dagger(\mathbf{r})\hat{\psi}(\mathbf{r}) - \hat{\psi}^\dagger(\mathbf{r})\nabla\hat{\psi}(\mathbf{r})\big\rangle_t + c\nabla\times\mathbf{M}(\mathbf{r},t), \tag{4.12}$$

which is the sum of the Schrödinger and spin current densities.[9] If orbital motion is important, i.e. if the simplification in Eq. (3.10) does not hold, the Schrödinger current density acquires an additional term $-\frac{q}{mc}\mathbf{A}(\mathbf{r},t)\rho_{\text{b}}(\mathbf{r},t)$ and the spin current density gets accompanied by an orbital magnetization current density, also contained in $c\nabla\times\mathbf{M}(\mathbf{r},t)$. Eqs. (4.10) and (4.12) can be thought of as the sources to Maxwell's equations in Eqs. (2.1)-(2.4). However, $\rho_{\text{b}}(\mathbf{r},t)$ and $\mathbf{J}_{\text{b}}(\mathbf{r},t)$ depend on the Hamiltonian operator, which contains the fields and thus leads to a feedback between fields and sources.

4.4 Wannier basis for electrons in solids

In the remainder of this thesis, the identical fermions are assumed to be electrons. Hence, $q=-e$, $m=m_{\text{e}}$ and $g\approx 2$ is assumed. Furthermore, Hartree's atomic units are also used from this point onwards, for which $\hbar = m_{\text{e}} = e = a_0 = 1$, where a_0 is the Bohr radius.

The field operator can be expanded in an orthonormal orbital basis as[10]

$$\hat{\psi}_\sigma(\mathbf{r}) = \sum_i \phi_i(\mathbf{r})\hat{c}_{i\sigma}, \tag{4.13}$$

[7] This easily extends to a thermal expectation value at finite temperature.

[8] The time-dependencies originate from the state Ψ used to define the expectation values.

[9] The Pauli (Schrödinger) current density is the non-relativistic limit of the Dirac (Gordon) current density.

[10] The Wannier functions are, apart from in Chap. 7, kept spin-independent to simplify the notation.

where $\hat{c}_{i\sigma}$ is the annihilation operator of a spin-σ fermion in orbital ϕ_i. The most common and useful localized basis for periodic solids is the Wannier basis, where $i = (\mathbf{R}, n)$ is a combination of a Bravais lattice vector $\mathbf{R}$ and a band index n. The Wannier functions are constructed from Bloch functions $\psi_{\mathbf{k}n}$, which fulfil $\hat{H}_0\psi_{\mathbf{k}n}(\mathbf{r}) = \epsilon_{\mathbf{k}n}\psi_{\mathbf{k}n}(\mathbf{r})$, where $\hat{H}_0$ is the mean-field Hamiltonian[11] and $\epsilon_{\mathbf{k}n}$ the eigenvalues. Mathematically,

$$\phi_{\mathbf{R}n}(\mathbf{r}) = \frac{1}{N}\sum_{\mathbf{k}} e^{-i\mathbf{k}\cdot\mathbf{R}}\tilde{\psi}_{\mathbf{k}n}(\mathbf{r}), \quad (4.14) \qquad \tilde{\psi}_{\mathbf{k}n}(\mathbf{r}) = \sum_m \psi_{\mathbf{k}m}(\mathbf{r})S_{mn}(\mathbf{k}), \quad (4.15)$$

where N is the number of unit cells (number of $\mathbf{k}$ vectors in the Brillouin zone) and the matrix $S_{mn}(\mathbf{k})$ guarantees that the band n is smooth in the Brillouin zone. This matrix can be optimized to minimize the spread of the Wannier functions [19]. Using the combined Wannier index i, the second-quantized Hamiltonian operator of Eq. (4.8) takes the form

$$\hat{H}(t) = \sum_{\sigma_1\sigma_2}\sum_{ij} h_{ij}^{\sigma_1\sigma_2}(t)\,\hat{c}_{i\sigma_1}^\dagger\hat{c}_{j\sigma_2} + \frac{1}{2}\sum_{\sigma_1\sigma_2}\sum_{ijkl} v_{ijkl}\,\hat{c}_{i\sigma_1}^\dagger\hat{c}_{l\sigma_2}^\dagger\hat{c}_{k\sigma_2}\hat{c}_{j\sigma_1}, \quad (4.16)$$

where

$$h_{ij}^{\sigma_1\sigma_2}(t) = \int d\mathbf{r}\,\phi_i^*(\mathbf{r})\Big(\delta_{\sigma_1\sigma_2}\big(\hat{T} - \phi_{\text{ext}}(\mathbf{r},t)\big) + \tfrac{1}{c}\mathbf{S}_{\sigma_1\sigma_2}\cdot\mathbf{B}_{\text{ext}}(\mathbf{r},t)\Big)\phi_j(\mathbf{r}), \quad (4.17)$$

$$v_{ijkl} = \int d\mathbf{r}d\mathbf{r}'\phi_i^*(\mathbf{r})\phi_j(\mathbf{r})\frac{1}{|\mathbf{r}-\mathbf{r}'|}\phi_k(\mathbf{r}')\phi_l^*(\mathbf{r}'). \quad (4.18)$$

$\gamma = -1/c$ has been inserted in the Zeeman term. The second 'interaction Hamiltonian' term of Eq. (4.16) is to be thought of as the two-electron scattering $j\sigma_1, k\sigma_2 \to i\sigma_1, l\sigma_2$. Both spins are conserved since the Coulomb interaction is non-magnetic.

4.5 Fierz ambiguity

By introducing the zeroth Pauli matrix σ^0 as the 2-by-2 unit matrix, the interaction Hamiltonian in Eq. (4.16) takes the form (μ and ν run over $0, x, y, z$)

$$\hat{H}_{\text{int}} = \frac{1}{2}\sum_{\substack{\sigma_1\sigma_2\\\sigma_3\sigma_4}}\sum_{ijkl} v_{ijkl}^{\sigma_1\sigma_2\sigma_3\sigma_4}\,\hat{c}_{i\sigma_1}^\dagger\hat{c}_{l\sigma_4}^\dagger\hat{c}_{k\sigma_3}\hat{c}_{j\sigma_2}, \quad (4.19)$$

$$v_{ijkl}^{\sigma_1\sigma_2\sigma_3\sigma_4} = \sum_{\mu\nu}\sigma_{\sigma_1\sigma_2}^{\mu}v_{ijkl}^{\mu\nu}\,\sigma_{\sigma_4\sigma_3}^{\nu}, \quad (4.20)$$

provided that the electromagnetic interaction $v^{\mu\nu}$ is restricted to the electric sector:

$$v_{ijkl}^{\mu\nu} = \delta_{\mu0}\delta_{\nu0}\,v_{ijkl}. \quad (4.21)$$

[11] Often, density functional theory [15, 16, 17, 18]. is used, which is a formally exact mean-field theory.

The absence of magnetic interaction has thus been expressed mathematically as the vanishing of $v^{\mu\nu}$ unless $\mu = \nu = 0$. However, due to the fermionic anti-commutation relations of Eqs. (4.5)-(4.6), which in the orbital representation take the form

$$\left\{\hat{c}_{i\sigma_1}, \hat{c}_{j\sigma_2}\right\} = \left\{\hat{c}^\dagger_{i\sigma_1}, \hat{c}^\dagger_{j\sigma_2}\right\} = 0\ , \ \ \left\{\hat{c}_{i\sigma_1}, \hat{c}^\dagger_{j\sigma_2}\right\} = \delta_{ij}\delta_{\sigma_1\sigma_2}, \tag{4.22}$$

the interaction Hamiltonian in Eq. (4.16) can also be written as

$$\hat{H}_{\text{int}}(t) = -\frac{1}{2}\sum_{\sigma_1\sigma_2}\sum_{ijkl} v_{ikjl}\, \hat{c}^\dagger_{i\sigma_1}\hat{c}^\dagger_{l\sigma_2}\hat{c}_{k\sigma_1}\hat{c}_{j\sigma_2}, \tag{4.23}$$

after a relabelling of the dummy variables j and k. Also this can be written in the form of Eqs. (4.19)-(4.20), with electromagnetic interaction

$$v^{\mu\nu}_{ijkl} = -\frac{\delta_{\mu\nu}}{2} v_{ikjl}. \tag{4.24}$$

In the case of scattering between two electrons with opposite spins, this interaction treats the vertex as a simultaneous flip of both spins so as to make the total spin conserved, whereas the interaction of Eq. (4.21) instead treats it as a conservation of both spins. More specifically, Eq. (4.24) has magnetic components (v^{xx}, v^{yy} and v^{zz}) while Eq.(4.21) is purely electric. The resolution of this apparent paradox, called the Fierz ambiguity [20], is the indistinguishability of electrons, which implies that the exact solutions when using Eq. (4.21) and (4.24) are the same. However, the exact solution is generally speaking inaccessible, and approximate schemes are required. It then turns out that the choice plays a role. An intriguing choice is to take the average of Eq. (4.21) and Eq. (4.24), so that

$$v^{\mu\nu}_{ijkl} = \frac{\delta_{\mu\nu}}{2}\Big(\delta_{\mu 0}\, v_{ijkl} - \tfrac{1}{2} v_{ikjl}\Big). \tag{4.25}$$

Using Eq. (4.20), this choice fulfils the crossing symmetry

$$v^{\sigma_1\sigma_2\sigma_3\sigma_4}_{ijkl} = -v^{\sigma_1\sigma_3\sigma_2\sigma_4}_{ikjl}, \tag{4.26}$$

which imposes the Pauli exclusion principle in each individual scattering vertex by forbidding two equal spins to interact in the same orbital, i.e. $v^{\sigma\sigma\sigma\sigma}_{iiii} = 0$. This is implicitly assumed when working with the famous Hubbard model, which means that the extension of such a treatment requires the choice in Eq. (4.25).

5

Green's function method

Finding the eigenstates to the many-body Schrödinger-Pauli equation (Eq. (4.7)) is an impossible task in solids. Therefore, this thesis focuses on Green's function-based methods of many-body perturbation theory. This framework was originally developed for weak correlations, where perturbation theory is justified, but has turned out to provide a useful picture also for strong correlations, where it can be combined with other methods if needed. This chapter starts by introducing Dirac's interaction picture, which will then be used when defining the Green's function and deriving its equation of motion. From this equation, the coupled integro-differential equations known as Hedin's equations [2] will be derived and applied to the linear spin-density response, which contains the plasmons and magnons of the system. Finally, the effect of phonons will be briefly discussed.

5.1 Dirac's interaction picture

The quantum formalism in Chap. 4 was presented in what is known as the Schrödinger picture. For closed systems, i.e. without external fields, this picture means that operators are time-independent and state vectors time-dependent. The time-dependence in the Hamiltonian operator of Eq. (4.16) thus stems exclusively from the external fields. In Sec. 5.3 and onwards, many-body correlations will be expressed as functional derivatives with respect to external fields taken in the closed system, but this is more conveniently formulated in Dirac's interaction picture. To arrive at this picture, the Schrödinger picture Hamiltonian[1] is split into two terms, $\hat{H}_{\mathrm{S}} = \hat{H}_0 + \hat{\varphi}_{\mathrm{S}}(t)$, where $\hat{H}_0$ is given by Eq. (4.16) due exclusively to the frozen background lattice, which is assumed spin-less, and $\hat{\varphi}_{\mathrm{S}}(t)$ is

[1] The Fierz ambiguity is not utilized here, i.e. the trivial choice of Eq. (4.21) is implicitly assumed.

the remaining contribution stemming from additional fields. More explicitly,

$$\hat{H}_0 = \sum_{\sigma_1} \sum_{ij} h_{ij}\, \hat{c}^\dagger_{i\sigma_1} \hat{c}_{j\sigma_1} + \frac{1}{2} \sum_{\sigma_1\sigma_2} \sum_{ijkl} v_{ijkl}\, \hat{c}^\dagger_{i\sigma_1} \hat{c}^\dagger_{l\sigma_2} \hat{c}_{k\sigma_2} \hat{c}_{j\sigma_1}, \tag{5.1}$$

$$h_{ij} = \int d\mathbf{r}\, \phi^*_i(\mathbf{r}) \big(\hat{T} - \phi_{\mathrm{lat}}(\mathbf{r})\big) \phi_j(\mathbf{r}), \tag{5.2}$$

where ϕ_{lat} is the electric scalar potential due to the background lattice, and

$$\hat{\varphi}_{\mathrm{S}}(t) = \sum_{\sigma_1\sigma_2} \sum_{ij} \varphi^{\sigma_1\sigma_2}_{ij}(t)\, \hat{c}^\dagger_{i\sigma_1} \hat{c}_{j\sigma_2}, \tag{5.3}$$

$$\varphi^{\sigma_1\sigma_2}_{ij}(t) = \int d\mathbf{r}\, \phi^*_i(\mathbf{r}) \Big(- \delta_{\sigma_1\sigma_2} \phi_{\mathrm{ext}}(\mathbf{r}, t) + \tfrac{1}{c} \mathbf{S}_{\sigma_1\sigma_2} \cdot \mathbf{B}_{\mathrm{ext}}(\mathbf{r}, t) \Big) \phi_j(\mathbf{r}), \tag{5.4}$$

where ϕ_{ext} and $\mathbf{B}_{\mathrm{ext}}$ are the external contributions to the electric scalar potential and the magnetic field, respectively.[2] An interaction picture operator $\hat{O}$ is then defined from a Schrödinger picture operator $\hat{O}_{\mathrm{S}}$ as [21]

$$\hat{O}(t) = e^{i\hat{H}_0 t} \hat{O}_{\mathrm{S}}(t) e^{-i\hat{H}_0 t}, \tag{5.5}$$

and an interaction picture state vector Ψ from a Schrödinger picture state vector Ψ_{S} as

$$|\Psi(t)\rangle = \hat{U}(t) |\Psi_{\mathrm{S}}(0)\rangle, \tag{5.6}$$

$$\hat{U}(t) = T \exp\Big(- i \int_0^t dt_1 \hat{\varphi}(t_1) \Big). \tag{5.7}$$

It follows that expectation values are picture independent, i.e.

$$O(t) = \langle \Psi(t) | \hat{O}(t) | \Psi(t) \rangle = \langle \Psi_{\mathrm{S}}(t) | \hat{O}_{\mathrm{S}}(t) | \Psi_{\mathrm{S}}(t) \rangle, \tag{5.8}$$

as should be the case. In fact, this is the reason for the possibility of residing to more than one picture. The exponential in Eq. (5.7) is defined from its Taylor series, and the time-ordering operator T ensures that operators in this series with the earliest times end up to the right. The S matrix is now defined as the operator that time-evolves the wavefunction in the interaction picture from time t_2 to t_1, i.e. $|\Psi(t_1)\rangle = \hat{S}(t_1, t_2) |\Psi(t_2)\rangle$. It is easily shown that $\hat{S}(t_1, t_2) = \hat{U}(t_1) \hat{U}^\dagger(t_2)$. From Eq. (5.7), it thus follows that

$$\hat{S}(t_1, t_2) = T \exp\Big(- i \int_{t_2}^{t_1} dt_3 \hat{\varphi}(t_3) \Big). \tag{5.9}$$

If Ψ is used to denote the ground state in the interaction picture and Ψ_0 the ground state of $\hat{H}_0$, then the important relation $|\Psi(0)\rangle = \hat{S}(0, -\infty) |\Psi_0\rangle$ follows, which means that $|\Psi(-\infty)\rangle = |\Psi_0\rangle$.

[2] This definition of external fields differs from that in Eq. (4.8), where the lattice contribution was included.

5.2 The Green's function for electrons

The electronic Green's function can either be defined in or out of thermal equilibrium. The discussion here is restricted to the zero-temperature (equilibrium) case. Extending it to finite temperature is straightforward in the imaginary time formalism by Matsubara [22]. In the orbital representation, the Green's function reads [23]

$$G_{ij}^{\sigma_1\sigma_2}(t_1t_2) = \frac{\langle\Psi_0|T\hat{S}\hat{c}_{i\sigma_1}(t_1)\hat{c}^\dagger_{j\sigma_2}(t_2)|\Psi_0\rangle}{\langle\Psi_0|\hat{S}|\Psi_0\rangle}\Big/i, \tag{5.10}$$

where $\hat{S} = \hat{S}(\infty, -\infty)$. G is a correlator between adding an electron in one spin-orbital at one time and removing an electron in another spin-orbital at another time. When $t_1 > t_2$ in Eq. (5.10), it describes the propagation of an added electron, and for $t_1 < t_2$ of a vacancy (or hole). The ground state expectation value of an arbitrary one-body operator

$$\hat{O}(t) = \sum_{\sigma_1\sigma_2}\sum_{ij} O_{ij}^{\sigma_1\sigma_2}(t)\hat{c}^\dagger_{i\sigma_1}(t)\hat{c}_{j\sigma_2}(t)\,, \tag{5.11}$$

where $O_{ij}^{\sigma_1\sigma_2}(t)$ denotes a matrix element of an operator $\hat{O}_{\sigma_1\sigma_2}(\mathbf{r}, t)$, takes the form

$$\langle\hat{O}(t)\rangle = \frac{\langle\Psi_0|\hat{S}\hat{O}(t)|\Psi_0\rangle}{\langle\Psi_0|\hat{S}|\Psi_0\rangle} = \sum_{\sigma_1\sigma_2}\sum_{ij} O_{ij}^{\sigma_1\sigma_2}(t)G_{ji}^{\sigma_2\sigma_1}(tt^+)/i \tag{5.12}$$

in terms of G, where $t^+ = t + \eta$ for a positive infinitesimal η. For example, the electronic (bound) charge and spin magnetization densities at $\mathbf{r}$ of Eqs. (4.10)-(4.11) are obtained using $\hat{O}_{\sigma_1\sigma_2}(\mathbf{r}') = -\delta_{\sigma_1\sigma_2}\delta(\mathbf{r}' - \mathbf{r})$ and $\hat{O}_{\sigma_1\sigma_2}(\mathbf{r}') = -\mathbf{S}_{\sigma_1\sigma_2}\delta(\mathbf{r}' - \mathbf{r})/c$:

$$\rho_{\rm b}(\mathbf{r}, t) = -\sum_{\sigma_1}\sum_{ij}\phi_i^*(\mathbf{r})\phi_j(\mathbf{r})G_{ji}^{\sigma_1\sigma_1}(tt^+)/i, \tag{5.13}$$

$$\mathbf{M}(\mathbf{r}, t) = -\sum_{\sigma_1\sigma_2}\sum_{ij}\phi_i^*(\mathbf{r})\mathbf{S}_{\sigma_1\sigma_2}\phi_j(\mathbf{r})G_{ji}^{\sigma_2\sigma_1}(tt^+)/ic. \tag{5.14}$$

In the absence of time-varying external fields, G depends on its two time variables t_1 and t_2 only through their difference $\tau = t_1 - t_2$. The Fourier transform of G is obtained as $G(\omega) = \int d\tau e^{i\omega\tau}G(\tau)$, in terms of which the spectral function reads $A(\omega) = |\operatorname{Im} G(\omega)|/\pi$. The spectral function is the 'many-body band structure', with peaks at the electron addition and removal energies of photoemission and inverse photoemission experiments.[3] Renormalization from correlations lead to life-time broadening and shifting of the spectral peaks compared to the mean field. G also yields the interacting ground state energy through the Galitskii-Migdal formula [24].

[3]Energy and angular frequency are interchangeable in quantum mechanics, through the relation $E = \hbar\omega$.

5.3 Equation of motion

The relation $\hat{c}_{i\sigma_1}(t_1) = e^{i\hat{H}_0 t_1}\hat{c}_{i\sigma_1}e^{-i\hat{H}_0 t_1}$ yields Heisenberg's equation of motion[4]

$$i\partial_{t_1}\hat{c}_{i\sigma_1}(t_1) = e^{i\hat{H}_0 t_1}\big[\hat{c}_{i\sigma_1}, \hat{H}_0\big]e^{-i\hat{H}_0 t_1}, \tag{5.15}$$

where ∂_{t_1} is compact notation for $\partial/\partial t_1$. Using $\hat{H}_0$ of Eq. (5.1), the anticommutation relations of Eq. (4.22) and Einstein's summation convention then leads to

$$i\partial_{t_1}\hat{c}_{i\sigma_1}(t_1) = h_{ij}\hat{c}_{j\sigma_1}(t_1) + v_{ijkl}\,\hat{c}^\dagger_{l\sigma_2}(t_1^+)\hat{c}_{k\sigma_2}(t_1)\hat{c}_{j\sigma_1}(t_1). \tag{5.16}$$

The Green's function definition of Eq. (5.10) then yields the equation of motion

$$\delta(t_1-t_2)\delta_{ij}\delta_{\sigma_1\sigma_2} = g^{-1}_{ik}(t_1)G^{\sigma_1\sigma_2}_{kj}(t_1t_2) - iv_{iklm}G_{2\,lkjm}^{\sigma_3\sigma_1\sigma_2\sigma_3}(t_1t_1;t_2t_1^+), \tag{5.17}$$

where $g^{-1}_{ik}(t_1) = i\partial_{t_1}\delta_{ik} - h_{ik}$ has been introduced for convenience and

$$G_{2\,ijkl}^{\sigma_1\sigma_2\sigma_3\sigma_4}(t_1t_2;t_3t_4) = -\langle T\hat{c}_{i\sigma_1}(t_1)\hat{c}_{j\sigma_2}(t_2)\hat{c}^\dagger_{l\sigma_4}(t_4)\hat{c}^\dagger_{k\sigma_3}(t_3)\rangle \tag{5.18}$$

is the two-electron Green's function. G_2 is thus required when solving for G, and similarly, G_3 is needed to find G_2, leading to a hierarchy problem of many-electron Green's functions. This issue is cured by utilizing Schwinger's functional derivative method, where

$$G_{2\,lijk}^{\sigma_4\sigma_1\sigma_2\sigma_3}(t_3t_1;t_2t_3^+) = \frac{\delta G_{ij}^{\sigma_1\sigma_2}(t_1t_2)}{\delta\varphi_{kl}^{\sigma_3\sigma_4}(t_3)} - G_{ij}^{\sigma_1\sigma_2}(t_1t_2)G_{lk}^{\sigma_4\sigma_3}(t_3t_3^+), \tag{5.19}$$

as can be verified by combining Eqs. (5.3), (5.5), (5.9) and (5.10).

5.4 Hedin's equations and the GW approximation

From Eqs. (5.17) and (5.19) and the chain rule $\delta GG^{-1} + G\delta G^{-1} = 0$, it follows that

$$G^{-1\,\sigma_1\sigma_2}_{ij}(t_1t_2) = G^{-1\,\sigma_1\sigma_2}_{\mathrm{H}\;ij}(t_1t_2) - \Sigma^{\sigma_1\sigma_2}_{ij}(t_1t_2), \tag{5.20}$$

$$G^{-1\,\sigma_1\sigma_2}_{\mathrm{H}\;ij}(t_1t_2) = \delta(t_1-t_2)\Big(\big(g^{-1}_{ij}(t_1) - V^{\mathrm{H}}_{ij}(t_1)\big)\delta_{\sigma_1\sigma_2} - \varphi^{\sigma_1\sigma_2}_{ij}(t_1)\Big), \tag{5.21}$$

$$\Sigma^{\sigma_1\sigma_2}_{ij}(t_1t_2) = -iv_{iklm}(t_1t_3)G^{\sigma_1\sigma_4}_{kn}(t_1t_4)\frac{\delta G^{-1\,\sigma_4\sigma_2}_{nj}(t_4t_2)}{\delta\varphi^{\sigma_3\sigma_3}_{ml}(t_3)}, \tag{5.22}$$

[4] $[\hat{A},\hat{B}] = \hat{A}\hat{B} - \hat{B}\hat{A}$.

where $v_{ijkl}(t_1t_2) = v_{ijkl}\,\delta(t_1-t_2)$. $G_{\rm H}^{-1}$ is the inverse Hartree Green's function and Σ the self-energy, which contains the exchange and correlation effects of the electronic system. $G_{\rm H}^{-1}$ contains the (classical) Hartree potential[5]

$$V_{ij}^{\rm H}(t_1) = -i\,v_{ijkl}\,G_{kl}^{\sigma\sigma}(t_1t_1^+) = v_{ijkl}\,n_{lk}(t_1). \tag{5.23}$$

Eq. (5.20) can be reformulated as

$$G_{ij}^{\sigma_1\sigma_2}(t_1t_2) = G_{{\rm H}ij}^{\sigma_1\sigma_2}(t_1t_2) + G_{{\rm H}ik}^{\sigma_1\sigma_3}(t_1t_3)\Sigma_{kl}^{\sigma_3\sigma_4}(t_3t_4)G_{lj}^{\sigma_4\sigma_3}(t_4t_2), \tag{5.24}$$

known as Dyson's equation. Hedin's formalism [2] uses the potential $V = \varphi + V^{\rm H}$ in the chain rule, so that Eq. (5.22) takes the form

$$\Sigma_{ij}^{\sigma_1\sigma_2}(t_1t_2) = i\,\sigma_{\sigma_3\sigma_2}^{\mu}G_{kl}^{\sigma_1\sigma_3}(t_1t_3)W_{mnki}(t_4t_1)\Lambda_{ljmn}^{\mu 0}(t_3t_2t_4), \tag{5.25}$$

where

$$\Lambda_{ijkl}^{\mu\nu}(t_1t_2t_3) = -\frac{1}{2}\sigma_{\sigma_2\sigma_1}^{\mu}\frac{\delta G^{-1}{}_{ij}^{\sigma_1\sigma_2}(t_1t_2)}{\delta V_{kl}^{\sigma_3\sigma_4}(t_3)}\sigma_{\sigma_3\sigma_4}^{\nu} \tag{5.26}$$

is the three-leg vertex and[6]

$$W_{ijkl}(t_1t_2) = \epsilon_{{\rm H}ijmn}^{-1}(t_1t_3)v_{mnkl}(t_3t_2), \quad (5.27) \qquad \epsilon_{{\rm H}ijkl}^{-1}(t_1t_2) = \frac{\delta V_{ij}(t_1)}{\delta\varphi_{kl}(t_2)}, \quad (5.28)$$

are, respectively, Hedin's screened interaction[7] and the inverse (Hartree) dielectric function. Only the $\mu 0$-component of Λ enters into Eq. (5.25). The chain rule implies that

$$\begin{aligned}\Lambda_{ijkl}^{\mu\nu}(t_1t_2t_3) &= \delta_{\mu\nu}\delta_{ik}\delta_{jl}\delta(t_1-t_2)\delta(t_1-t_3) \\ &\quad + \frac{1}{2}\,\sigma_{\sigma_2\sigma_1}^{\mu}\sigma_{\sigma_7\sigma_8}^{\eta}\frac{\delta\Sigma_{ij}^{\sigma_1\sigma_2}(t_1t_2)}{\delta G_{mn}^{\sigma_5\sigma_6}(t_5t_6)}G_{mo}^{\sigma_5\sigma_7}(t_5t_7)G_{pn}^{\sigma_8\sigma_6}(t_8t_6)\Lambda_{opkl}^{\eta\nu}(t_7t_8t_3),\end{aligned} \tag{5.29}$$

$$W_{ijkl}(t_1t_2) = v_{ijkl}(t_1t_2) + v_{ijmn}(t_1t_3)\,P_{mnop}(t_3t_4)\,W_{opkl}(t_4t_2), \tag{5.30}$$

$$P_{ijkl}(t_1t_2) = -i\,G_{im}^{\sigma_1\sigma_3}(t_1t_3)G_{nj}^{\sigma_3\sigma_1}(t_4t_1^+)\Lambda_{mnkl}^{00}(t_3t_4t_2), \tag{5.31}$$

where P is the density polarization propagator and $i\delta\Sigma/\delta G$ is a four-point correction to the Coulomb interaction due to exchange and correlations. Since the Hamiltonian contains no explicit spin-spin interaction, this is exclusively contained in this quantity. Since $W = W^{00}$, the closure of Eq. (5.30) follows from the decoupling between charge-charge and spin-spin interactions in the absence of the spin-orbit effect. Eqs. (5.24), (5.25),

[5]Potentials V without spin variables denote the charge components $\frac{1}{2}\varphi^{\sigma\sigma}$ and $\frac{1}{2}V^{\sigma\sigma}$.

[6]The reader is encouraged to prove that $\epsilon_{\rm H}^{-1}$ is an approximation to the inverse relative permittivity of Sec. 2.5, but also to relate other quantities in Chap. 5 to those in Chap. 2.

[7]W has dimension of energy in frequency domain and power in time domain.

(5.29), (5.30) and (5.31) are called Hedin's equations [2], which in principle yield the exact electronic structure. However, approximations are required in practice, and the most famous is the GW approximation, justified for weakly correlated metals. In this approximation, only the first term of Eq. (5.29) is kept, which leads to the self-energy

$$\Sigma_{\mathrm{GW}}{}_{ij}^{\sigma_1\sigma_2}(t_1t_2) = iG_{kl}^{\sigma_1\sigma_2}(t_1t_2)W_{ljki}(t_2t_1), \tag{5.32}$$

where Eq. (5.30) for W is unchanged but Eq. (5.31) for P is simplified to $P = -iGG$, schematically. The argument behind the GW approximation is that, when the screening is strong, it should work to expand Σ to linear order in W. However, this argument is flawed for the short-range components of W, which are big. To accurately describe short-range correlations, the GW approximation is often combined with other methods, such as dynamical mean-field theory [25, 26, 27] and configuration interaction [28]. An alternative route is to include vertex correction in Eq. (5.29) stemming from $\delta\Sigma/\delta G$ [29].

5.5 Charge and spin fluctuations

The spin-density operator $\hat{n}_{ij}^{\sigma_1\sigma_2}(t) = \hat{c}_{i\sigma_1}^\dagger(t)\hat{c}_{j\sigma_2}(t)$ can be split into an expectation value n and a fluctuation $\Delta\hat{n}$, i.e. $\hat{n} = n + \Delta\hat{n}$. It can then be shown that

$$R_{ijkl}^{\sigma_1\sigma_2\sigma_3\sigma_4}(t_1t_3) = \frac{\delta n_{ji}^{\sigma_2\sigma_1}(t_1)}{\delta\varphi_{kl}^{\sigma_3\sigma_4}(t_3)} = \langle T\Delta\hat{n}_{kl}^{\sigma_3\sigma_4}(t_3)\Delta\hat{n}_{ji}^{\sigma_2\sigma_1}(t_1)\rangle/i, \tag{5.33}$$

i.e. that the (time-ordered) linear spin-density response R equals the correlator between two spin-density fluctuations. It is intrinsic to the system, and so are the higher-order responses. In four-vector representation, $R^{\mu\nu} = \sigma_{\sigma_2\sigma_1}^{\mu}R^{\sigma_1\sigma_2\sigma_3\sigma_4}\sigma_{\sigma_3\sigma_4}^{\nu}$ takes the form

$$R_{ijkl}^{\mu\nu}(t_1t_3) = \frac{\delta n_{ji}^{\mu}(t_1)}{\delta\varphi_{kl}^{\nu}(t_3)} = \langle T\Delta\hat{n}_{kl}^{\nu}(t_3)\Delta\hat{n}_{ji}^{\mu}(t_1)\rangle/i. \tag{5.34}$$

Importantly, this contains $\delta\mathbf{M}/\delta\mathbf{B}_{\mathrm{ext}}$ since $n^\mu = -2cM^\mu$ ($\mu > 0$) in the absence of orbital magnetization and $\varphi^\nu = B_{\mathrm{ext}}^\nu/2c$ ($\nu > 0$), and it is left as an exercise to show that $\delta\mathbf{M}/\delta\mathbf{B}_{\mathrm{ext}} = \overleftrightarrow{\chi}_{\mathrm{m}}(\mathbb{I}-4\pi\overleftrightarrow{\chi}_{\mathrm{m}})^{-1}$, in terms of $\overleftrightarrow{\chi}_{\mathrm{m}}$ of Sec. 2.3. The magnetoelectric susceptibility components, however, vanish without spin-orbit interaction. The $\mu\nu$-components $|\operatorname{Im} R^{\mu\nu}(\omega)|/\pi$ are spectral functions containing the charge ($\mu = 0, \nu = 0$) and spin ($\mu > 0$, $\nu > 0$) (electron-hole) excitation energies, i.e. the plasmon and magnon spectras.

5.6 Bethe-Salpeter equation

To treat charge and spin fluctuations equally, the Hedin chain rule behind Eq. (5.25) should be avoided, and the mass operator $M = V^{\mathrm{H}} + \Sigma$ take over the role of V^{H}. By

writing R as a two-time contraction[8] of its four-time extension $\mathcal{R}_{IJKL} = -i\,\frac{\delta G_{IJ}}{\delta \varphi_{KL}}$, where the combined index $I = (i, \sigma_i, t_i)$ has been introduced, the modified chain rule implies the Bethe-Salpeter equation [30, 31]

$$\mathcal{R}_{IJKL} = \mathcal{P}_{IJKL} + \mathcal{P}_{IJMN}\,\mathcal{V}_{MNOP}\,\mathcal{R}_{OPKL}, \tag{5.35}$$

where

$$\mathcal{P}_{IJKL} = -iG_{IK}G_{LJ}, \tag{5.36}$$

$$\mathcal{V}_{IJKL} = i\frac{\delta M_{IJ}}{\delta G_{KL}}. \tag{5.37}$$

$\mathcal{P}$ is vertex-free, contrary to P in Eq. (5.31). The information from the vertex is instead absorbed in the electromagnetic interaction $\mathcal{V}$, which contains both charge-charge and spin-spin components. In many situations, like when computing magnon spectra, it is customary to split the mass operator between the Hartree-Fock potential[9] and the correlations, i.e. $M = V^{\mathrm{HF}} + \Sigma^{\mathrm{c}}$, where Σ^{c} is the correlation part of Eq. (5.25). This split is used in Sec. 8.2, and turns the Bethe-Salpeter equation into two equations

$$\mathcal{R}_{IJKL} = \mathcal{R}^{\mathrm{HF}}_{IJKL} + \mathcal{R}^{\mathrm{HF}}_{IJMN}\,\Delta_{MNOP}\,\mathcal{R}_{OPKL}, \tag{5.38}$$

$$\mathcal{R}^{\mathrm{HF}}_{IJKL} = \mathcal{P}_{IJKL} + \mathcal{P}_{IJMN}\,\mathcal{V}^{\mathrm{HF}}_{MNOP}\,\mathcal{R}^{\mathrm{HF}}_{OPKL}, \tag{5.39}$$

where

$$\mathcal{V}^{\mathrm{HF}}_{IJKL} = i\frac{\delta V^{\mathrm{HF}}_{IJ}}{\delta G_{KL}}, \tag{5.40}$$

$$\Delta_{IJKL} = i\frac{\delta \Sigma^{\mathrm{c}}_{IJ}}{\delta G_{KL}}. \tag{5.41}$$

The typical strategy is to first find reference magnons and plasmons, by computing $\mathcal{R}_{\mathrm{HF}}$ of Eq. (5.39). This is possible since the Hartree-Fock interaction $\mathcal{V}^{\mathrm{HF}}$ of Eq. (5.40) is known. While generally demanding, it gets rather simple in the context of the Hubbard model. The interaction Δ of Eq. (5.41) can then be interpreted as the interaction between the reference bosons in Eq. (5.38), i.e. as the magnon-magnon or plasmon-plasmon interaction, depending on the particular component. Eq. (5.38) is to be thought of as the bosonic analog of Dyson's equation (Eq. (5.24)), and the task of finding good bosonic spectra thus boils down to finding a good approximation to Δ.

5.7 Effect of phonons on the electronic structure

The clamped-nuclei assumption used so far is not justified for some lighter nuclei (or ions), such as oxygen. Phonons are included by introducing operators for the nuclear positions. Nucleus κ (with charge Z_κ and mass M_κ) in unit cell p is associated with a position operator

[8] $R^{\sigma_1\sigma_2\sigma_3\sigma_4}_{ijkl}(t_1t_3) = \lim_{t_2\to t_1}\lim_{t_4\to t_3}\mathcal{R}^{\sigma_1\sigma_2\sigma_3\sigma_4}_{ijkl}(t_1t_2^+t_3t_4)$

[9] $V^{\mathrm{HF}\,\sigma_1\sigma_2}_{ij}(t_1t_2) = -i\delta(t_1-t_2)\big(\delta_{\sigma_1\sigma_2}v_{ijkl}G^{\sigma\sigma}_{kl}(t_1t_1^+) - v_{ljki}G^{\sigma_1\sigma_2}_{kl}(t_1t_1^+)\big)$

$\hat{\boldsymbol{\tau}}_{\kappa p}(t_1)$. If the equilibrium position is $\boldsymbol{\tau}^0_{\kappa p}$, it follows that $\hat{\boldsymbol{\tau}}_{\kappa p}(t_1) = \boldsymbol{\tau}^0_{\kappa p} + \Delta\hat{\boldsymbol{\tau}}_{\kappa p}(t_1)$, where the last term is the nuclear displacement (or fluctuation) operator, with vanishing expectation value. Eq. (5.2) for h_{ij} then extends to

$$h_{ij}(t_1) = \int d\mathbf{r}_1\, \phi_i^*(\mathbf{r}_1)\bigg(\hat{T} - \int d\mathbf{r}_2 dt_2 \frac{\delta(t_1-t_2)}{|\mathbf{r}_1-\mathbf{r}_2|}\rho_{\mathrm{n}}(\mathbf{r}_2,t_2)\bigg)\phi_j(\mathbf{r}_1), \tag{5.42}$$

where $\rho_{\mathrm{n}}(\mathbf{r},t) = \sum_{\kappa p} Z_\kappa \langle\delta(\mathbf{r} - \boldsymbol{\tau}^0_{\kappa p} - \Delta\hat{\boldsymbol{\tau}}_{\kappa p}(t))\rangle$ is the nuclear charge density and Einstein's summation convention temporarily has been abandoned. For small displacements, the harmonic approximation is justified, in which [32, 33]

$$\rho_{\mathrm{n}}(\mathbf{r},t) = \Big(1 + \frac{i}{2}\nabla\cdot\overleftrightarrow{\mathbf{D}}_{\kappa p,\kappa p}(t^+t)\cdot\nabla\Big) Z_\kappa \delta(\mathbf{r}-\boldsymbol{\tau}^0_{\kappa p}), \tag{5.43}$$

$$\overleftrightarrow{\mathbf{D}}_{\kappa p,\kappa' p'}(t_1t_2) = \langle T\Delta\hat{\boldsymbol{\tau}}_{\kappa p}(t_1)\Delta\hat{\boldsymbol{\tau}}_{\kappa' p'}(t_2)\rangle/i, \tag{5.44}$$

where $\overleftrightarrow{\mathbf{D}}$ is the nuclear displacement-displacement correlation tensor. Skipping details, phonons enter Hedin's formalism through the extension [34, 35]

$$W_{ijkl}(\omega) \mapsto W_{ijkl}(\omega) + W^{\mathrm{ph}}_{ijkl}(\omega) \tag{5.45}$$

of Eq. (5.30) in frequency domain. The last term is a phonon contribution obtained by an integral of the form of Eq. (4.18), but with $1/|\mathbf{r}_1-\mathbf{r}_2|$ replaced by

$$W^{\mathrm{ph}}(\mathbf{r}_1\mathbf{r}_2,\omega) = \epsilon^{-1}_{\mathrm{H}}(\mathbf{r}_1\mathbf{r}_3,\omega)\,\mathbf{F}_{\kappa p}(\mathbf{r}_3)\cdot\overleftrightarrow{\mathbf{D}}_{\kappa p,\kappa' p'}(\omega)\cdot\mathbf{F}_{\kappa' p'}(\mathbf{r}_4)\,\epsilon^{-1}_{\mathrm{H}}(\mathbf{r}_4\mathbf{r}_2,\omega), \tag{5.46}$$

where $\epsilon^{-1}_{\mathrm{H}}$ is the position representation of Eq. (5.28) and

$$\mathbf{F}_{\kappa p}(\mathbf{r}_1) = Z_\kappa \frac{\mathbf{r}_1 - \boldsymbol{\tau}^0_{\kappa p}}{|\mathbf{r}_1 - \boldsymbol{\tau}^0_{\kappa p}|^3} \tag{5.47}$$

is the force from a clamped nucleus κ in unit cell p. In the adiabatic (Born-Oppenheimer) approximation, which holds if the plasmon energies are much higher than the phonon energies,[10] $\epsilon^{-1}_{\mathrm{H}}(\omega)$ is replaced by its static value. An important consequence is that the phonon spectrum acquires sharp peaks that follow well-defined phonon dispersions $\omega_{\mathbf{q}\nu}$ for the different phonon modes ν, which leads to the simple relation

$$\overleftrightarrow{\mathbf{D}}_{\kappa p,\kappa' p'}(\omega) = \sum_\nu \int d\mathbf{q}\, \frac{e^{-i\mathbf{q}\cdot(\mathbf{R}_p-\mathbf{R}_{p'})}}{\sqrt{M_\kappa M_{\kappa'}}} \frac{\mathbf{e}^*_{\mathbf{q}\nu,\kappa}\mathbf{e}_{\mathbf{q}\nu,\kappa'}}{\omega^2 - \omega^2_{\mathbf{q}\nu}}, \tag{5.48}$$

where Einstein's summation convention has been abandoned. The phonon polarization vector of mode ν at nucleus κ is denoted by $\mathbf{e}_{\mathbf{q}\nu,\kappa}$. The phonons are treated as a perturbation in this thesis. The phonon dispersions and polarization vectors are thus assumed as known inputs, although they generally have to be computed self-consistently together with the electronic structure, using the so-called Hedin-Baym equations [35].

[10] Adiabaticity fails in metals, but the metallic contribution can be separated out and treated analytically.

Part II

Project summary & key results

6

Spatiotemporal view of screening

This chapter introduces and summarizes Paper I, titled "Position representation of effective electron-electron interactions in solids". The screened interaction W and its partially screened analog U enter into Hedin's equations and low-energy models, respectively. In Paper I, a formula is derived for obtaining the position representation of W (U) from matrix elements of the linear density response R (R^{r}) in a Bloch product basis. The causal interaction in time domain due to the insertion of an impurity at time $\tau = 0$ is also derived. As a test, W (U) is computed within the (constrained) random-phase approximation for the cuprate parent compounds La_2CuO_4 and $HgBa_2CuO_4$ and the correlated metal $SrVO_3$, based on the spin-unpolarized local density approximation. The major finding is the presence of spatial regions with a strong negative U in the cuprates, which are short-lived in the 3-band model but stable in the 1-band model.

6.1 Fully and partially screened interaction

In the random-phase approximation (RPA), $\delta\Sigma/\delta G$ is neglected, which simplifies the three-leg vertex $\Lambda^{\mu\nu}$ of Eq. (5.29) and the electromagnetic interaction $\mathcal{V}^{\mu\nu}$ of Eq. (5.37). With short-hand notation R for the 00-component of Eq. (5.34), it follows that

$$R_{ijkl}(\omega) = P_{ijkl}(\omega) + \sum_{mnop} P_{ijmn}(\omega)\, v_{mnop} R_{opkl}(\omega), \tag{6.1}$$

$$P_{ijkl}(\omega) = -i \sum_{\sigma} \int \frac{d\omega'}{2\pi} e^{i\omega'\eta} G^{\sigma\sigma}_{ik}(\omega+\omega') G^{\sigma\sigma}_{lj}(\omega'), \tag{6.2}$$

in frequency domain. In practice, it is common to approximate the Green's function G by that computed using density functional theory (DFT) [15, 16, 17, 18]. For spin-

unpolarized periodic systems, the DFT Bloch electrons are described by one-body eigenstates $\psi_{\mathbf{k}n}$ and eigenvalues $\epsilon_{\mathbf{k}n}$, so that

$$G^{\sigma\sigma}_{ik}(\omega) = \sum_{\mathbf{k}n}^{\text{occ}} \frac{O^i_{\mathbf{k}n} O^{k*}_{\mathbf{k}n}}{\omega - \epsilon_{\mathbf{k}n} - i\eta} + \sum_{\mathbf{k}n}^{\text{unocc}} \frac{O^i_{\mathbf{k}n} O^{k*}_{\mathbf{k}n}}{\omega - \epsilon_{\mathbf{k}n} + i\eta}, \tag{6.3}$$

where $O^i_{\mathbf{k}n} = \langle \phi_i | \psi_{\mathbf{k}n} \rangle$. The two terms are restricted to occupied and unoccupied states, respectively. Eq. (6.3) combined with Eq. (6.2) yields

$$P_{ijkl}(\omega) = 2 \sum_{\mathbf{k}n}^{\text{occ}} \sum_{\mathbf{k}'n'}^{\text{unocc}} \left(\frac{O^i_{\mathbf{k}'n'} O^{k*}_{\mathbf{k}'n'} O^l_{\mathbf{k}n} O^{j*}_{\mathbf{k}n}}{\omega + \epsilon_{\mathbf{k}n} - \epsilon_{\mathbf{k}'n'} + i\eta} - \frac{O^i_{\mathbf{k}n} O^{k*}_{\mathbf{k}n} O^l_{\mathbf{k}'n'} O^{j*}_{\mathbf{k}'n'}}{\omega - \epsilon_{\mathbf{k}n} + \epsilon_{\mathbf{k}'n'} - i\eta} \right), \tag{6.4}$$

known as the Lindhard formula [36]. By combining Eq. (5.30) and Eq. (6.1), the fully screened interaction W can be written as

$$W_{ijkl}(\omega) = v_{ijkl} + \sum_{mnop} v_{ijmn} P_{mnop}(\omega) W_{opkl}(\omega) \tag{6.5}$$

$$= v_{ijkl} + \sum_{mnop} v_{ijmn} R_{mnop}(\omega) v_{opkl}, \tag{6.6}$$

in terms of R, which is used to find the position representation of W in Sec. 6.2. It is also possible to construct a partially screened interaction U, which can be thought of as an effective interaction in a low-energy subspace. Physically, U excludes the screening which stems from transitions within the low-energy subspace itself. To define U, the one-body (DFT) Hilbert space is split into a low-energy window d, and the rest r. It then follows that $P = P^{\mathrm{d}} + P^{\mathrm{r}}$, where P^{d} is restricted to the d subspace and P^{r} contains all other transitions. But the low-energy band structure is not always separated from the rest of the band structure. In the disentanglement method [37], this issue is dealt with by fitting suitable Wannier functions to the band structure in an energy window, which is restricted but wide enough to yield convergence. The subspace spanned by these Wannier functions is then chosen as the d subspace, in which the one-body (DFT) Hamiltonian is diagonalized, yielding low-energy eigenfunctions $\bar{\psi}_{\mathbf{k}n}$ and eigenvalues $\bar{\epsilon}_{\mathbf{k}n}$, where $\mathbf{k}n \in \mathrm{d}$. These may differ slightly from the original bands close to the edge of the energy window. P^{d} is then computed using the approximate band structure as

$$P^{\mathrm{d}}_{ijkl}(\omega) = 2 \sum_{\mathbf{k}n \in \mathrm{d}}^{\text{occ}} \sum_{\mathbf{k}'n' \in \mathrm{d}}^{\text{unocc}} \left(\frac{\bar{O}^i_{\mathbf{k}'n'} \bar{O}^{k*}_{\mathbf{k}'n'} \bar{O}^l_{\mathbf{k}n} \bar{O}^{j*}_{\mathbf{k}n}}{\omega + \bar{\epsilon}_{\mathbf{k}n} - \bar{\epsilon}_{\mathbf{k}'n'} + i\eta} - \frac{\bar{O}^i_{\mathbf{k}n} \bar{O}^{k*}_{\mathbf{k}n} \bar{O}^l_{\mathbf{k}'n'} \bar{O}^{j*}_{\mathbf{k}'n'}}{\omega - \bar{\epsilon}_{\mathbf{k}n} + \bar{\epsilon}_{\mathbf{k}'n'} - i\eta} \right), \tag{6.7}$$

where $\bar{O}^i_{\mathbf{k}n} = \langle \phi_i | \bar{\psi}_{\mathbf{k}n} \rangle$. By defining the d-subspace projector $\hat{\mathcal{P}} = \sum_{\mathbf{k}n \in \mathrm{d}} |\bar{\psi}_{\mathbf{k}n}\rangle\langle\bar{\psi}_{\mathbf{k}n}|$, the r subspace is obtained by acting with the operator $1 - \hat{\mathcal{P}}$ on the full one-body Hilbert space, so as to render it orthogonal to the d subspace. The resulting orthonormalized r-subspace eigenvectors $\bar{\psi}_{\mathbf{k}n}$, where $\mathbf{k}n \in \mathrm{r}$, are all orthogonal to those in the d subspace.

The full polarization propagator of Eq. (6.4) is then approximated by the modified band structure in the full Hilbert space, i.e. its expression is identical to Eq. (6.7) but without restricting the summations to the d subspace. The replacement of Eq. (6.4) by this approximation is important in order to guarantee that $P^{\mathrm{r}} = P - P^{\mathrm{d}}$ contains no low-energy transitions. In analogy with the fully screened interaction W of Eq. (6.5), the partially screened interaction U is defined as [38, 39, 40]

$$U_{ijkl}(\omega) = v_{ijkl} + \sum_{mnop} v_{ijmn} P^{\mathrm{r}}_{mnop}(\omega) U_{opkl}(\omega) \tag{6.8}$$

$$= v_{ijkl} + \sum_{mnop} v_{ijmn} R^{\mathrm{r}}_{mnop}(\omega) v_{opkl}(\omega), \tag{6.9}$$

where $R^{\mathrm{r}} = P^{\mathrm{r}} + P^{\mathrm{r}} v R^{\mathrm{r}}$. Eq. (6.9) is used to find the position representation of U in Sec. 6.2. It follows that $W = U + U P^{\mathrm{d}} W$, which shows that U indeed is the effective interaction in the d subspace. In fact, U is a dynamical and non-local extension of the U of the famous Hubbard model. It is common to include effects beyond the RPA stemming from $\delta\Sigma/\delta G$ in the d subspace. Such an approach is known as the constrained RPA (cRPA), and is justified when the correlations are strong only close to the Fermi energy.

6.2 From product basis to position representation

In position representation, the screened interaction W of Eq. (5.30) reads[1]

$$W(\mathbf{r}_1\mathbf{r}_2,\omega) = \frac{1}{|\mathbf{r}_1-\mathbf{r}_2|} + W^{\mathrm{c}}(\mathbf{r}_1\mathbf{r}_2,\omega), \tag{6.10}$$

$$W^{\mathrm{c}}(\mathbf{r}_1\mathbf{r}_2,\omega) = \int d\mathbf{r}_3 d\mathbf{r}_4 \frac{R(\mathbf{r}_3\mathbf{r}_4,\omega)}{|\mathbf{r}_1-\mathbf{r}_3||\mathbf{r}_4-\mathbf{r}_2|}, \tag{6.11}$$

where the known spatial dependence of the bare Coulomb interaction v has been written explicitly. The correlated part W^{c}, which physically is the potential at $\mathbf{r}_1$ due to the screening hole created by an added test charge at $\mathbf{r}_2$, contains all the material-specific spatial dependence of W. Fig. 6.1 gives two simplified sketches, for weak and strong screening, of v, W^{c} and W as a function of the distance between two electrons in an isotropic and homogeneous medium. Notably, while v and W^{c} decay algebraically at long distances, W decays exponentially.[2] The strong-screening case illustrates that W can turn negative at short distances, indicating a bound state. The task is to find the spatial dependence of W^{c} in Eq. (6.11) from the components $R_{ijkl}(\omega)$ of Eq. (6.1), which comprise a common output from first-principle codes. R, contrary to W^{c}, decays exponentially at long

[1] All results for W carry over to U by replacing R by R^{r}.

[2] U decays algebraically, contrary to W.

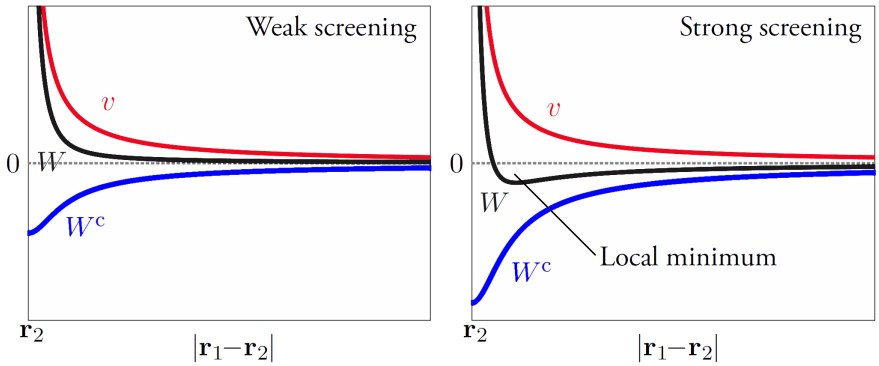

Figure 6.1: Position representation of v, static W^{c} and static W in an isotropic and homogeneous system, for weak (left) and strong screening (right). A local (radial) minimum of W is possible when the screening is strong.

distances and can thus be expanded in a workably small basis. More precisely, the (Bloch) product basis $B_{\mathbf{k}\alpha}$ ($= \phi_i\phi_j^*$) used for P is also complete for R since the v's in Eq. (6.1) are sandwiched between P's. Consequently, [41]

$$R(\mathbf{r}_1\mathbf{r}_2,\omega) = \sum_{\alpha\beta}\sum_{\mathbf{k}} B_{\mathbf{k}\alpha}(\mathbf{r}_1)R_{\alpha\beta}(\mathbf{k},\omega)B^*_{\mathbf{k}\beta}(\mathbf{r}_2), \tag{6.12}$$

where R is diagonal in wave vector due to the discrete translational symmetry of the lattice. Combining Eq. (6.11) and Eq. (6.12) finally yields

$$W^{\mathrm{c}}(\mathbf{r}_1\mathbf{r}_2,\omega) = \sum_{\alpha\beta}\sum_{\mathbf{k}} I_{\mathbf{k}\alpha}(\mathbf{r}_1)R_{\alpha\beta}(\mathbf{k},\omega)I^*_{\mathbf{k}\beta}(\mathbf{r}_2), \tag{6.13}$$

$$I_{\mathbf{k}\alpha}(\mathbf{r}_1) = \int d\mathbf{r}_2 \frac{B_{\mathbf{k}\alpha}(\mathbf{r}_2)}{|\mathbf{r}_1-\mathbf{r}_2|}. \tag{6.14}$$

This has the same form as R in Eq. (6.12), but with $B_{\mathbf{k}\alpha}$ replaced by the convolution $I_{\mathbf{k}\alpha}$. The task of Sec. 6.2, which is included in the flowchart of Fig. 6.2, is thus reduced to computing all convolutions $I_{\mathbf{k}\alpha}$ and using them together with $R_{\alpha\beta}(\mathbf{k},\omega)$ in Eq. (6.13).

6.3 Time-domain picture: Impulse and step response

In Sec. 6.2, $W(\omega)$ is the Fourier transform of the time-ordered $W(\tau)$.[3] To access the causal $W(\tau)$ from $W(\omega)$, the imaginary part of the latter has to be multiplied by $\mathrm{sign}(\omega)$, as can easily be verified. Here, this factor is absorbed into $W(\omega)$ for convenience, making its real and imaginary parts even and odd functions of ω, respectively. All information is

[3] In the absence of external fields, $W(t_1t_2)$ depends only on the time-difference $\tau = t_1 - t_2$.

thus contained in the $\omega > 0$ components. The causal $W(\tau)$ is then obtained from the inverse Fourier transform (see Fig. 6.2)

$$W_\delta(\mathbf{r}_1\mathbf{r}_2,\tau) = \int \frac{d\omega}{2\pi} e^{-i\omega\tau} W(\mathbf{r}_1\mathbf{r}_2,\omega). \tag{6.15}$$

Subscript δ highlights that it, in linear response theory, is the change of potential $V(\mathbf{r}_1,\tau)$ of Sec. 5.4 due to an impulse density perturbation at position $\mathbf{r}_2$ and time 0 ($\varphi(\mathbf{r}_1,\tau) = \delta(\tau)/|\mathbf{r}_1-\mathbf{r}_2|$). If instead, a frozen impurity is added ($\varphi(\mathbf{r}_1,\tau) = \theta(\tau)/|\mathbf{r}_1-\mathbf{r}_2|$, where θ is the Heaviside step function), the induced change of $V(\mathbf{r}_1,\tau)$ reads

$$W_\theta(\mathbf{r}_1\mathbf{r}_2,\tau) = \frac{\theta(\tau)}{|\mathbf{r}_1-\mathbf{r}_2|} + \int d\mathbf{r}_3 d\mathbf{r}_4 dt \frac{R(\mathbf{r}_3\mathbf{r}_4,\tau-t)\theta(t)}{|\mathbf{r}_1-\mathbf{r}_3||\mathbf{r}_4-\mathbf{r}_2|}, \tag{6.16}$$

The factor $\theta(t)$ in the last term requires that $t > 0$, whereas the causality of R requires that $t < \tau$. From the variable change $\tau - t \mapsto t$, it then follows that (see Fig. 6.2)

$$W_\theta(\mathbf{r}_1\mathbf{r}_2,\tau) = \int_{0^-}^{\tau} dt\, W_\delta(\mathbf{r}_1\mathbf{r}_2,t) = \int_{-\infty}^{\tau} dt\, W_\delta(\mathbf{r}_1\mathbf{r}_2,t), \tag{6.17}$$

where the last equality follows from causality. W_θ is thus the anti-derivative of W_δ. While W_δ has dimension of power, W_θ has dimension of energy, like $W(\omega)$. It has the limits

$$W_\theta(\mathbf{r}_1\mathbf{r}_2,\tau) = \begin{cases} 1/|\mathbf{r}_1-\mathbf{r}_2| & , \quad \tau \to 0^+ \\ W(\mathbf{r}_1\mathbf{r}_2,\omega=0) & , \quad \tau \to \infty. \end{cases} \tag{6.18}$$

To the best of the author's knowledge, this quantity has not been studied before. Physically, it implicitly assumes that the impurity has a large mass to render it frozen. Yet, it provides a minimal way to study semi-bound states since it is possible that W_θ is negative after some finite time-delay τ even though both limits in Eq. (6.18) turn out to be positive.

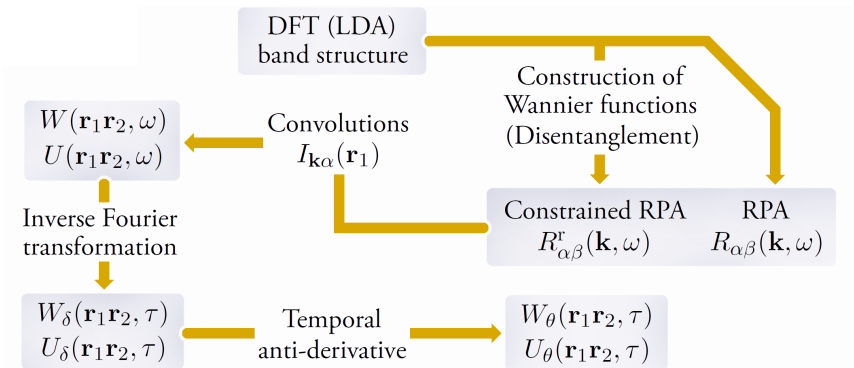

Figure 6.2: Flowchart for obtaining W and U in position representation and time domain, from an initial density functional calculation.

6.4 Results: Cuprate superconductors versus $SrVO_3$

The schemes of Secs. 6.2-6.3 are applied to the cuprate superconductor parent compounds[4] La_2CuO_4 [42] and $HgBa_2CuO_4$ [43] and to the correlated metal $SrVO_3$ [44]. G is computed using the full-potential linearized augmented plane-wave DFT code FLEUR [45] from the band structure of the (spin-unpolarized) local density approximation (LDA), see Fig. 6.3. Product basis matrix elements of R and $R^{\rm r}$ are obtained from the code SPEX [46], which enter a project-specific code used to find W and U of Eqs. (6.5) and (6.8) in position representation and time domain. Low-energy models are constructed using the disentanglement method of Sec. 6.1. For the cuprates, the 3-band and 1-band models are used to define two alternative d subspaces for computing U within cRPA (see Sec. 6.1), whereas the t_{2g} model is applied to $SrVO_3$. The 3-band model consists of two occupied bands with mainly oxygen $2p_x$ and $2p_y$ characters and an antibonding band with mainly copper $3d_{x^2-y^2}$ character.[5] The 3-band model thus assumes that the low-energy physics

[4]The parent compounds are by definition undoped, and Mott insulating (of charge transfer type) due to the strong repulsion between the low-energy 3d electrons (principal quantum number $n = 3$; orbital angular momentum $l = 2$). In the local density approximation they are described by a spurious metallic band crossing the Fermi energy, which sometimes is used as a minimal model of the doped cuprates.

[5]Here, x, y, xy, yz, xz and $x^2 - y^2$ specify "real harmonics" $Y_{1,1}$, $Y_{1,-1}$, $Y_{2,-2}$, $Y_{2,-1}$, $Y_{2,1}$ and $Y_{2,2}$.

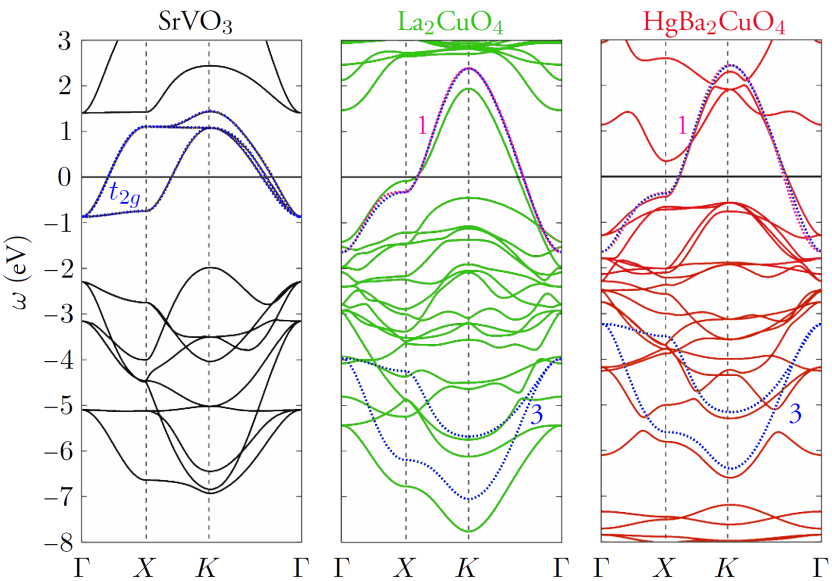

Figure 6.3: LDA band structures of $SrVO_3$ (black), La_2CuO_4 (green) and $HgBa_2CuO_4$ (red). For $SrVO_3$, the t_{2g} model bands are shown with blue dotted lines. For the cuprates, the 3-band and 1-band model bands are shown with blue and magenta dotted lines, respectively. $\Gamma = (0, 0, 0)$, $X = (\pi/a, 0, 0)$ and $K = (\pi/a, \pi/a, 0)$.

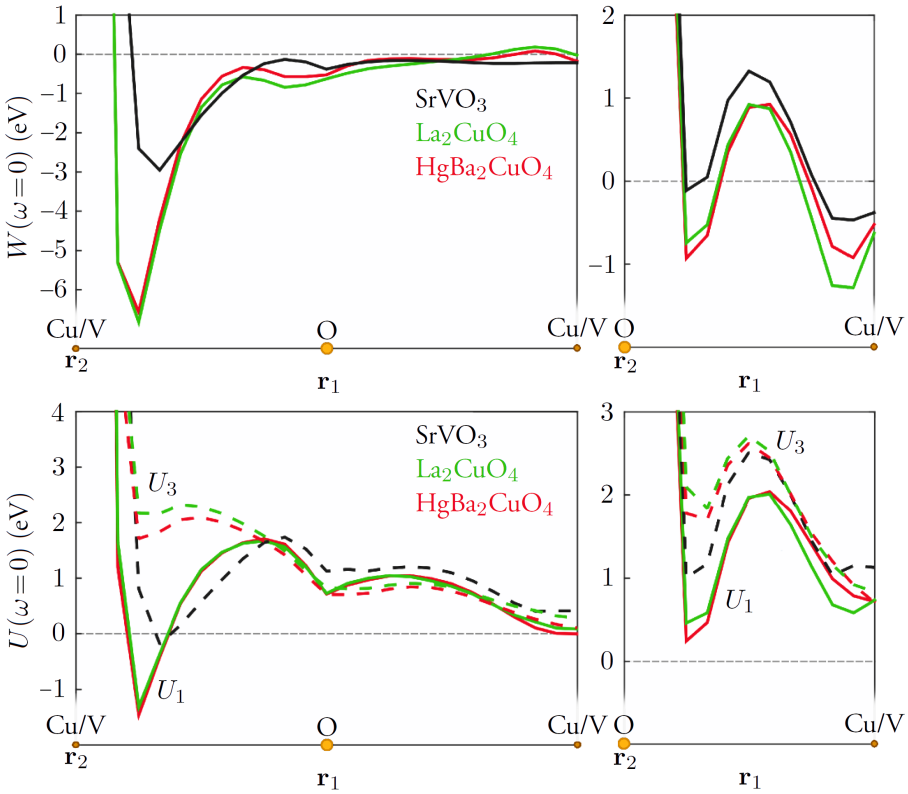

Figure 6.4: Static W (top) and U (bottom) in position representation in a CuO_2 plane of La_2CuO_4 and $HgBa_2CuO_4$ and in a VO_2 plane of $SrVO_3$. The test charge coordinate $\mathbf{r}_2$ is at the (copper or vanadium) atom to the left and at the oxygen atom to the right. Both the 1- and 3-band U are presented for the cuprates.

takes place in the CuO_2 planes.[6] The 1-band model further simplifies the picture by only keeping a single antibonding band of copper $3d_{x^2-y^2}$ character. The t_{2g} model for $SrVO_3$ approximates the three bands across the Fermi energy as stemming from the hybridization of vanadium $3d_{xy}$, $3d_{yz}$ and $3d_{xz}$ orbitals. The screening from the spurious metallic LDA-band in the cuprates is excluded from U, which partially justifies the LDA calculation. The schemes of Secs. 6.2-6.3, however, are applicable to arbitrary DFT energy functionals.

The position representations of the static W and U obtained from the band structures of Fig. 6.3 are presented in Fig. 6.4 in a CuO_2 plane of the cuprates and in a VO_2 plane of $SrVO_3$.[7] The $\mathbf{r}_1$-dependence is studied in two cases: with the test charge coordinate $\mathbf{r}_2$ at the transition metal atom (copper and vanadium) and at the oxygen atom. For the cuprates,

[6] If a is the lattice constant in the CuO_2 planes, the unit cell copper coordinate is $(0, 0)$ whereas the oxygen coordinates are $(a/2, 0)$ and $(0, a/2)$. In $SrVO_3$, the VO_2 planes have the same geometry.

[7] The convolution of Eq. (6.14) is achieved using Ewald summation and Gaussian integration, as is explained in Paper I along with computational details regarding unit cell specifications [42, 43, 44], the product basis, convergence and the treatment of the contribution to Eq. (6.13) from the Γ point ($\mathbf{k} = \mathbf{0}$).

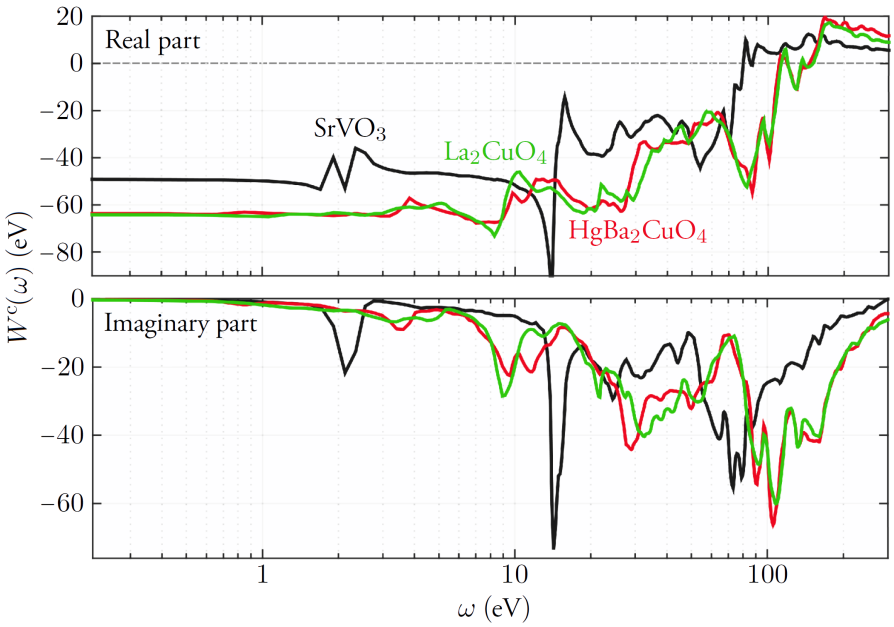

Figure 6.5: $W^{\mathrm{c}}(\omega)$ in La_2CuO_2, $HgBa_2CuO_4$ and $SrVO_3$ with $\mathbf{r}_1 = \mathbf{r}_2$ at the same (copper or vanadium) atom.

both the 1-band and the 3-band U's are presented. With $\mathbf{r}_2$ at copper, U goes from exclusively positive in the 3-band model to including a negative (bound) region in the 1-band model. The negative region is caused by transitions between the occupied oxygen $2p_x$ and $2p_y$ bands and the unoccupied part of the copper $3d_{x^2-y^2}$ band, which leads to a slightly reduced screening close to the neighboring oxygen sites but a drastically enhanced screening close to the copper site with the test charge. The shape of the negative region is shown in Paper I, which also shows that it overlaps to a large extent with that of the 1-band electron density. In $SrVO_3$, a 1-band model cannot be constructed, and the t_{2g} interaction remains essentially positive. The existence of a negative 1-band (charge-charge) interaction in the cuprates is curious, since the pairing mechanism of the doped superconducting cuprates is known to involve the electron spin [47]. The findings would most probably be modified by going beyond cRPA or by including spin-orbit interaction. Indeed, at weak coupling, the charge and spin fluctuations affect each other perturbatively, which could eliminate the negative regions seen in Fig. 6.4 but also convert the effect to the spin-spin interaction. The SCDFT (DFT for superconductors) gap equation [48, 49] is used in Paper I to show that a sufficiently negative W should open up a d-wave superconducting gap. However, W is not very reliable and requires vertex corrections since it includes unphysical metallic screening from the LDA band structure.

$W^{\mathrm{c}}(\omega)$ is presented in Fig. 6.5 in the three compounds, with $\mathbf{r}_1$ and $\mathbf{r}_2$ at the same transition metal atom (copper or vanadium). The causal $W_\delta(\tau)$, which is obtained from

$W^{\mathrm{c}}(\omega)$ using Eq. (6.15), is presented in Fig. 6.6. The latter looks similar in all three compounds. Shortly after the repulsive impulse (not shown in the plot since described by a delta function at $\tau = 0$) the interaction becomes negative due to the build-up of a screening hole caused by the repulsion. This hole then attracts some electrons back into the region, and the cycle is repeated, albeit damped. The time-scale is set by the dominating spectral features in Fig. 6.5, as can be understood in a simplified picture if $W^{\mathrm{c}}(\omega)$ is approximated by a train of infinite-lifetime plasmons, with weights $W_i > 0$ and frequencies $\omega_i > 0$. Eq. (6.15) applied to this approximation yields

$$W_\delta(\tau) = -\frac{2}{\pi} \sum_i W_i \sin(\omega_i \tau)\theta(\tau). \tag{6.19}$$

The short-time behavior in the three compounds is determined by $W^{\mathrm{c}}(\omega)$ in a broad range of frequencies whereas, due to destructive interference, the long-time behavior is predominantly determined by the structure of $W^{\mathrm{c}}(\omega)$ at low frequencies. The bulk plasmon, seen in all three compounds as a broad structure in the imaginary part of $W^{\mathrm{c}}(\omega)$ in Fig. 6.5, therefore strongly influences the short-time behavior in Fig. 6.6. Since the bulk plasmons are similar in the two cuprates, their short-time behaviors are also similar.

Fig. 6.7 presents $U_{3,\theta}(\tau)$ for the cuprates, i.e. the analog of Eq. (6.17) due to an impurity, but for U of the 3-band model. To avoid the divergence stemming from the bare Coulomb interaction, $\mathbf{r}_1$ and $\mathbf{r}_2$ are placed close to each other but not at the same place. $\mathbf{r}_1$ is placed

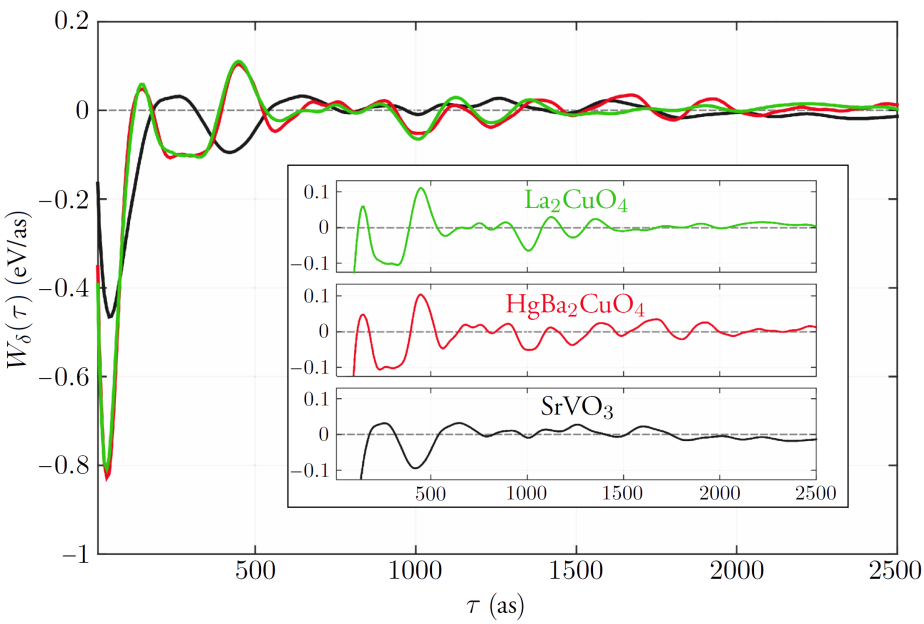

Figure 6.6: $W_\delta(\tau)$ in La_2CuO_2, $HgBa_2CuO_4$ and $SrVO_3$ with $\mathbf{r}_1 = \mathbf{r}_2$ at the same (copper or vanadium) atom.

at the copper atom and $\mathbf{r}_2$ a quarter along the path between the copper and oxygen atom. Despite the positivity of both the short- and long-time (static) limits, time-intervals are found with a negative interaction. La_2CuO_4 shows a single negative time-interval while $HgBa_2CuO_4$ shows two. It is most likely a coincidence that $HgBa_2CuO_4$ also has the highest critical temperature when doped (95 K [50] compared to 38 K [51]).

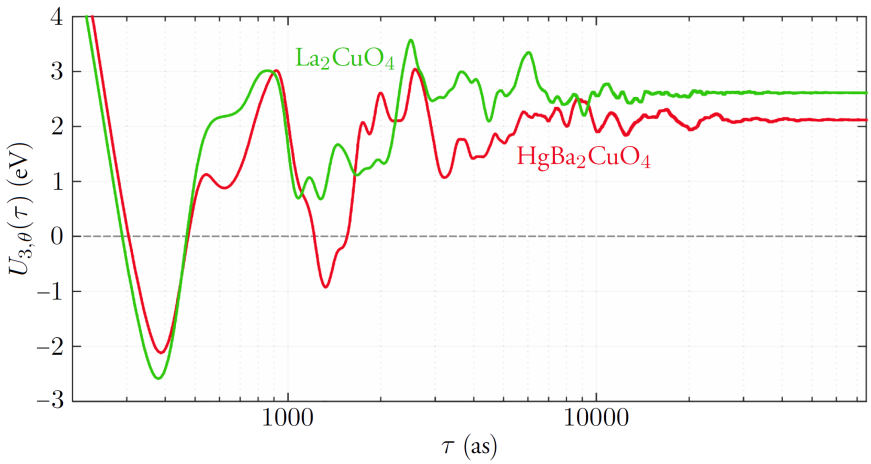

Figure 6.7: $U_{3,\theta}(\tau)$ in La_2CuO_2 and $HgBa_2CuO_4$ with $\mathbf{r}_1$ at copper and $\mathbf{r}_2$ moved a quarter towards oxygen from copper.

7

Correlations in orbital magnetism

This chapter introduces and summarizes Paper II, titled "Influence of correlations on the orbital magnetization of the spin-1/2 Haldane-Hubbard model". The orbital magnetization has been accessible in the mean-field approximation for general solids for less than two decades. In Paper II, the recent extension to correlated electron systems [52] is used to study the effect of charge fluctuations on the orbital magnetization, by applying it to the spin-1/2 Haldane-Hubbard model within the one-shot [1] GW approximation. For a small local repulsion U, the charge fluctuations are shown to boost the orbital magnetization if the staggered potential Δ_{AB} of the model is larger than the nearest-neighbor hopping t_1. This boost stems from interband correlations and occurs for all time-reversal symmetry-breaking phases φ of the next-nearest neighbor hopping t_2.

7.1 Orbital magnetization using the Green's function

The classical orbital magnetic moment for a particle i reads $\boldsymbol{\mu}_i^{\mathrm{orb}} = \frac{q_i}{2c}\mathbf{r}_i \times \mathbf{v}_i$, as follows from Eq. (3.9). In a second quantized description of electrons, the expectation value of Eq. (5.12) can be applied to the total orbital magnetic moment. By dividing by the volume V of the system, the spatially averaged orbital magnetization $\mathbf{M}^{\mathrm{orb}} = \langle \hat{\boldsymbol{\mu}}^{\mathrm{orb}} \rangle / V$ is obtained. Choosing a spin-dependent Wannier basis, then yields

$$\mathbf{M}^{\mathrm{orb}} = \frac{i}{2Vc} \sum_{\mathbf{R}_1 \mathbf{R}_2} \langle \phi^{\sigma}_{\mathbf{R}_1 n_1} | \hat{\mathbf{r}} \times \hat{\mathbf{v}} | \phi^{\sigma}_{\mathbf{R}_2 n_2} \rangle G^{\sigma}_{\mathbf{R}_2 n_2, \mathbf{R}_1 n_1}, \tag{7.1}$$

where $G^{\sigma} = G^{\sigma\sigma}(tt^{+})$. Einstein summation is used only for band and spin indices, n_i and

[1] The one-shot GW approximation is not self-consistent but uses an approximate mean-field G in the self-energy as well as in the polarization used to compute W.

σ. App. D summarizes the derivation [52] for $\mathbf{M}^{\rm orb}$ in periodic insulators with vanishing Chern invariant[2] (defined in Eq. (7.5)), without residing to Hartree's atomic units. It splits into a local part $\mathbf{M}^{\rm L}$ due to self-rotation of the Wannier functions and an itinerant part $\mathbf{M}^{\rm I}$ due to rotation of the Wannier functions around the origin:

$$\mathbf{M}^{\rm L} = \frac{-1}{2c}\int\frac{d\mathbf{k}}{(2\pi)^3}\langle\tilde{\boldsymbol{u}}^{\prime\sigma}_{\mathbf{k}n_1}|\times\Big(\hat{H}_{\mathbf{k}}|\tilde{\boldsymbol{u}}^{\prime\sigma}_{\mathbf{k}n_2}\rangle + \tilde{\epsilon}^{\sigma}_{\mathbf{k}n_3n_2}|\tilde{u}^{\sigma}_{\mathbf{k}n_3}\rangle\nabla_{\mathbf{k}}\Big)G^{\sigma}_{n_2n_1}(\mathbf{k}), \tag{7.2}$$

$$\mathbf{M}^{\rm I} = \frac{-1}{2c}\int\frac{d\mathbf{k}}{(2\pi)^3}\langle\tilde{\boldsymbol{u}}^{\prime\sigma}_{\mathbf{k}n_1}|\times\Big(\delta_{n_1n_4}\tilde{\epsilon}^{\sigma}_{\mathbf{k}n_2n_3}|\tilde{\boldsymbol{u}}^{\prime\sigma}_{\mathbf{k}n_2}\rangle - \delta_{n_1n_2}\tilde{\boldsymbol{\epsilon}}^{\prime\sigma}_{\mathbf{k}n_4n_2}|\tilde{u}^{\sigma}_{\mathbf{k}n_3}\rangle\Big)G^{\sigma}_{n_3n_4}(\mathbf{k}). \tag{7.3}$$

The ingredients are defined in the footnote.[3] Despite that the itinerant contribution is often viewed as a surface property, as in Eq. (3.9), it is expressed solely by bulk quantities in Eq. (7.3). Eqs. (7.2)-(7.3) contain one-body information from $|\tilde{u}^{\sigma}_{\mathbf{k}n}\rangle$ and $\tilde{\epsilon}^{\sigma}_{\mathbf{k}n_1n_2}$ and correlation effects from the Green's function. They can be applied to systems with band crossings since the unitary matrix $S^{\sigma}_{mn}(\mathbf{k})$ ensures that the Bloch states vary smoothly. Without interactions and band crossings, $S^{\sigma}_{mn}(\mathbf{k}) = \delta_{mn}$ and $G^{\sigma}_{n_1n_2}(\mathbf{k}) = in_{\rm F}(\epsilon^{\sigma}_{\mathbf{k}n})\delta_{n_1n_2}$, where $n_{\rm F}$ is the Fermi occupation,[4] and it follows that

$$\mathbf{M}^{\rm orb} = \frac{1}{2c}\int\frac{d\mathbf{k}}{(2\pi)^3}n_{\rm F}(\epsilon^{\sigma}_{\mathbf{k}n})\,{\rm Im}\langle\boldsymbol{u}^{\prime\sigma}_{\mathbf{k}n}|\times(\hat{H}_{\mathbf{k}}+\epsilon^{\sigma}_{\mathbf{k}n})|\boldsymbol{u}^{\prime\sigma}_{\mathbf{k}n}\rangle\,. \tag{7.4}$$

7.2 Heuristic extension to metals and Chern insulators

Eqs. (7.2)-(7.3) can be extended to metals and Chern insulators, like Eq. (7.4) was by Ceresoli *et al.* [53], by introducing a chemical potential μ. $\partial\mathbf{M}^{\rm orb}/\partial\mu = \mathbf{0}$ in a normal insulator at zero temperature, but for Chern insulators with non-zero Chern invariant[5]

$$\mathbf{C} = \frac{1}{2\pi}\int d\mathbf{k}\,n_{\rm F}(\epsilon^{\sigma}_{\mathbf{k}n})\boldsymbol{\Omega}^{\sigma}_{\mathbf{k}n}, \tag{7.5}$$

where $\boldsymbol{\Omega}^{\sigma}_{\mathbf{k}n} = i\langle\boldsymbol{u}^{\prime\sigma}_{\mathbf{k}n}|\times|\boldsymbol{u}^{\prime\sigma}_{\mathbf{k}n}\rangle = -\,{\rm Im}\langle\boldsymbol{u}^{\prime\sigma}_{\mathbf{k}n}|\times|\boldsymbol{u}^{\prime\sigma}_{\mathbf{k}n}\rangle$ is the Berry curvature [54],[6] it should hold that $\partial\mathbf{M}^{\rm orb}/\partial\mu \propto \mathbf{C}$ due to the presence of surface states. With regards to Eq. (7.4), this is achieved by enforcing energy shift invariance by extending it to

$$\mathbf{M}^{\rm orb} = \frac{1}{2c}\int\frac{d\mathbf{k}}{(2\pi)^3}n_{\rm F}(\epsilon^{\sigma}_{\mathbf{k}n})\,{\rm Im}\langle\boldsymbol{u}^{\prime\sigma}_{\mathbf{k}n}|\times(\hat{H}_{\mathbf{k}}+\epsilon^{\sigma}_{\mathbf{k}n}-2\mu)|\boldsymbol{u}^{\prime\sigma}_{\mathbf{k}n}\rangle\,. \tag{7.6}$$

[2] In Chern insulators, the Chern invariant of Eq. (7.5) does not vanish.

[3] $\tilde{u}^{\sigma}_{\mathbf{k}n}$ ($u^{\sigma}_{\mathbf{k}m}$) is the Bloch-periodic part of $\tilde{\psi}^{\sigma}_{\mathbf{k}n}$ ($\psi^{\sigma}_{\mathbf{k}m}$) in Eq. (4.15), $G^{\sigma}_{n_2n_1}(\mathbf{k}) = \sum_{\mathbf{R}}e^{-i\mathbf{k}\cdot\mathbf{R}}G^{\sigma}_{\mathbf{R}n_2,\mathbf{0}n_1}$, $|\tilde{\boldsymbol{u}}^{\prime\sigma}_{\mathbf{k}n}\rangle = |\nabla_{\mathbf{k}}\tilde{u}^{\sigma}_{\mathbf{k}n}\rangle$ and $\tilde{\boldsymbol{\epsilon}}^{\prime\sigma}_{\mathbf{k}n_1n_2} = \nabla_{\mathbf{k}}\tilde{\epsilon}^{\sigma}_{\mathbf{k}n_1n_2}$, where $\tilde{\epsilon}^{\sigma}_{\mathbf{k}n_1n_2} = S^{\sigma\dagger}_{n_1n_3}(\mathbf{k})\epsilon^{\sigma}_{\mathbf{k}n_3}S^{\sigma}_{n_3n_2}(\mathbf{k})$. The eigenvalues $\epsilon^{\sigma}_{\mathbf{k}n}$ fulfil $\hat{H}|\psi^{\sigma}_{\mathbf{k}n}\rangle = \epsilon^{\sigma}_{\mathbf{k}n}|\psi^{\sigma}_{\mathbf{k}n}\rangle$ and $\hat{H}_{\mathbf{k}}|u^{\sigma}_{\mathbf{k}n}\rangle = \epsilon^{\sigma}_{\mathbf{k}n}|u^{\sigma}_{\mathbf{k}n}\rangle$, where $\hat{H}_{\mathbf{k}} = e^{-i\mathbf{k}\cdot\hat{\mathbf{r}}}\hat{H}e^{i\mathbf{k}\cdot\hat{\mathbf{r}}}$.

[4] Since the zero-temperature Green's function is used, $n_{\rm F}(\epsilon_{\mathbf{k}n})$ is 1 (0) for (un-)occupied states.

[5] $\mathbf{C}$ stems from non-conservation of charge and (parallel) momentum on the edge of the system, which is equal and opposite to the bulk non-conservation. $\mathbf{C}$ is thus simultaneously an edge and bulk quantity.

[6] The Berry curvature is a gauge-independent geometric property of the band structure.

The correction from the 2μ-term in Eq. (7.6) can be written as

$$\Delta\mathbf{M}^{\rm orb} = \frac{\mu}{c(2\pi)^2}\mathbf{C}. \tag{7.7}$$

This has been shown [55] to yield the correct linear μ-dependence for Chern insulators. Numerical tests have also confirmed Eq. (7.6) for metals, making it valid for all solids. It constitutes the core of the *modern theory* of orbital magnetization,[7] developed in the early 2000s [56, 57, 53, 12, 58, 55, 59, 60, 61, 62]. This theory drastically outperforms the famous atomic sphere approximation in metals. Chern insulators acquire a non-vanishing $\mathbf{C}$ due to a spontaneously broken time-reversal (T) symmetry, which stems either from magnetic ordering, orbital ordering or both. This is understood from Eq. (7.5), which shows that the crucial quantity is the Berry curvature, which can be written in the "magnetic field form" $\mathbf{\Omega}^\sigma_{\mathbf{k}n} = \nabla_{\mathbf{k}} \times \mathbf{A}^\sigma_{\mathbf{k}n}$, where the vector potential $\mathbf{A}^\sigma_{\mathbf{k}n} = i\langle u^\sigma_{\mathbf{k}n}|\nabla_{\mathbf{k}}|u^\sigma_{\mathbf{k}n}\rangle$ is the gauge-dependent Berry connection.[8] $\mathbf{\Omega}^\downarrow_{-\mathbf{k}n} = -\mathbf{\Omega}^\uparrow_{\mathbf{k}n}$ for T symmetric systems [59], so that $\mathbf{C} = \mathbf{0}$ after integration in Eq. (7.5).

The same argument can be made for interacting many-body systems by replacing $\hat{H}$ by $\hat{H} - \mu$ in the velocity formula of Eq. (D1) in App. D. The extensions of Eqs. (7.2)-(7.3) to general solids then take the form ($\tilde{\xi}^\sigma_{\mathbf{k}n_1n_2} = \tilde{\epsilon}^\sigma_{\mathbf{k}n_1n_2} - \mu\delta_{n_1n_2}$ and $\tilde{\boldsymbol{\xi}}'^\sigma_{\mathbf{k}n_1n_2} = \tilde{\boldsymbol{\epsilon}}'^\sigma_{\mathbf{k}n_1n_2}$)

$$\mathbf{M}^{\rm L} = \frac{-1}{2c}\int\frac{d\mathbf{k}}{(2\pi)^3}\langle\tilde{\boldsymbol{u}}'^\sigma_{\mathbf{k}n_1}|\times\Big((\hat{H}_{\mathbf{k}}-\mu)|\tilde{\boldsymbol{u}}'^\sigma_{\mathbf{k}n_2}\rangle + \tilde{\xi}^\sigma_{\mathbf{k}n_3n_2}|\tilde{u}^\sigma_{\mathbf{k}n_3}\rangle\nabla_{\mathbf{k}}\Big)G^\sigma_{n_2n_1}(\mathbf{k}), \tag{7.8}$$

$$\mathbf{M}^{\rm I} = \frac{-1}{2c}\int\frac{d\mathbf{k}}{(2\pi)^3}\langle\tilde{\boldsymbol{u}}'^\sigma_{\mathbf{k}n_1}|\times\Big(\delta_{n_1n_4}\tilde{\xi}^\sigma_{\mathbf{k}n_2n_3}|\tilde{\boldsymbol{u}}'^\sigma_{\mathbf{k}n_2}\rangle - \delta_{n_1n_2}\tilde{\boldsymbol{\xi}}'^\sigma_{\mathbf{k}n_4n_2}|\tilde{u}^\sigma_{\mathbf{k}n_3}\rangle\Big)G^\sigma_{n_3n_4}(\mathbf{k}). \tag{7.9}$$

7.3 Anomalous Hall effect

The Berry curvature $\mathbf{\Omega}^\sigma_{\mathbf{k}n}$ modifies the wave packet group velocity $\partial\epsilon^\sigma_{\mathbf{k}n}/\partial\mathbf{k}$ by an additional "Luttinger anomalous velocity" $d\mathbf{k}/dt \times \mathbf{\Omega}^\sigma_{\mathbf{k}n}$, which violates Liouville's theorem [59]. In T symmetry breaking systems, the anomalous velocity underlies the intrinsic (scattering-free) quantum anomalous Hall effect (QAHE) [63]. To understand the QAHE, it is imperative to first understand the (classical) anomalous Hall effect (AHE),[9] since the effect of quantum mechanics is merely to yield a discretized Hall conductivity (see Sec. 7.4). A simple classical picture starts by revisiting the Lorentz-Stern-Gerlach force of Eq. (3.4), but boosting it from the material's to the (slowly) moving electron's rest

[7] The modern theory also covers electric polarization due to spontaneously broken inversion symmetry [6].

[8] $\mathbf{\Omega}^\sigma_{\mathbf{k}n}$ and $\mathbf{A}^\sigma_{\mathbf{k}n}$ generalize the magnetic field and vector potential to extended coordinate spaces, and yield the Berry phase — a path-dependent phase contribution accumulated during adiabatic time-evolution. $\mathbf{\Omega}^\sigma_{\mathbf{k}n}$ becomes singular at points of degeneracy.

[9] AHE is used to probe magnetic order in solids, and is more convenient than optical methods.

frame. The boost is obtained by the replacements $\mathbf{E}_i(t) \mapsto \mathbf{E}_i(t) + \frac{1}{c}\mathbf{v}_i(t) \times \mathbf{B}_i(t)$, $\mathbf{B}_i(t) \mapsto \mathbf{B}_i(t) - \frac{1}{c}\mathbf{v}_i(t) \times \mathbf{E}_i(t)$ and $\mathbf{v}_i(t) \mapsto \mathbf{0}$, and results in the force

$$\begin{aligned}\mathbf{F}_i(t) = &-\Big(\mathbf{E}_i(t) + \frac{1}{c}\mathbf{v}_i(t) \times \mathbf{B}_i(t)\Big) + \nabla\Big(\boldsymbol{\mu}_i^{\mathrm{S}}(t) \cdot \mathbf{B}_i(\mathbf{r}, t)\Big)\Big|_{\mathbf{r}=\mathbf{r}_i(t)} \\ &- \frac{1}{c}\nabla\Big(\boldsymbol{\mu}_i^{\mathrm{S}}(t) \cdot \big(\mathbf{v}_i(t) \times \mathbf{E}_i(\mathbf{r}, t)\big)\Big)\Big|_{\mathbf{r}=\mathbf{r}_i(t)}.\end{aligned} \tag{7.10}$$

The Lorentz force alone is not altered by the boost but the Stern-Gerlach force results in the spin-orbit force in the second line,[10] which sets in if the magnetic moment is not in the plane spanned by the velocity and the electric field, provided that the latter varies at the position of electron i. The ordinary Hall effect (OHE) originates from the Lorentz force terms in Eq. (7.10), due to a constant external magnetic field $\mathbf{B}_i^{\mathrm{ext}}(t) = \mathbf{H}$ and average driven current density $\langle \mathbf{J}(t) \rangle = -n\langle \mathbf{v}(t) \rangle = -\frac{n}{N}\sum_i \mathbf{v}_i(t)$ (n: average electron density). Adding a Drude relaxation term $\frac{1}{n\tau}\langle \mathbf{J}(t) \rangle$ to the average Lorentz force, where τ is the relaxation time, results in the steady-state condition

$$\text{OHE}: \qquad \langle \mathbf{P} \rangle = -\frac{1}{4\pi n\tau}\langle \mathbf{J} \rangle + \frac{1}{4\pi nc}\langle \mathbf{J} \rangle \times \mathbf{H}, \tag{7.11}$$

where $\langle \mathbf{P} \rangle$ is the average electric polarization, with a component perpendicular to $\langle \mathbf{J} \rangle$ and $\mathbf{H}$. In the AHE, $\mathbf{H}$ is replaced by 4π times the spontaneous magnetization $\langle \mathbf{M} \rangle$, so that[11]

$$\text{AHE}: \qquad \langle \mathbf{P} \rangle = -\frac{1}{4\pi n\tau}\langle \mathbf{J} \rangle + \frac{1}{nc}\langle \mathbf{J} \rangle \times \langle \mathbf{M} \rangle. \tag{7.12}$$

The usual definition of AHE requires that $\langle \mathbf{J} \rangle$, $\langle \mathbf{M} \rangle$ and $\langle \mathbf{P} \rangle$ are established without external fields. To get a finite $\langle \mathbf{M} \rangle$, the magnetic moments have to correlate due to dipole-dipole or exchange interaction. The spin-orbit force term in Eq. (7.10) correlates the velocity and magnetic moment of an electron, but if different magnetic moments correlate, different velocities correlate too. This 'spin Hall effect' (SHE) is needed to get a spontaneous current density $\langle \mathbf{J} \rangle$ in Eq. (7.12).[12] All terms in Eq. (7.10) are thus required to obtain a finite AHE, which relies on the SHE. However, Eq. (7.12) is generally incomplete, since it does not include the Stern-Gerlach and spin-orbit force terms in steady state.

7.4 The Haldane-Hubbard model

The QAHE is important in two-dimensional systems, say in the xy plane, with Berry curvature along the z-axis . The Chern invariant of Eq. (7.5) then reads $\mathbf{C} = C\mathbf{e}_z$, where

[10] Despite being derived in the electron's rest frame, Eq. (7.10) will be assumed to hold also in the material's rest frame. Under this assumption, the total force in Eq. (7.10) is not altered by the boost.

[11] More generally, $\langle \mathbf{J} \rangle \times \langle \mathbf{M} \rangle$ is replaced by $\langle \mathbf{J} \times \mathbf{M} \rangle$, as is important in frustrated spin liquids, where AHE can exist without a macroscopic magnetization $\langle \mathbf{M} \rangle$ [64].

[12] SHE does not require T symmetry breaking, contrary to AHE.

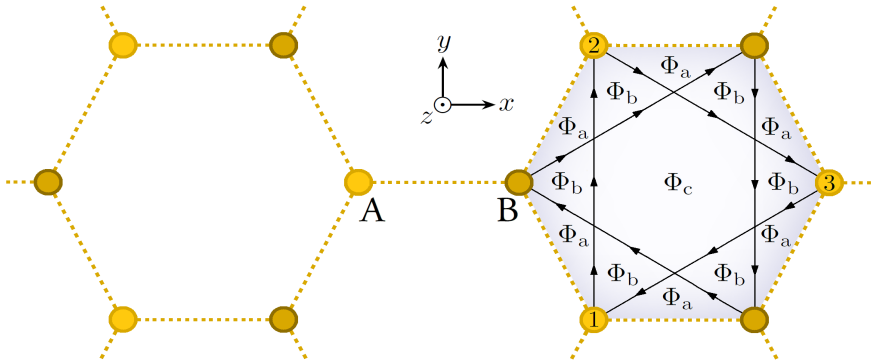

Figure 7.1: The Haldane (honeycomb) lattice, where sublattice A (B) is shown in gold (bronze) and fluxes (Φ_a, Φ_b and Φ_c) are indicated for different regions of a Wigner-Seitz unit cell. The arrows between next-nearest neighbors indicate the hopping direction with positive phase accumulation due to the broken T symmetry.

$\mathbf{e}_z$ is the z-axis unit vector and C the Chern number (integer). C counts the magnetic vortices in the Brillouin zone, and the quantum anomalous Hall conductivity equals the von Klitzing constant $1/2\pi$ times C. The difference ΔC between two adjacent materials is the number of gapless chiral edge states propagating on their shared boundary.

The Haldane model [65] is the simplest model of QAHE, where T symmetry is broken due to a periodic magnetic field $\mathbf{B}(\mathbf{r})$, albeit without a net magnetic flux in the unit cell, allowing for a periodic gauge[13] and the use of Bloch functions. The model is a generalization of graphene and consists of a honeycomb lattice with hexagonal Wigner-Seitz unit cells, depicted in Fig. 7.1, with two sublattices A and B. Since the unit cell, with vanishing magnetic flux, can be enclosed by repeated nearest-neighbor (NN) hoppings, the NN hopping integral t_1 can be chosen as real-valued. However, the next-nearest-neighbor (NNN) hopping cannot. To see this, it is helpful to define (for sublattice A and similarly for sublattice B) the NNN hopping integral $t_{12} = |t_{12}|e^{i\phi_{\alpha\beta}}$ between atoms 1 and 2 in Fig. 7.1, and similarly t_{23} and t_{31}, all with magnitudes t_2. With S denoting the triangular surface enclosed by the path $1 \to 2 \to 3 \to 1$, it follows from the Aharonov-Bohm effect that

$$t_{12}t_{23}t_{31} = (t_2)^3 e^{i(\phi_{12}+\phi_{23}+\phi_{31})} = (t_2)^3 e^{-\frac{i}{c}\iint_S dS\hat{\mathbf{n}}\cdot\mathbf{B}(\mathbf{r})}, \tag{7.13}$$

where the unit normal vector $\hat{\mathbf{n}} = -\mathbf{e}_z$ due to the right-hand rule. As pointed out by Haldane [65], the physical origin of the magnetic field can be the presence of magnetic moments in the z direction located at the centres of the hexagonal Wigner-Seitz unit cells. While each hopping phase is gauge-dependent, the total accumulated (Berry) phase in Eq. (7.13) is not. If the latter is denoted as 3ϕ, the simplest gauge choice is to choose the phase ϕ for each hopping, so that $t_{12} = t_{23} = t_{31} = t_2 e^{i\phi}$. If the path is reversed, the normal vector and thus the phase flips, which results in complex conjugated hopping integrals. The total magnetic flux through S is $\Phi = 6\Phi_a + 3\Phi_b$, as verified from Fig. 7.1, in terms

[13] In the periodic gauge, both the scalar potential and the vector potential are lattice-periodic.

of which the total phase reads $3\phi = \Phi/c$, which implies that $\phi = (2\Phi_\mathrm{a} + \Phi_\mathrm{b})/c$. In the half-filled spin-1/2 Haldane model, each unit cell (which contains two sites, A and B) has two electrons. The magnetic field $\mathbf{B}(\mathbf{r})$ generally leads to Zeeman splitting between the spin-up and -down states, but this effect is neglected here and magnetically unpolarized electrons are assumed. This is possible despite a non-zero NNN hopping phase ϕ, since the latter depends on $\mathbf{B}(\mathbf{r})$ in the entire region S whereas the Zeeman effect depends on it only where the electronic orbitals have a high amplitude.[14] Having laid the groundwork for the spin-1/2 Haldane model, the Hamiltonian can be written down. It reads

$$\hat{H}_\mathrm{H} = t_1 \sum_\sigma \sum_{\langle ij \rangle} \hat{c}^\dagger_{i\sigma} \hat{c}_{j\sigma} + t_2 \sum_\sigma \sum_{\langle\langle ij \rangle\rangle} e^{i\phi_{ij}} \hat{c}^\dagger_{i\sigma} \hat{c}_{j\sigma} + \Delta_\mathrm{AB} \sum_\sigma \sum_i \xi_i \hat{c}^\dagger_{i\sigma} \hat{c}_{i\sigma}, \tag{7.14}$$

where $\langle ij \rangle$ ($\langle\langle ij \rangle\rangle$) restricts the summation to NN (NNN) sites, $\phi_{ij} = \phi\,(-\phi)$ for hoppings parallel (anti-parallel) to the arrows in Fig. 7.1 and $\Delta_\mathrm{AB}\xi_i$, where $\xi_{i\in\mathrm{A}} = 1$ and $\xi_{i\in\mathrm{B}} = -1$, is an inversion symmetry-breaking staggered potential present if sublattices A and B contain different atoms. For small t_2, a mass-less Dirac semimetal is obtained if $\Delta_\mathrm{AB} = 0$ and $\phi = 0 \pmod{\pi}$, a normal insulator with $C = 0$ if $\Delta_\mathrm{AB} \neq 0$ and $\phi = 0 \pmod{\pi}$ and a Chern insulator with $C = 1$ (per spin channel) if $\Delta_\mathrm{AB} = 0$ and $\phi \neq 0 \pmod{\pi}$. The Haldane-Hubbard model extends the model to correlated electrons [66, 67] . If the important Coulomb integrals are the (site-independent) on-site and NN interactions U and U', Eq. (7.14) extends to (with $\hat{n}_{i\sigma} = \hat{c}^\dagger_{i\sigma}\hat{c}_{i\sigma}$)

$$\hat{H}_\mathrm{HH} = \hat{H}_\mathrm{H} + U \sum_i \hat{n}_{i\uparrow}\hat{n}_{i\downarrow} + \frac{U'}{2} \sum_{\sigma_1\sigma_2} \sum_{\langle ij \rangle} \hat{n}_{i\sigma_1}\hat{n}_{j\sigma_2}. \tag{7.15}$$

[14] This most likely requires more than one background magnetic moment per unit cell, to cancel out $\mathbf{B}(\mathbf{r})$ in the electronic orbitals. An alternative, not considered here, is to assume that the electrons are fully spin polarized, which results in the spinless version of the model.

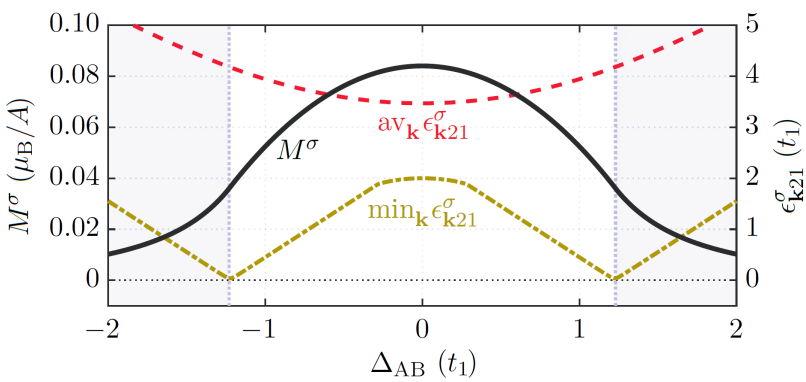

Figure 7.2: Orbital magnetization M^σ (black) for the non-interacting Haldane model with $t_1 = E_\mathrm{h}$, $t_2 = t_1/3$ and $\phi = \pi/4$ as a function of staggered potential Δ_AB, with average and minimum band splittings (red and gold) included for comparison. White background: $C = 2$. Lavender background: $C = 0$.

7.5 Results: Orbital magnetization with GW correlations

The orbital magnetization $\mathbf{M}^{\rm orb} = M^{\rm orb}\mathbf{e}_z$ (Eqs. (7.8)-(7.9)) is computed for the half-filled Haldane-Hubbard model (Eq. 7.15), with the G computed within the GW and Hartree approximations, i.e. with and without exchange and correlations due to electronic charge fluctuations. The GW self-energy (Eq. (5.32)) is computed at the one-shot level from a self-consistent Hartree reference,[15] as is customary but leads to spin-unpolarized solutions. Since GW self-consistency is avoided, also the Hamiltonian $\hat{H}^\sigma_{\mathbf{k}}$ used in Eqs. (7.8)-(7.9) is computed in the Hartree approximation. Future topics involve the study of the spin-polarized and spinless (fully polarized) cases as well as the extension to the self-consistent GW approximation, where not only G is self-consistent but where also the 2×2 Hamiltonian in Eqs. (7.8)-(7.9) reads $\hat{H}^\sigma_{\mathbf{k}} = -G^\sigma(\mathbf{k},\omega=0)^{-1}$. The spin-unpolarized treatment of this work implies that $M^{\rm orb}$ gets equal contributions $M^\sigma = M^{\rm orb}/2$ from spin $\uparrow$ and $\downarrow$. The same holds for C, which thus equals 0 or 2 (1 requires spin polarization). $S^\sigma_{mn}(\mathbf{k})$ is reduced to δ_{mn} since the employed $\mathbf{k}\cdot\mathbf{p}$ perturbation formula [68]

$$|\boldsymbol{u}'^\sigma_{\mathbf{k}n_1}\rangle = \sum_{n_2\neq n_1} \frac{|u^\sigma_{\mathbf{k}n_2}\rangle\langle u^\sigma_{\mathbf{k}n_2}|\nabla_{\mathbf{k}}\hat{H}_{\mathbf{k}}|u^\sigma_{\mathbf{k}n_1}\rangle}{\epsilon^\sigma_{\mathbf{k}n_1}-\epsilon^\sigma_{\mathbf{k}n_2}} \tag{7.16}$$

requires no smooth gauge, as is convenient since diagonalizing $\hat{H}^\sigma_{\mathbf{k}}$ yields random phases for each $\mathbf{k}$. G is computed with a small numerical temperature ($k_{\rm B}T = 0.025t_1$) using the Matsubara formalism [22] and the one-shot GW calculation includes a shift of μ needed to conserve the electron number. The plots for M^σ below also specify C and the average and minimum band splittings, $\mathrm{av}_{\mathbf{k}}\{\epsilon^\sigma_{\mathbf{k}21}\}$ and $\min_{\mathbf{k}}\{\epsilon^\sigma_{\mathbf{k}21}\}$ (the direct gap). In the GW approximation, these splittings are obtained from the eigenvalues of $-G^\sigma(\mathbf{k},\omega=0)^{-1}$, mentioned above. Computational details are found in Paper II.

The dependence of M^σ on $\Delta_{\rm AB}$ in the absence of interactions is presented in Fig. 7.2 for the values $t_1 = E_{\rm h}$ (Hartree energy unit), $t_2 = t_1/3$ and $\phi = \pi/4$ of the seminal paper by Thonhauser *et al.* of Ref. [56], in units of $\mu_{\rm B}/A$, where $\mu_{\rm B} = 1/2c$ is the Bohr magneton and A the unit cell area. The monotonic decrease of M^σ with $|\Delta_{\rm AB}|$ is understood by the increase of $\mathrm{av}_{\mathbf{k}}\{\epsilon^\sigma_{\mathbf{k}21}\}$ caused by the latter. More specifically, inserting Eq. (7.16) into Eq. (7.6) shows that M^σ picks up a factor of $(\epsilon^\sigma_{\mathbf{k}21})^{-2}$ for each $\mathbf{k}$. If $\min_{\mathbf{k}}\{\epsilon^\sigma_{\mathbf{k}21}\}$ is not too small, this factor can roughly be approximated by $(\mathrm{av}_{\mathbf{k}}\{\epsilon^\sigma_{\mathbf{k}21}\})^{-2}$. The reciprocal relationship between M^σ and $\mathrm{av}_{\mathbf{k}}\{\epsilon^\sigma_{\mathbf{k}21}\}$ is evident from Fig. 7.2. The system is a Chern insulator with $C=2$ below $\Delta_{\rm AB}\approx 1.2t_1$, but a normal insulator above this value. When crossing the transition, the gap $\min_{\mathbf{k}}\{\epsilon^\sigma_{\mathbf{k}21}\}$ is closed and reopened, yielding a semimetal at the transition point, as expected. The value of M^σ at $\Delta_{\rm AB} = 2t_1$ agrees with Ref. [56].

[15] An erratum to Paper II is to be published. The results are correct but based on a Hartree rather than Hartree-Fock reference, as stated in the paper. It also states that the intersite exchange potential vanishes, which is incorrect but not assumed in the code. A Hartree-Fock reference yields spin ordering for large U [66].

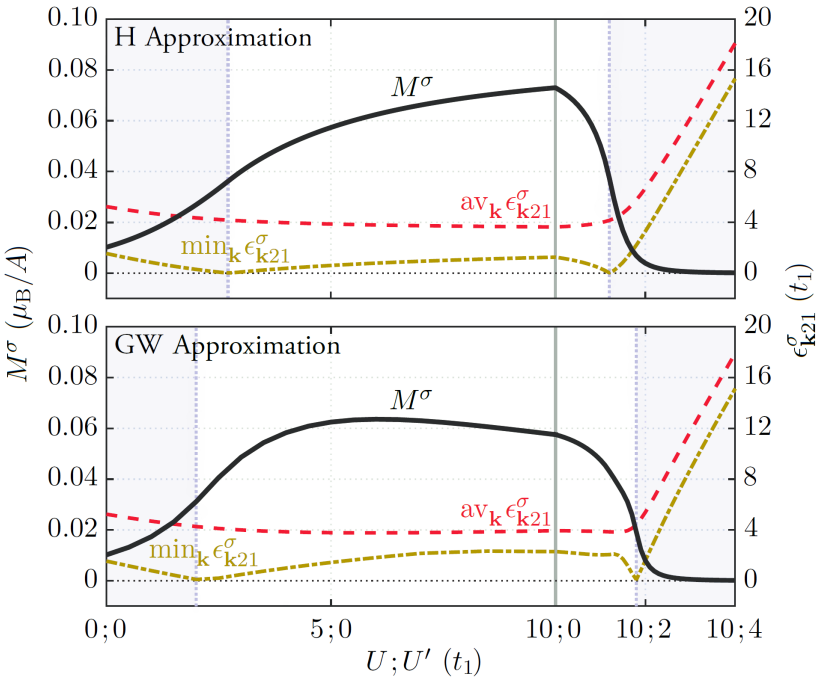

Figure 7.3: Orbital magnetization M^σ (black) for the spin-1/2 Haldane-Hubbard model with $t_1 = E_\mathrm{h}$, $t_2 = t_1/3$, $\Delta_\mathrm{AB} = 2t_1$ and $\phi = \pi/4$ as a function of on-site and intersite interactions U and U', with average and minimum band splittings (red and gold) included for comparison. White background: $C = 2$. Lavender background: $C = 0$. Top: Hartree approximation. Bottom: GW approximation.

The Hartree and GW approximations for M^σ are compared in Fig. 7.3 for different U and U' of the spin-1/2 Haldane-Hubbard model (Eq. (7.15)), with $\Delta_\mathrm{AB} = 2t_1$. In the Hartree approximation, U counteracts Δ_AB, which is observed through the reduction of $\mathrm{av}_\mathbf{k}\{\epsilon^\sigma_{\mathbf{k}21}\}$. M^σ thus increases with U and approaches its value for $\Delta_\mathrm{AB} = 0$ in Fig. 7.2. U' has the opposite effect. Charge fluctuations contained in the GW approximation are seen to boost M^σ additionally. This boost, however, has nothing to do with the splitting $\mathrm{av}_\mathbf{k}\{\epsilon^\sigma_{\mathbf{k}21}\}$, which essentially is the same as in the Hartree approximation. Instead, the boost is attributed to the two terms of Eqs. (7.8)-(7.9) that vanish in the mean field and are switched on by interband correlations.

Fig. 7.4 presents the analogous results for $\Delta_\mathrm{AB} = 0$. The U-independence of M^σ in the Hartree approximation is a consequence of the electrons already being delocalized at $U = 0$. On the other hand, increasing U' beyond a certain threshold has a localizing effect and leads to charge segregation. All electrons end up on one of the sublattices, which breaks the inversion symmetry of the $U' = 0$ solution. An effective Δ_AB is thus generated, which drastically reduces M^σ. Contrary to the findings for $\Delta_\mathrm{AB} = 2t_1$, the additional charge fluctuations of the GW approximation are seen to reduce M^σ. The reason for this is a suppression of the interband correlations when $\Delta_\mathrm{AB} = 0$, which previously were shown

to boost M^σ. Instead, the important effect is the reduction of the band splitting due to intraband correlations, which from the arguments made earlier leads to a reduced M^σ. A general finding common to Figs. 7.2-7.4 is that M^σ typically is large in the Chern insulating phase and small in the normal insulating phase. Paper II contains figures not included here, including a plot that presents the change of M^σ due to charge fluctuations in the plane of U and Δ_{AB}, for $U' = 0$. For small U it is found that a boost occurs essentially for $\Delta_{\mathrm{AB}} > t_1$, i.e. if the staggered potential dominates the nearest-neighbor hopping. For large U, boost occurs essentially if $\Delta_{\mathrm{AB}} > U/3$.

As a final result, the dependence of M^σ on the complex hopping phase φ is shown in Fig. 7.5 for the non-interacting system as well as the on-site interacting system with $U = 5t_1$, within both the Hartree and the GW approximation. The staggered potential $\Delta_{\mathrm{AB}} = 2t_1$ is used. The non-interacting results agree with Ref. [56]. Apart from the rescaling of M^σ due to U, the overall shapes of all three curves are very similar. Importantly, the maximum is still close to $\varphi = \pi/4$, as in the non-interacting system.

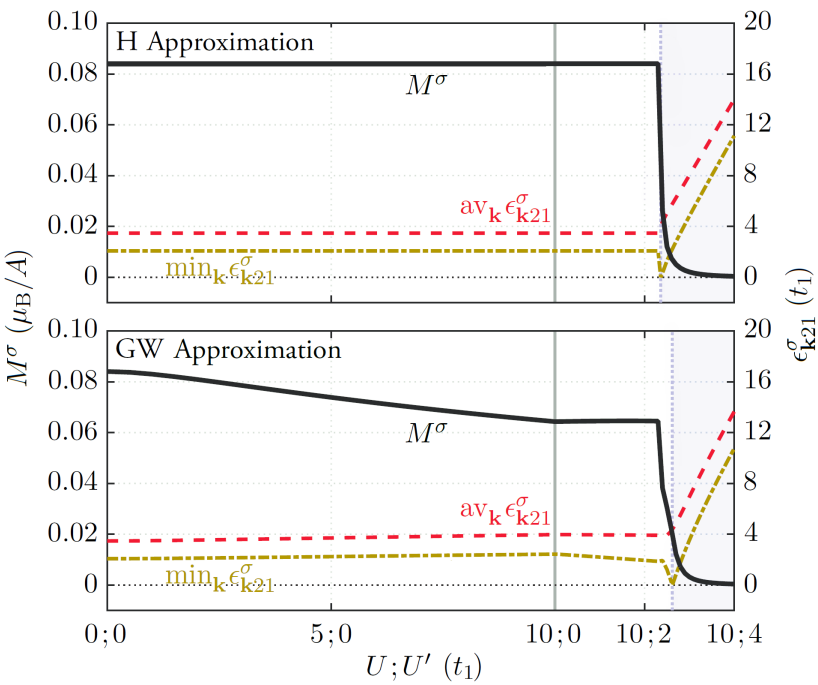

Figure 7.4: Orbital magnetization M^σ (black) for the spin-1/2 Haldane-Hubbard model with $t_1 = E_{\mathrm{h}}$, $t_2 = t_1/3$, $\Delta_{\mathrm{AB}} = 0$ and $\phi = \pi/4$ as a function of on-site and intersite interactions U and U', with average and minimum band splittings (red and gold) included for comparison. White background: $C = 2$. Lavender background: $C = 0$. Top: Hartree approximation. Bottom: GW approximation.

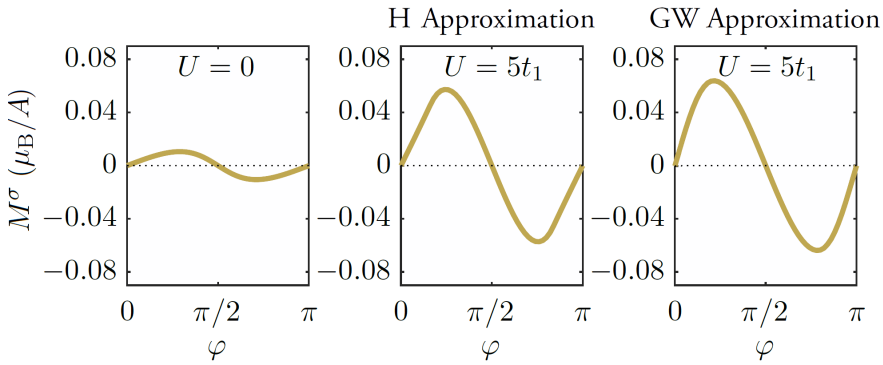

Figure 7.5: Orbital magnetization M^σ for the spin-1/2 Haldane-Hubbard model with $t_1 = E_\mathrm{h}$, $t_2 = t_1/3$ and $\Delta_\mathrm{AB} = 2t_1$ for vanishing U (left) and $U = 5\,t_1$ in the Hartree approximation (middle) and GW approximation (right).

8

Ab initio exchange-mediated magnon-phonon interaction

This chapter introduces and summarizes Paper III, titled "Magnon-phonon interaction and the underlying role of the Pauli exclusion principle". The magnon-phonon interaction $\mathcal{A}$ is crucial in many solid-state devices and technologies. It enters spin caloritronics since it affects the interplay between heat and spin currents [69] and acoustic spintronics since it can be used for spin pumping [70, 71]. It also yields phononic spin [72, 73, 74] and a mechanism for the thermal Hall effect [75]. The non-relativistic exchange contribution is less understood than the spin-orbit contribution and therefore derived in Paper III from the underlying electronic structure. First, the finite-temperature interaction Δ between reference (Hartree-Fock) magnons is derived by utilizing the Fierz ambiguity and Schwinger's functional derivative method. After a Hubbard approximation, Δ is iterated, contracted to a two-point quantity and extended to account for phonons. The result indirectly yields a microscopic formula for $\mathcal{A}$ and is applied to a three-dimensional model with isotropic magnon dispersion and a dispersion-free optical phonon. Increasing $\mathcal{A}$ from zero induces a magnon band splitting at finite temperatures by phonon absorption, which increases the low-energy magnon density of states and thus decreases the Curie temperature.

8.1 Independent magnons and phonons

As discussed in Sec. 5.5, the dynamical information contained in the linear spin-density response $R^{\mu\nu}$ of Eq. (5.34) can be used to find the collective charge and spin excitation spectra of the electrons in a solid. The collectivity stems from the pairwise interaction between the electrons. For the spin part of the response, the dominant interaction is the

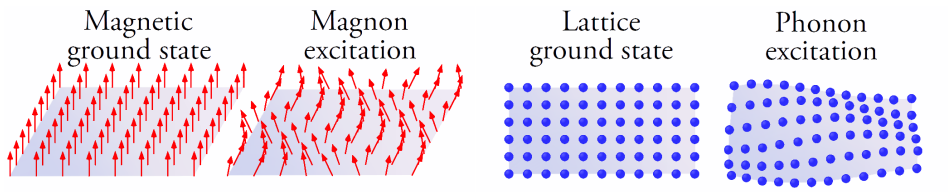

Figure 8.1: Simple illustration in two dimensions of how a magnetic ground state is altered by a magnon excitation (left) and how a lattice ground state is altered by a phonon excitation (right).

exchange interaction, which stems from the Coulomb interaction and the Pauli exclusion principle of electrons. The transverse components R^{+-} and R^{-+}, where $\sigma^+ = \sigma^x + i\sigma^y$ and $\sigma^- = \sigma^x - i\sigma^y$, describe right- and left-handed circularly polarized magnons, i.e. quantized spin waves. The focus here is on right-handed magnons, which reduce the total spin of the system by 1.[1] These are bosonic low-energy spin excitations in (z-axis) ferromagnets [76, 77, 78], antiferromagnets [79], ferrimagnets [80], multiferroics [81, 82] and in more complicated set-ups, such as magnetic nano devices, and play a key role in spintronics. From Eqs. (5.33)-(5.34), it follows that the right-handed spin response reads

$$R^{+-}_{ijkl}(t_1t_2) = 4R^{\Uparrow\Uparrow}_{ijkl}(t_1t_2) = 4\mathcal{R}^{\Uparrow\Uparrow}_{ijkl}(t_1t_1^+t_2t_2), \tag{8.1}$$

The left panel of Fig. 8.1 depicts a magnon mode in a two-dimensional ferromagnet. Similarly, a two-dimensional phonon mode is depicted in the right panel. Phonons, which were discussed in Sec. 5.7, are bosonic quasiparticles that describe low-energy lattice excitations, i.e. quantized lattice vibrations, and acquire their collectivity from the Coulomb interaction between the ions. In addition to magnons and phonons, the most important bosonic quasiparticles are plasmons, contained in R^{00}, which describe electronic charge fluctuations and acquire their collectivity from the Coulomb interaction between electrons.

8.2 Deriving the magnon-phonon interaction

Magnons, phonons and plasmons are in general interdependent, but since plasmon energies are typically higher than that of magnons and phonons, it often suffices to study the magnetoelastic excitations steeming exclusively from the interplay between magnons and phonons, as can be imagined from Fig. 8.1 as a situation where the spin solid angles correlate with the lattice displacements. More specifically, reference magnons and phonons are initially computed separately, followed by the inclusion of a magnon-phonon interaction between the two. This approach is suitable if the interaction is sufficiently weak. The magnon-phonon interaction has two origins: the spin-orbit interaction [83, 84] and the exchange interaction [85]. The former, which leads to magnon-phonon interconversion[2]

[1] Left-handed and right-handed magnons are connected by the relation $R^{-+}_{ijkl}(t_1t_2) = R^{+-}_{lkji}(t_2t_1)$.

[2] Magnon-phonon interconversion means that magnons can propagate into phonons, and vice versa.

and avoided crossing between the magnon and phonon spectra, enters through a relativistic extension of the random-phase approximation, and is thus well-understood. Less understood is the latter, which forbids magnon-phonon interconversion (i.e. conserves the magnon number) due to the non-relativistic spin conservation requirement and stems from the dependence of the exchange interaction between two spins on their positions relative to the background lattice, and thus on lattice vibrations. The main goal of Paper III is to derive this contribution from the underlying electronic structure. A good starting point is to consider the well-known [86] form for the phonon-induced magnon-magnon interaction in a model with a single magnon and phonon band. Its Fourier space expression is[3]

$$\Delta^{\Uparrow\Uparrow}(\mathbf{k},\omega)=\int\frac{d\mathbf{q}}{\Omega_{\mathrm{BZ}}}\left|\mathcal{A}_{\mathbf{q}}\right|^2\left(\frac{n^{\mathrm{P}}_{\mathbf{q}}-n^{\mathrm{M}}_{\mathbf{k}-\mathbf{q}}}{\omega+\omega^{\mathrm{P}}_{\mathbf{q}}-\omega^{\mathrm{M}}_{\mathbf{k}-\mathbf{q}}+i\eta}+\frac{1+n^{\mathrm{P}}_{\mathbf{q}}+n^{\mathrm{M}}_{\mathbf{k}-\mathbf{q}}}{\omega-\omega^{\mathrm{P}}_{\mathbf{q}}-\omega^{\mathrm{M}}_{\mathbf{k}-\mathbf{q}}+i\eta}\right),\tag{8.2}$$

where $\omega^{\mathrm{P}}_{\mathbf{q}}$ is the phonon dispersion, $\omega^{\mathrm{M}}_{\mathbf{q}}$ the magnon dispersion and $n^{\mathrm{P}}_{\mathbf{q}}$ and $n^{\mathrm{M}}_{\mathbf{q}}$ the associated Bose occupations. Most importantly, $\mathcal{A}_{\mathbf{q}}$ is the exchange-mediated magnon-phonon interaction, which enters to second order. The goal is thus to derive Eq. (8.2) using the Green's function formalism of Chap. 5, and by doing so also to derive the magnon-phonon interaction $\mathcal{A}_{\mathbf{q}}$. If the reference magnons are obtained from the Hartree-Fock interaction (see Eqs. (5.39)-(5.40)), the starting point of the derivation is the magnon-magnon component of the four-point interaction Δ of Eq. (5.41), namely

$$\Delta^{\Uparrow\Uparrow}_{ijkl}(t_1t_2t_3t_4)=i\frac{\delta\Sigma^{\mathrm{c}\Uparrow}_{ij}(t_1t_2)}{\delta G^{\Uparrow}_{kl}(t_3t_4)},\tag{8.3}$$

where Σ^{c} is the correlation part of Eq. (5.25). By expressing Δ in terms of the screened interaction W of Eq. (5.30), phonons can be accounted for at the end by deforming W as in Eq. (5.45). While details are found in Paper III, the derivation involves the steps:

1. Since magnons and phonons are excited thermally, the zero-temperature formalism is replaced by a finite-temperature formalism, where the Hamiltonian $\hat{H}_0$ of Eq. (5.1) is replaced by the grand canonical Hamiltonian $\hat{H}_0-\mu\hat{N}$ ($\hat{N}$: number operator) and the real-time G by the imaginary-time Green's function $\mathcal{G}$.

2. The Fierz ambiguity of Sec. 4.5 is utilized to turn the Coulomb interaction into the crossing symmetric spin-dependent interaction of Eq. (4.26), schematically denoted by v below. Crossing symmetry is important in order to treat charge and spin on equal footing, as shows to be essential to derive the magnon-phonon interaction.

3. Σ^{c} is expressed in terms of a crossing-symmetric four-point generalization of W, denoted by $\mathcal{W}$. Schematically, $\Sigma^{\mathrm{c}}=-v\mathcal{G}^3\mathcal{W}$ where $\mathcal{W}=\mathcal{V}+\mathcal{V}\mathcal{P}\mathcal{W}$, $\mathcal{V}=\delta M/\delta\mathcal{G}$ and $\mathcal{P}=\mathcal{G}\mathcal{G}$. M is the finite-temperature extension of the mass operator $M=V^{\mathrm{HF}}+\Sigma^{\mathrm{c}}$. Factors of i are lacking due to the finite-temperature formalism.

[3]Term one (two) describes phonon absorption (emission). In the $T\to 0$ limit, only the emission survives.

4. This step is included for simplicity and can be skipped. v is assumed to be diagonal in the Wannier basis $i = (\mathbf{R}, n)$ to mimic the short-range interaction in a low-energy model. Mathematically, this means taking[4]

$$v_{ijkl}^{\sigma_1\sigma_2\sigma_3\sigma_4} = \frac{U_i}{2}(\delta_{\sigma_1\sigma_2}\delta_{\sigma_3\sigma_4} - \delta_{\sigma_1\sigma_3}\delta_{\sigma_2\sigma_4})\delta_{ij}\delta_{jk}\delta_{kl}. \tag{8.4}$$

5. The magnon-magnon interaction $\delta\Sigma^{\mathrm{c}\downarrow\uparrow}/\delta\mathcal{G}^{\downarrow\uparrow}$ acquires three categories of terms containing $\mathcal{W}^{\uparrow\uparrow\uparrow\uparrow}$, $\mathcal{W}^{\downarrow\uparrow\downarrow\uparrow}$ and $\delta\mathcal{W}^{\downarrow\uparrow\uparrow\uparrow}/\delta\mathcal{G}^{\downarrow\uparrow}$, respectively. With $\mathcal{W} = \mathcal{V} + \mathcal{W}^{\mathrm{c}}$ ($\mathcal{W}^{\mathrm{c}} = \mathcal{V}\mathcal{P}\mathcal{W}$), $\mathcal{V}$ is replaced by the Hartree-Fock interaction (2$\times$Eq. (8.4)) and $\mathcal{W}^{\mathrm{c}}$ by

$$\mathcal{W}^{\mathrm{c}}{}_{ijkl}^{\sigma_1\sigma_2\sigma_3\sigma_4} = \delta_{ij}\delta_{kl}W_{\mathrm{c}}{}_{ik}^{\sigma_1\sigma_2\sigma_3\sigma_4} - \delta_{ik}\delta_{jl}W_{\mathrm{c}}{}_{ij}^{\sigma_1\sigma_3\sigma_2\sigma_4}, \tag{8.5}$$

where $W_{\mathrm{c}} = 2vR_{\mathrm{HF}}2v$ and R_{HF} is the Hartree-Fock two-point spin-density response. Using crossing symmetry, the (second) exchange term is written as a spin-permuted direct term. Particle-particle contractions of $\mathcal{P}$ are neglected.

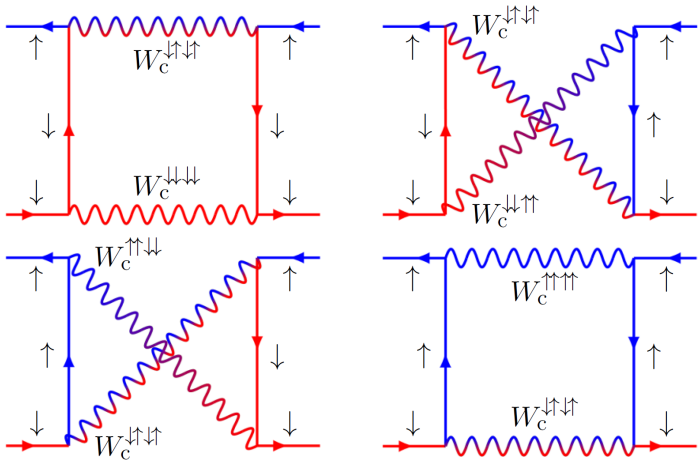

Figure 8.2: The four terms in the four-point magnon-magnon interaction $\Delta^{\downarrow\uparrow\downarrow\uparrow}$ amenable to phonons in such a way as to lead to Eq. (8.2). Green's function arrows point from the first to second time argument.

6. The resulting four-point magnon-magnon interaction $\Delta^{\downarrow\uparrow\downarrow\uparrow}$ is contracted to a two-point direct (i.e. 'bubble-bubble') interaction. This involves imaginary time integration of $\mathcal{G}$, for which an accurate yet simple approximation is proposed (details in Paper III). Out of the three categories of terms in $\Delta^{\downarrow\uparrow\downarrow\uparrow}$, only that containing $\delta\mathcal{W}^{\downarrow\uparrow\uparrow\uparrow}/\delta\mathcal{G}^{\downarrow\uparrow}$ (which is comprised of the the four terms depicted in Fig. 8.2) retains spatiotemporal dispersion effects after contraction. The others (which include the screened T matrix [87]) reduce to point interactions and are dropped since they can be absorbed in a parameter used to enforce the Goldstone criterion for the magnons.[5]

[4]Here and in Eq. (8.5), the time variable is absorbed in the orbital index.

[5]The Goldstone criterion requires that the magnon energy vanishes in the long-wavelength limit.

In a 1-band model, the band index drops out and (the finite-temperature extension [22] of) Eq. (5.38) for the renormalized magnons reduces to[6]

$$R^{\Uparrow\Uparrow}(\mathbf{k}, i\omega_m) = \frac{R^{\Uparrow\Uparrow}_{\mathrm{HF}}(\mathbf{k}, i\omega_m)}{1 - R^{\Uparrow\Uparrow}_{\mathrm{HF}}(\mathbf{k}, i\omega_m)\Delta^{\Uparrow\Uparrow}(\mathbf{k}, i\omega_m)}, \tag{8.6}$$

$$\Delta^{\Uparrow\Uparrow}(\mathbf{k}, i\omega_m) = -\frac{1}{N\beta}\sum_{\mathbf{q}\omega_n}\sum_{\sigma_1\sigma_2} \overline{\mathcal{G}}^{\sigma_1}\overline{\mathcal{G}}^{\sigma_2} W_{\mathrm{c}}^{\Uparrow\Uparrow}(\mathbf{k}-\mathbf{q}, i\omega_m - i\omega_n) \times W_{\mathrm{c}}^{\sigma_1\sigma_1\sigma_2\sigma_2}(\mathbf{q}, i\omega_n), \tag{8.7}$$

in Fourier space, where $\omega_m = 2\pi m/\beta$ (with $m \in \mathbb{Z}$) are bosonic Matsubara freqiencies and $\beta = 1/k_{\mathrm{B}}T$ is the thermodynamic beta. With mean-field [88] electronic dispersion (Fermi occupation) $\epsilon^\sigma_{\mathbf{k}}$ ($n^\sigma_{\mathbf{k}}$), the approximate contraction of $\mathcal{G}$ reads

$$\overline{\mathcal{G}}^\sigma = \frac{1}{N}\sum_{\mathbf{k}} \frac{n^\sigma_{\mathbf{k}} - 1/2}{|\epsilon^\sigma_{\mathbf{k}} - \mu|}. \tag{8.8}$$

7. The spin-conserving part of W_{c} in Eq. (8.7) is deformed by phonons through a finite-temperature version of the replacement scheme by Hedin and Lundqvist [34, 35] outlined in Sec. 5.7. Eq. (5.46) is extended to account for spin through the replacement $\mathbf{r} \mapsto (\mathbf{r}, \sigma)$. The deformation for a single phonon mode reads

$$W_{\mathrm{c}}^{\sigma_1\sigma_1\sigma_2\sigma_2}(\mathbf{q}, i\omega_n) \mapsto W_{\mathrm{c}}^{\sigma_1\sigma_1\sigma_2\sigma_2}(\mathbf{q}, i\omega_n) + g^{\sigma_1}_{\mathbf{q}} D(\mathbf{q}, i\omega_n) g^{\sigma_2 *}_{\mathbf{q}}, \tag{8.9}$$

where the last term is the spin-dependent extension of W^{ph}, $g^\sigma_{\mathbf{q}}$ the one-momentum electron-phonon interaction[7] and

$$D(\mathbf{q}, i\omega_n) = \frac{2\omega^{\mathrm{P}}_{\mathbf{q}}}{(i\omega_n)^2 - (\omega^{\mathrm{P}}_{\mathbf{q}})^2} \tag{8.10}$$

the adiabatic phonon propagator, with phonon dispersion $\omega^{\mathrm{P}}_{\mathbf{q}}$. Eqs. (8.7) and (8.9)-(8.10) and the (usually valid) quasiparticle ansatz $R^{\Uparrow\Uparrow}_{\mathrm{HF}}(\mathbf{k}, i\omega_m) = 1/(i\omega_m - \omega^{\mathrm{M}}_{\mathbf{k}})$ lead to the desired expression (i.e. Eq. (8.2)) for the phonon-induced magnon-magnon interaction after Matsubara summation and analytic continuation ($i\omega_m \mapsto \omega + i\eta$),[8] but with an *ab initio* exchange-mediated magnon-phonon interaction[9]

$$\mathcal{A}_{\mathbf{q}} = U\sum_\sigma \overline{\mathcal{G}}^\sigma g^\sigma_{\mathbf{q}}. \tag{8.11}$$

[6] In practice, Eq. (8.7) is complemented by a shift to enforce the Goldstone criterion.

[7] In Ref. [35], $g^\sigma_{\mathbf{q}}$ is shown to be related to the screened force of Sec. 5.7.

[8] The first (plasmonic) term in Eq. (8.9) is dropped and the continuous limit $\frac{1}{N}\sum_{\mathbf{k}} \to \int \frac{d\mathbf{q}}{\Omega_{\mathrm{BZ}}}$ is taken.

[9] U is the Hubbard interaction of Eq. (8.4) with dropped band index.

8.3 A minimal three-dimensional model

To illustrate how a typical magnon spectrum is renormalized (and shifted) by the magnon-phonon interaction $\mathcal{A}_{\mathbf{q}}$ of Eq. (8.11), a minimal model is considered. Future studies should aim at computing $\mathcal{A}_{\mathbf{q}}$ in real materials. The renormalized magnon spectrum is obtained by analytically continuing Eq. (8.6) and inserting the magnon-magnon interaction Δ of Eq. (8.2), which depends on $\mathcal{A}_{\mathbf{q}}$ only through its squared magnitude

$$\left|\mathcal{A}_{\mathbf{q}}\right|^2 = U^2\Big(\left(\overline{\mathcal{G}}^{\uparrow}\right)^2\left|g_{\mathbf{q}}^{\uparrow}\right|^2 + \left(\overline{\mathcal{G}}^{\downarrow}\right)^2\left|g_{\mathbf{q}}^{\downarrow}\right|^2 + 2\,\overline{\mathcal{G}}^{\uparrow}\overline{\mathcal{G}}^{\downarrow}\mathrm{Re}\left(g_{\mathbf{q}}^{\uparrow}g_{\mathbf{q}}^{\downarrow *}\right)\Big). \tag{8.12}$$

From this expression it follows that the usual momentum average approximation [89] for the electron-phonon interaction, i.e. for $\left|g_{\mathbf{q}}^{\uparrow}\right|^2$, $\left|g_{\mathbf{q}}^{\downarrow}\right|^2$ and $2\,\mathrm{Re}\left(g_{\mathbf{q}}^{\uparrow}g_{\mathbf{q}}^{\downarrow *}\right)$, also implies a momentum average approximation for the magnon-phonon interaction, so that $\left|\mathcal{A}_{\mathbf{q}}\right|^2$ reduces to $\mathcal{A}^2$ for some positive 'magnon-phonon interaction strength' $\mathcal{A}$. A minimal three-dimensional model with a wave vector-independent Δ is obtained by assuming a flat optical phonon dispersion $\omega_{\mathbf{q}}^{\mathrm{P}} = \omega^{\mathrm{P}}$ and isotropic magnon dispersion $\omega_{\mathbf{q}}^{\mathrm{M}} = \omega_q^{\mathrm{M}}$. By approximating the Brillouin zone by a sphere with radius $K = \left(\frac{3\Omega_{\mathrm{BZ}}}{4\pi}\right)^{1/3}$, the momentum integral in Eq. (8.2) reduces to a radial momentum integral, resulting in

$$\Delta^{\downarrow\uparrow\downarrow\uparrow}(\omega) = \mathcal{A}^2\int_0^K \frac{4\pi q^2 dq}{\Omega_{\mathrm{BZ}}}\left(\frac{n^{\mathrm{P}} - n_q^{\mathrm{M}}}{\omega + \omega^{\mathrm{P}} - \omega_q^{\mathrm{M}} + i\eta} + \frac{1 + n^{\mathrm{P}} + n_q^{\mathrm{M}}}{\omega - \omega^{\mathrm{P}} - \omega_q^{\mathrm{M}} + i\eta}\right). \tag{8.13}$$

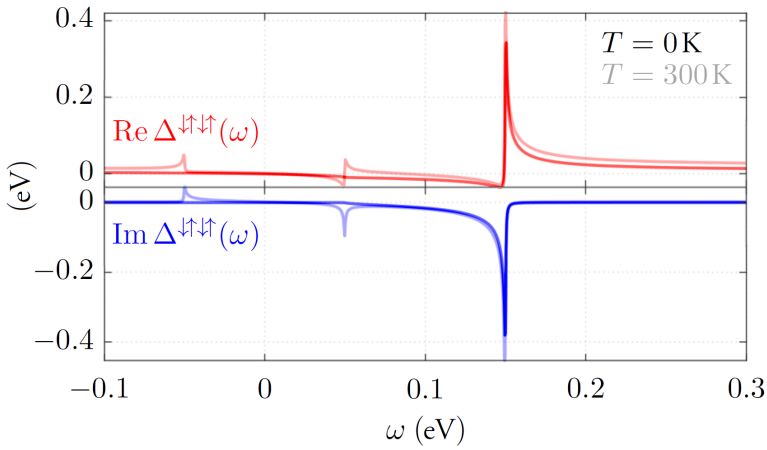

Figure 8.3: Real and imaginary parts (red and blue) of the phonon-induced magnon-magnon interaction $\Delta^{\downarrow\uparrow\downarrow\uparrow}(\omega)$ with $\mathcal{A} = 32$ meV, $\omega^{\mathrm{P}} = 50$ meV, $\omega_q^{\mathrm{M}} = 100\sin^2\left(\frac{\pi q}{2K}\right)$ meV, $K = \frac{\pi}{a}$ ($a = 7$ a.u.) and convergence parameter $\eta = 0.3$ meV. Dark colors: $T = 0$ K. Bright colors: $T = 300$ K.

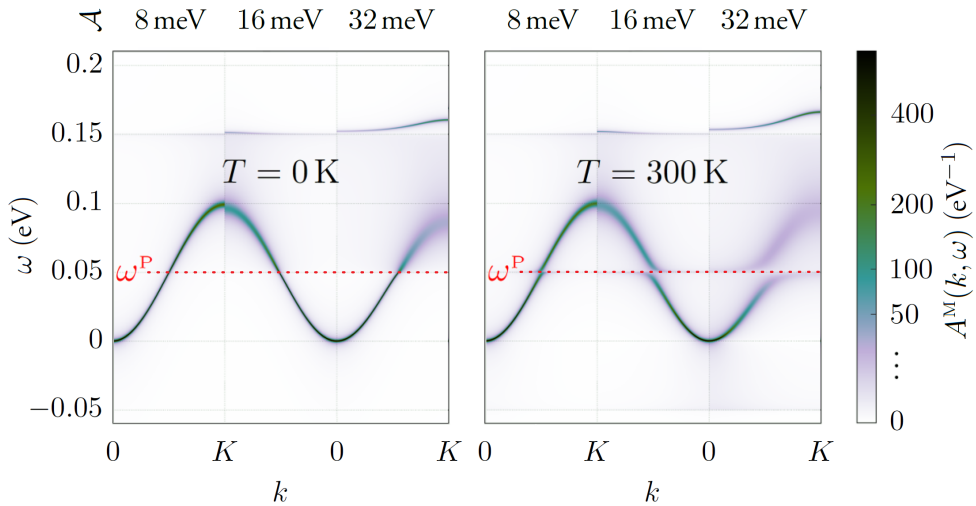

Figure 8.4: Magnitude of the renormalized magnon spectral function, $A^{\mathrm{M}}(k,\omega)$, for three values of $\mathcal{A}$ (8 meV, 16 meV and 32 meV) with $\omega^{\mathrm{P}} = 50$ meV, $\omega_q^{\mathrm{M}} = 100\sin^2\left(\frac{\pi q}{2K}\right)$ meV, $K = \frac{\pi}{a}$ ($a = 7$ a.u.) and convergence parameter $\eta = 0.3$ meV. Left: $T = 0$ K. Right: $T = 300$ K.

8.4 Results: Renormalized magnons

The phonon-induced magnon-magnon interaction $\Delta^{\downarrow\uparrow\downarrow\uparrow}(\omega)$ of Eq. (8.13) is presented at both zero temperature ($T = 0$ K) and room temperature ($T = 300$ K) in Fig. 8.3, with magnon-phonon interaction strength $\mathcal{A} = 32$ meV, a typical optical phonon energy of $\omega^{\mathrm{P}} = 50$ meV and quadratic (ferromagnetic) isotropic magnon dispersion $\omega_q^{\mathrm{M}} = 100\sin^2\left(\frac{\pi q}{2K}\right)$ meV. The representative value of $K = \frac{\pi}{a}$ ($a = 7$ a.u.) is chosen. The dominant dispersion feature centered at the sum energy $\omega_K^{\mathrm{M}} + \omega^{\mathrm{P}} = 150$ meV stems from phonon emission, which is present at $T = 0$ K. The two low-energy features at $T = 300$ K are due to phonon absorption and centered at the difference energies $\omega_K^{\mathrm{M}} - \omega^{\mathrm{P}} = 50$ meV and $\omega_0^{\mathrm{M}} - \omega^{\mathrm{P}} = -50$ meV, where the latter stems from a large Bose occupation factor. Since the phonon energy is chosen in the middle of the magnon band, the positive difference energy equals the phonon energy. The magnitude of the renormalized magnon spectral function,

$$A^{\mathrm{M}}(k,\omega) = \tfrac{1}{\pi}\left|\mathrm{Im}\,R^{\downarrow\uparrow\downarrow\uparrow}(k,\omega)\right| = \frac{\frac{1}{\pi}\left|\mathrm{Im}\,\Delta^{\downarrow\uparrow\downarrow\uparrow}(\omega)\right|}{\left(\omega - \omega_k^{\mathrm{M}} - \mathrm{Re}\,\Delta^{\downarrow\uparrow\downarrow\uparrow}(\omega)\right)^2 + \left(\mathrm{Im}\,\Delta^{\downarrow\uparrow\downarrow\uparrow}(\omega)\right)^2}, \quad (8.14)$$

is shown in Fig. 8.4 for the same parameters except with a variable magnon-phonon interaction strength $\mathcal{A}$.[10] At $T = 0$ K, phonon emission leads to magnon line broadening in the 'sum energy interval' $[\omega_0^{\mathrm{M}} + \omega^{\mathrm{P}}, \omega_K^{\mathrm{M}} + \omega^{\mathrm{P}}] = [50, 150]$ meV, for which the second

[10] The magnitude is presented since bosonic spectral functions turn negative for $\omega < 0$. Strictly speaking, the last equality in Eq. (8.14) only holds if $\eta \to 0$.

term in the denominator of Eq. (8.14) dominates, and to a satellite feature above the maximum sum energy $\omega_K^{\mathrm{M}} + \omega^{\mathrm{P}} = 150$ meV, for which the first term in the denominator of Eq. (8.14) dominates, provided that $\omega \approx \omega_k^{\mathrm{M}} + \mathrm{Re}\,\Delta^{\downarrow\uparrow\downarrow\uparrow}(\omega)$. For $\mathcal{A} = 32$ meV, Fig. 8.3 can be used to understand the satellite energy graphically. At $T = 300$ K, phonon absorption leads to additional magnon line broadening in the 'difference energy interval' $[\omega_0^{\mathrm{M}} - \omega^{\mathrm{P}}, \omega_K^{\mathrm{M}} - \omega^{\mathrm{P}}] = [-50, 50]$ meV and, in particular, to a suppression of spectral density at the dominant difference energy $\omega_K^{\mathrm{M}} - \omega^{\mathrm{P}} = 50$ meV. While the magnon density of states does not vanish, the effect approximates to a splitting of the magnon band, typically attributed to spin-orbit interaction [90]. Integrating the product of the Brillouin zone-averaged A^{M} and the absolute value of the Bose occupation factor over ω yields the z-axis magnetization reduction due to magnons in units of $\gamma/V = -g\mu_{\mathrm{B}}/V$, where V is the unit cell volume. Assuming the magnetization $0.5\ \gamma/V$ at $T = 0$ K yields the T- and $\mathcal{A}$-dependent z-axis spin magnetization M of Fig. 8.5. Deviations from the famous $T^{3/2}$ law is observed when increasing $\mathcal{A}$ from 0, together with a reduction of the Curie temperature T_{C} (except for very large $\mathcal{A}$), whose $\mathcal{A}$-dependence is also included in Fig. 8.5. This reduction stems from the increased low-energy magnon density of states, caused by the thermal splitting due to phonon absorption, as observed in Fig. 8.4.

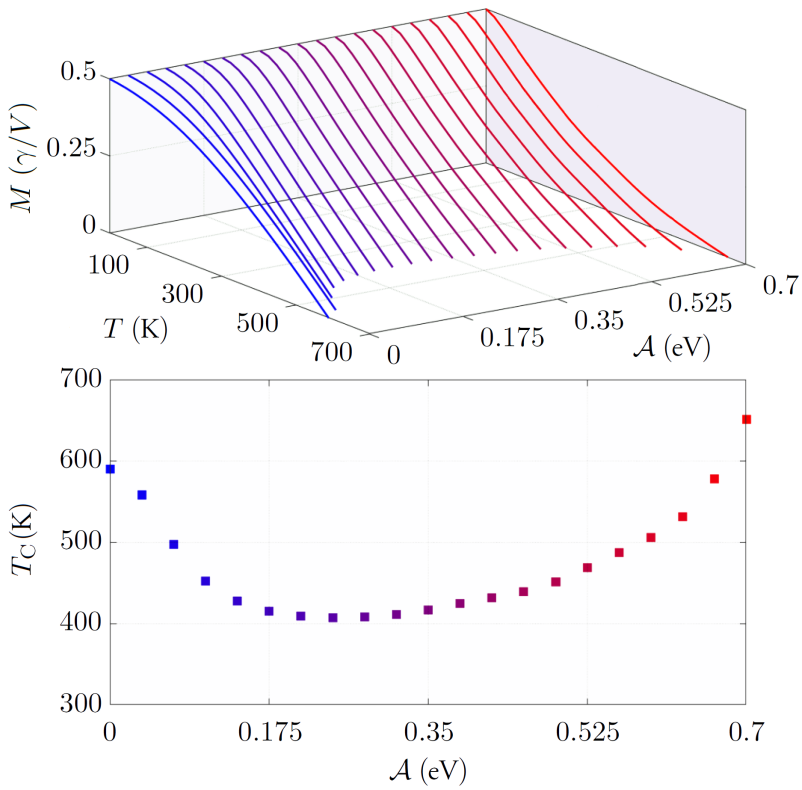

Figure 8.5: Top: Magnetization M as a function of T and $\mathcal{A}$. Bottom: Curie temperature T_{C} as a function of $\mathcal{A}$.

9

Dynamic exchange-correlation method for the Green's function

This chapter introduces and summarizes Paper IV, titled "Spectral functions of the half-filled one-dimensional Hubbard chain within the exchange-correlation potential formalism". The Green's function G is a useful tool to determine, among other things, the Fermi surface in conductors and band gap in semiconductors and insulators. Unlike the wave-function, it depends on only two spatial (and spin) coordinates in many-electron systems. Since the emergence of Green's function theory in the 1950s, self-energy methods based on Dyson's equation [23, 91] have been the standard for computing G. It was recently shown [1] that the equation of motion for G is naturally reformulated so as to replace the convolution term ΣG by a multiplicative term $V_{\mathrm{xc}}G$, where V_{xc} is the *time-dependent* exchange-correlation potential, caused by the exchange-correlation hole density n_{xc}. In Paper IV, the formalism is applied to the spectral function of the half-filled 1-band Hubbard chain, using the exact V_{xc} of the Hubbard dimer. At the one-shot level, analytic spectra are available and found to be close to those of the more sophisticated dynamic density-matrix renormalization group method, and the U-dependent band gap is similar to the exact one, found using the Bethe ansatz.

9.1 Time-dependent exchange-correlation potential

The Hierarchy problem refers to the fact that in order to solve the equation of motion for the one-electron Green's function G, the two-electron Green's function G_2 is needed, which in turn requires G_3, and so on. This is cured with Schwinger's functional derivative method, as described in Sec. 5.3. Combining Eqs. (5.17) and (5.19) and changing to

position representation, with brief notation $r = (\mathbf{r}, \sigma)$, yields $\delta(\tau)\delta(r_1 r_2)$

$$= \Big(i\frac{\partial}{\partial\tau} - h(r_1) - V_{\rm H}(r_1,\tau)\Big)G(r_1 r_2,\tau) - i\int dr_3\, v(r_1 r_3)\frac{\delta G(r_1 r_2,\tau)}{\delta\varphi(r_3,\tau)}, \qquad (9.1)$$

where $V_{\rm H}(r_1,\tau) = \int dr_3 v(r_1 r_3) n(r_3,\tau)$ is the Hartree potential, written in terms of the electron number density $n(r_3,\tau)$. Eq. (9.1) uses that G only depends on the relative time $\tau = t_1 - t_2$ in the absence of time-varying fields.[1] While Eq. (9.1) formally solves the Hierarchy problem, it does not do so in practice. This is where the self-energy Σ enters. First, imagine ignoring the $\delta G/\delta\varphi$ term. This immediately yields G as the inverse of the parenthesis in the first term, i.e. as the Hartree Green's function $G_{\rm H}$. When including $\delta G/\delta\varphi$, G can be solved for in exactly the same way by factorizing out a factor of G, as is achieved by defining the self-energy Σ from the convolution

$$-\int dr_3 d\tau' \Sigma(r_1 r_3, \tau-\tau')G(r_3 r_2,\tau') = -i\int dr_3\, v(r_1 r_3)\frac{\delta G(r_1 r_2,\tau)}{\delta\varphi(r_3,\tau)}. \qquad (9.2)$$

This turns Eq. (9.1) into a matrix equation $(G_{\rm H}^{-1} - \Sigma)G = \mathbb{I}$, known as Dyson's equation, which is more commonly written in the forms $G^{-1} = G_{\rm H}^{-1} - \Sigma$ and $G = G_{\rm H} + G_{\rm H}\Sigma G$. Despite being one of the most important many-body tools, Σ does not have a clear physical interpretation, unlike the exchange-correlation potential in density functional theory, which acts locally rather than non-locally in space and time. A new way of expressing Schwinger's Hierarchy truncation was recently found [1], where the *time-dependent* exchange-correlation potential[2] $V_{\rm xc}$ is defined from the alternative relation

$$-V_{\rm xc}(r_1 r_2,\tau)G(r_1 r_2,\tau) = -i\int dr_3\, v(r_1 r_3)\frac{\delta G(r_1 r_2,\tau)}{\delta\varphi(r_3,\tau)}, \qquad (9.3)$$

so that

$$\delta(\tau)\delta(r_1 r_2) = \Big(i\frac{\partial}{\partial\tau} - h(r_1) - V_{\rm H}(r_1,\tau) - V_{\rm xc}(r_1 r_2,\tau)\Big)G(r_1 r_2,\tau), \qquad (9.4)$$

Eq. (9.3) is similar to yet different from Eq. (9.2), since $V_{\rm xc}$ is defined from a product rather than a convolution. It is useful to think of r_2 in Eq. (9.4) as fixed so that the equation is equivalent to a Schrödinger equation for the Green's function if $\tau \neq 0$ and $r_1 \neq r_2$. Due to Coulomb interaction, $V_{\rm xc}$ is generally non-Hermitian, which leads to a time-decaying Green's function and thus to line broadening. The multiplicative property of $V_{\rm xc}$ separates the equation of motion into one for the hole ($t < 0$) and another for the electron ($t > 0$). This is in contrast to the self-energy approach in which solving for the hole Green's function requires explicit knowledge of the electron Green's function

[1] The field φ is to be regarded as vanishing, but not derivatives with respect to it.

[2] This time-dependence is not a dependence on absolute time but on relative time (time delay).

and vice versa. On the other hand, the self-energy formalism is more natural in frequency domain, since Dyson's equation can be solved for each frequency separately whereas the exchange-correlation potential formalism involves a frequency convolution. Thus, the two approaches complement one another. It follows from Eqs. (9.2)-(9.3) that $V_{\rm xc}$ and Σ are related through the relation

$$V_{\rm xc}(r_1r_2,\tau)G(r_1r_2,\tau) = \int dr_3 d\tau' \Sigma(r_1r_3,\tau-\tau')G(r_3r_2,\tau'). \tag{9.5}$$

In contrast to the self-energy approach, which can be extremely time consuming for large systems, a universal exchange-correlation potential with the ground-state density as input would allow for applications to large systems. The self-energy approach was recently called into question in the context of the half-filled two-dimensional Hubbard model [92], yielding a metal rather than an insulator due to the implicit summation of reducible diagrams when solving Dyson's equation, so that it differs from the direct expansion at each order. The exchange-correlation potential formalism, on the other hand, does not rely on Dyson's equation but rather on direct construction based on known results of model systems and on exact properties of the exchange-correlation hole.

9.2 Time-dependent exchange-correlation hole

When an electron is added it induces a density fluctuation $n_{\rm xc}$ called an exchange-correlation hole, which generates an exchange-correlation potential

$$V_{\rm xc}(r_1r_2,\tau) = \int dr_3\, v(r_1r_3) n_{\rm xc}(r_1r_2r_3,\tau) \tag{9.6}$$

that acts back on the electron. Eq. (9.3) then yields[3]

$$n_{\rm xc}(r_1r_2r_3,\tau)G(r_1r_2,\tau) = i\frac{\delta G(r_1r_2,\tau)}{\delta\varphi(r_3,\tau)}. \tag{9.7}$$

G_2 in the equation of motion (Eq. (5.17)) can be written in terms of $n_{\rm xc}$ as

$$\langle T[\hat{n}(r_3,\tau)\hat{\psi}(r_1,\tau)\hat{\psi}^\dagger(r_2,0))]\rangle = iG(r_1r_2,\tau)\big(n(r_3)+n_{\rm xc}(r_1r_2r_3,\tau)\big), \tag{9.8}$$

but also naturally defines the correlator g from the ansatz

$$\langle T[\hat{n}(r_3,\tau)\hat{\psi}(r_1,\tau)\hat{\psi}^\dagger(r_2,0))]\rangle = iG(r_1r_2,\tau)g(r_1r_2r_3,\tau)n(r_3), \tag{9.9}$$

[3] $n_{\rm xc}$ can be deformed and set to fulfil $n_{\rm xc}(r_1r_2r_3,\tau t_3)G(r_1r_2,\tau) = i\delta G(r_1r_2,\tau)/\delta\varphi(r_3,t_3)$. The relation $\delta G = -G\delta G^{-1}G$ then yields an expression in terms of the screening $\epsilon^{-1} = -\delta G^{-1}/\delta\varphi$.

which implies the relation

$$n_{\rm xc}(r_1 r_2 r_3, \tau) = \big(g(r_1 r_2 r_3, \tau) - 1\big) n(r_3) \tag{9.10}$$

between the exchange-correlation hole and the correlator. It is left as an exercise to show that by integrating G_2 over r_3, first for $\tau < 0$ and then for $\tau > 0$, leads to the sum rule[4]

$$\int d\mathbf{r}_3 \, n_{\rm xc}(r_1 r_2 r_3, \tau) = -\delta_{\sigma_1 \sigma_3} \theta(-\tau), \tag{9.11}$$

which justifies the hole terminology. Locally, $n_{\rm xc}$ can be complex, but the imaginary part integrates to zero. g is independent of the Coulomb interaction v, and does therefore not lump it together with other quantities, like Σ does. The exchange-correlation formalism can therefore exploit the simple distance-dependence of v, which implies that only the spherical average of the exchange-correlation hole is relevant [93, 17], which simplifies the search for a good approximation for the exchange-correlation potential. The time-dependent exchange-correlation hole of Eq. (9.10) generalizes the static exchange-correlation hole. The latter, which is obtained when $\tau \to 0^-$ and $r_2 \to r_1$, determines the exchange-correlation energy [94, 17, 18] in density functional theory [15, 16, 17, 18]. The connection to density functional theory suggests that some very successful approximations may be applied also to the time-dependent formalism based on the Green's function, such as the local density approximation [94].

9.3 Results: From the dimer to the chain

In the previous work [1], the formalism was illustrated by deriving the exact $V_{\rm xc}$ of the Hubbard dimer analytically by means of reverse engineering. In Paper IV, the formalism is applied by using this dimer $V_{\rm xc}$ to calculate G in the one-dimensional half-filled Hubbard chain. The exact Bethe ansatz provides a good benchmark for the dispersion and yields two (holon and spinon)[5] branches of collective excitations [95, 96]. Spinons and holons are also found in real materials, such as $SrCuO_2$ [97, 98]. In addition to the dispersion, dynamical density-matrix renormalization group spectra [99] furnish a benchmark for the spectral distributions. The Hamiltonian of the Hubbard dimer reads

$$\hat{H} = -\Delta \sum_{i \neq j} \hat{c}^\dagger_{i\sigma} \hat{c}_{j\sigma} + U \sum_i \hat{n}_{i\uparrow} \hat{n}_{i\downarrow}, \tag{9.12}$$

[4]For $t > 0$ (addition of an electron), $n_{\rm xc}$ integrates to zero. Indeed, there is no hole created and the added electron is not part of the electron density that generates the Hartree potential, in contrast to the electron-removal case, in which the system has lost one electron and necessitates the removal of self-interaction.

[5]The electron can be thought of as a bound state of spinons, holons and orbitons, which carry spin, charge and orbital degrees of freedom. Systems with strong confinement can display spin-charge separation, which means that the spinons and holons behave rather independently.

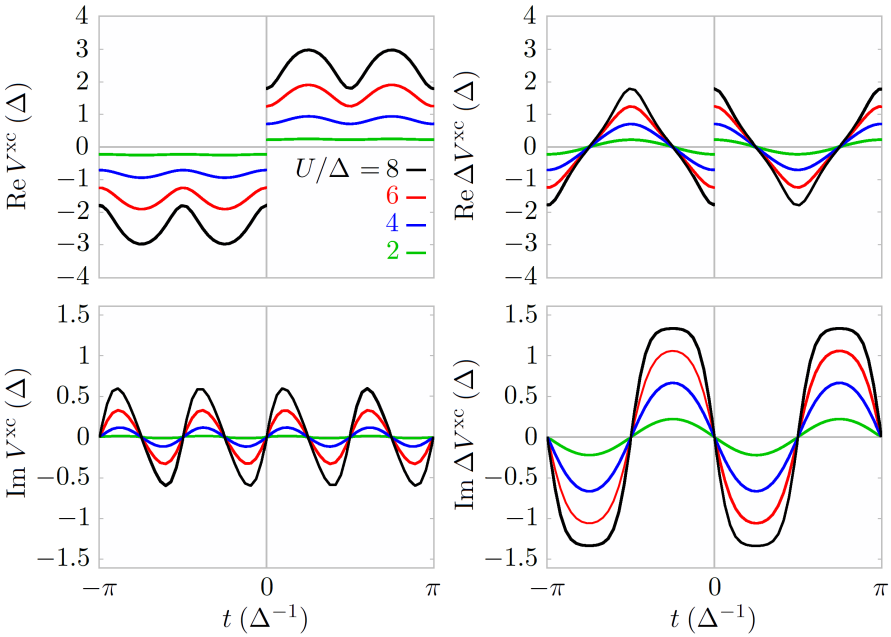

Figure 9.1: Real and imaginary parts of the two distinct time-dependent components of the exchange-correlation potential of the Hubbard dimer, $V^{\rm xc}$ and $\Delta V^{\rm xc}$, for different values of U/Δ.

where $i, j = 1, 2$. The exact $V_{\rm xc}$ components in the bonding and anti-bonding orbitals, $V^{\rm xc}_{\rm aaaa}$ and $V^{\rm xc}_{\rm bbbb}$,[6] are both given by (α defined in the footnote[7]) [1]

$$V^{\rm xc}(t>0) = \frac{\alpha U}{2}\frac{1-\alpha^2 e^{-i4\Delta t}}{1-\alpha^4 e^{-i4\Delta t}}, \tag{9.13}$$

and the other non-vanishing components, $V^{\rm xc}_{\rm abab}$ and $V^{\rm xc}_{\rm baba}$, by

$$\Delta V^{\rm xc}(t>0) = \frac{\alpha U}{2}\frac{(1-\alpha^2) e^{-i2\Delta t}}{1-\alpha^4 e^{-i4\Delta t}}. \tag{9.14}$$

From particle-hole symmetry, $V^{\rm xc}(-t) = -V^{\rm xc}(t)$. The two complex time-dependent functions of Eqs. (9.13)-(9.14) are plotted in Fig. 9.1 for different relative interaction strengths U/Δ. High-amplitude oscillations are shown to be attributed to strong correlations, and low-amplitude oscillations to weak correlations. This is expected since weakly correlated systems are known to be well-described by a static mean field. Another feature, which is shared by the static exchange-correlation potential of density functional theory [100], is the discontinuity in $V^{\rm xc}$ at $t = 0$, equal to the difference between the electron

[6] The components $V^{\rm xc}_{ijkl}$ are ordered like v_{ijkl} of Eq. (4.18).

[7] $\alpha = (1-x)/(1+x)$ is the ratio between the gap and the interaction U and $x = (\sqrt{U^2+16U^2}-U)/4\Delta$ the relative weight of double-occupancy configurations in the ground state.

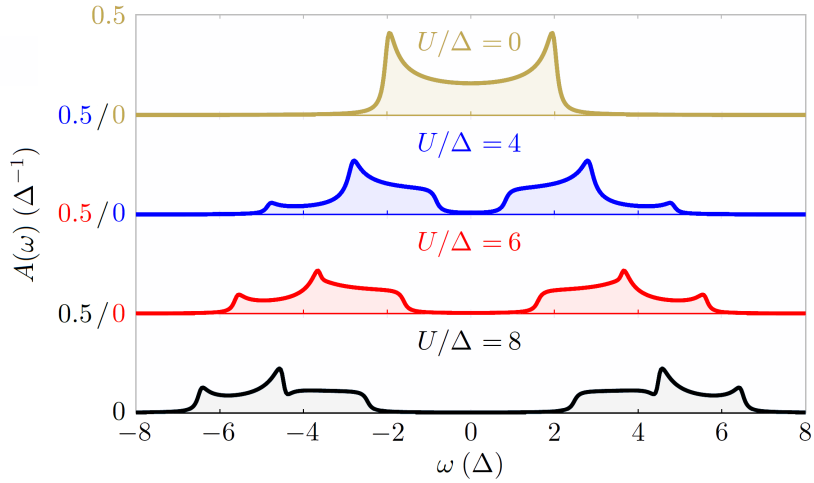

Figure 9.2: The total spectral functions of the 1D Hubbard chain for $U/\Delta = 2$, 4, 6 and 8 obtained using the approximations described in the text. A broadening of 0.1Δ is used.

($t = 0^+$) and hole ($t = 0^-$) values. The time dependence is seen to be dictated by the excitation energies of the $(N \pm 1)$ systems. For many-electron systems, this should include collective excitations, like plasmons with a field variation $e^{i\omega_{\rm P}t}$, exchanging plasmon energy $\omega_{\rm P}$ with the system. This expectation is confirmed in Paper IV when considering the Holstein Hamiltonian (not included here).

In the Hubbard chain, the Hamiltonian is the same but with unrestricted i and j. The equation of motion in the Bloch functions $\psi_k(r)$ reads[8]

$$\big(i\partial_t - \varepsilon_q\big)G(q,t) - \sum_k V^{\rm xc}(qk,t)G(k,t) = \delta(t), \tag{9.15}$$

where $\varepsilon_q = -2\Delta\cos qa$ and a is the lattice constant of the chain. The constant Hartree potential is absorbed into the chemical potential. An approximation is made where the exact $V_{\rm xc}$ components of the Hubbard dimer, Eqs. (9.13)-(9.14), are employed by replacing $V^{\rm xc}(qq,t)$ by $V^{\rm xc}(t)$ and, for $q \neq k$, $V^{\rm xc}(qk,t)$ by $\Delta V^{\rm xc}(t)/N$, so that

$$\Big(i\partial_t - \varepsilon_q - V^{\rm xc}(t)\Big)G(q,t) - \frac{1}{N}\sum_k \Delta V^{\rm xc}(t)G(k,t) = \delta(t) \tag{9.16}$$

for large N. The second term is written as $-\Delta V^{\rm xc}(q,t)G(q,t)$, with

$$\Delta V^{\rm xc}(q,t) = \frac{1}{N}\sum_k \frac{G(k,t)}{G(q,t)}\Delta V^{\rm xc}(t) \approx \frac{1}{N}\sum_k e^{-i(\varepsilon_k-\varepsilon_q)t}\Delta V^{\rm xc}(t). \tag{9.17}$$

[8] $V^{\rm xc}(qk,t) = V^{\rm xc}_{qkqk}(t)$. Other components vanish.

In the last step, a non-interacting G has been assumed as a first approximation. Furthermore, $V^{\rm xc}$ and $\Delta V^{\rm xc}$ in Eqs. (9.13)-(9.14) can be expanded to linear order in α as[9]

$$V^{\rm xc}(t) \approx \frac{\alpha U}{2}, \qquad (9.18) \qquad\qquad \Delta V^{\rm xc}(t) \approx \frac{\alpha U}{2} e^{-i2\Delta t}. \qquad (9.19)$$

The constant component in Eq. (9.18) shifts the one-particle energy whereas the excitation term of Eq. (9.19) generates the main satellite through its time-dependence $e^{-i2\Delta t}$. To first order in $\Delta V^{\rm xc}$, the hole Green's function takes the form (in t and ω domain)

$$G^{\rm h}(q,t) = i\theta(-t) e^{-i(\varepsilon_q - \frac{\alpha U}{2})t} \left(1 - \frac{\alpha U}{2N} \sum_k \frac{e^{-i(\varepsilon_k - \varepsilon_q - 2\Delta)t} - 1}{\varepsilon_k - \varepsilon_q - 2\Delta} \right), \qquad (9.20)$$

$$G^{\rm h}(q,\omega) = \frac{A_0^{\rm h}}{\omega - \left(\varepsilon_q - \frac{\alpha U}{2}\right) - i\eta} - \frac{1}{N} \sum_k \frac{A^{\rm h}(k)}{\omega - (\varepsilon_k - \frac{\alpha U}{2} - 2\Delta) - i\eta}, \qquad (9.21)$$

where $A_0^{\rm h} = 1 + \frac{1}{N}\sum_k A^{\rm h}(k)$ and $A^{\rm h}(k) = \frac{\alpha U}{2}/(\varepsilon_k - \varphi_q - 2\Delta)$. In Paper IV and the results below, the α^3-correction to $\Delta V^{\rm xc}(t)$ is kept, which changes the weights $\alpha U/2$ into $\alpha U(1-\alpha^2)/2$. The α^3-correction to $V^{\rm xc}(t)$ is dropped, despite being of the same order, since only the main (lowest-energy) excitation is of interest in this first study. A similar derivation is carried out for the electron Green's function in Paper IV. For the electron/hole case it is understood that both ε_k and ε_q correspond to unoccupied/occupied states.

The total hole spectral functions with $U/\Delta = 2$, 4, 6 and 8 are shown in Fig. 9.2 and the k-resolved spectra with $U/\Delta = 7.74$ in Fig. 9.3, at k points for which dynamical density-matrix renormalization group results are available [99]. Due to the approximation of replacing G by the non-interacting value in Eq. (9.17), there is no spectral weight

[9] α^2 remains small for quite big U/Δ. For example, it is 0.172 for $U/\Delta = 4$ and 0.382 for $U/\Delta = 8$.

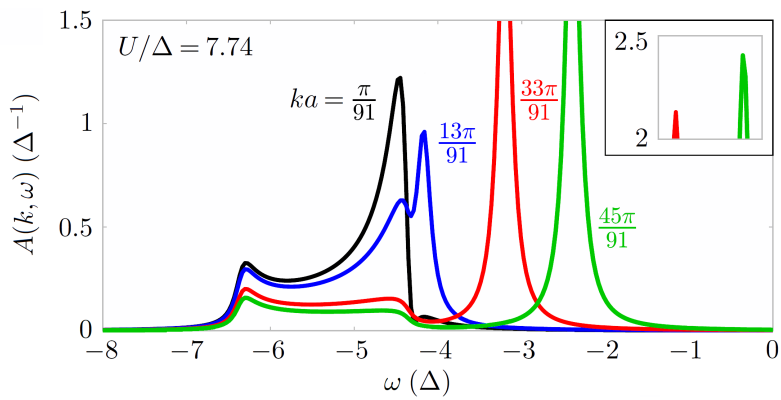

Figure 9.3: The k-resolved spectral functions of the 1D Hubbard chain for $U/\Delta = 7.74$. U and k have been chosen to facilitate comparison with Fig. 11 of Benthien and Jeckelmann [99]. A broadening of 0.1 is used.

above the chemical potential for the hole Green's function. Despite the simplicity of the approximation used, the k-resolved spectra in Fig. 9.3 are in favorable agreement with Ref. [99]. A notable discrepancy is the dispersion widths for both the spinon and the holon branches, which results in small-k peaks with lower energy compared to Ref. [99]. This is a consequence of using the non-interacting G and the Hubbard dimer V^{xc}, which neglects long-range correlations and thus suppresses band dispersion. The advantage of analytical calculations is that the structure of the k-resolved hole spectra in Fig. 9.3 can be understood from G^{h} of Eq. (9.21). The first term yields the main peak centered at $\omega = \varepsilon_q - \frac{\alpha U}{2}$, interpreted as the spinon excitation. The second term with the weight $A^{\mathrm{h}}(k)$ set to unity yields the non-interacting occupied density of states shifted by $-(\frac{\alpha U}{2} + 2\Delta)$. A more detailed explanation is in Paper IV. The calculated band gap, which is given by αU, is displayed in Fig. 9.4 and compared with the exact result [101],

$$E_{\mathrm{gap}} = \frac{16\Delta^2}{U}\int_1^\infty \frac{ds\sqrt{s^2-1}}{\sinh\left(\frac{2\pi\Delta s}{U}\right)}, \tag{9.22}$$

obtained from the Bethe ansatz. The agreement between the analytically calculated gap and the exact gap is quite striking, considering the simple approximations used. In the limit of large U the calculated gap approaches the exact gap. Importantly, a gap opens up for all positive U. It should be noted that in the widely used dynamical mean-field theory (DMFT) [102] within the single-site approximation, the gap is not opened up until $U/\Delta > 6$. Only within the cluster DMFT with an even number of sites does the gap form for all positive U [103].

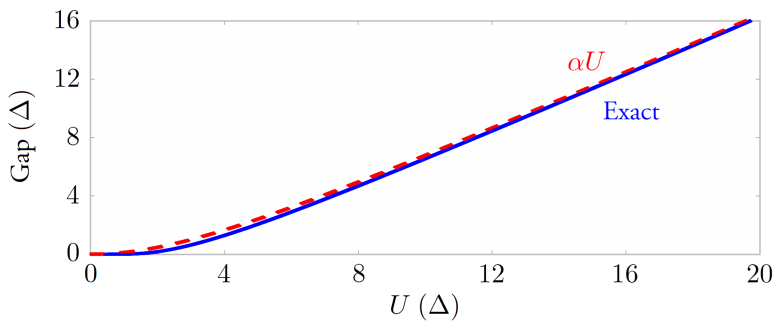

Figure 9.4: The calculated band gap, αU, compared with the exact gap obtained from the Bethe ansatz as a function of U. The calculated gap approaches the exact result as U increases.

Appendices (Parts I-II)

A: Deriving the Lorentz-Stern-Gerlach force

Integrating $\boldsymbol{\mathcal{F}}_i$ of Eq. (3.1) yields

$$\mathbf{F}_i(t) = q_i\Big(\mathbf{E}_i(t) + \frac{1}{c}\mathbf{v}_i(t)\times\mathbf{B}_i(t)\Big) + \int d\mathbf{r}\,\Big(\nabla\times\big(\boldsymbol{\mu}_i^{\mathrm{S}}(t)\delta(\mathbf{r}-\mathbf{r}_i(t))\big)\Big)\times\mathbf{B}_i(\mathbf{r},t), \quad \text{(A1)}$$

where the fields $\mathbf{E}_i(t)$ and $\mathbf{B}_i(t)$ are evaluated at the time-dependent position $\mathbf{r}_i(t)$ of the particle. Vector calculus the yields (with $\nabla\cdot\mathbf{B}_i(\mathbf{r},t)=0$)

$$\begin{aligned}
&\int d\mathbf{r}\,\Big(\nabla\times\big(\boldsymbol{\mu}_i^{\mathrm{S}}(t)\delta(\mathbf{r}-\mathbf{r}_i(t))\big)\Big)\times\mathbf{B}_i(\mathbf{r},t)\\
&= \boldsymbol{\mu}_i^{\mathrm{S}}(t)\int d\mathbf{r}\,\big(\mathbf{B}_i(\mathbf{r},t)\cdot\nabla\delta(\mathbf{r}-\mathbf{r}_i(t))\big) - \int d\mathbf{r}\,\big(\boldsymbol{\mu}_i^{\mathrm{S}}(t)\cdot\mathbf{B}_i(\mathbf{r},t)\big)\nabla\delta(\mathbf{r}-\mathbf{r}_i(t)) \quad \text{(A2)}\\
&= -\boldsymbol{\mu}_i^{\mathrm{S}}(t)\int d\mathbf{r}\,\big(\nabla\cdot\mathbf{B}_i(\mathbf{r},t)\big)\delta(\mathbf{r}-\mathbf{r}_i(t)) + \int d\mathbf{r}\nabla\big(\boldsymbol{\mu}_i^{\mathrm{S}}(t)\cdot\mathbf{B}_i(\mathbf{r},t)\big)\delta(\mathbf{r}-\mathbf{r}_i(t)) \quad \text{(A3)}\\
&= \nabla\big(\boldsymbol{\mu}_i^{\mathrm{S}}(t)\cdot\mathbf{B}_i(\mathbf{r},t)\big)\big|_{\mathbf{r}=\mathbf{r}_i(t)}. \quad \text{(A4)}
\end{aligned}$$

The force thus takes the form of Eq. (3.4).

B: Deriving the Pauli coupling Hamiltonian

Vector calculus and the divergence theorem yields (with $\mathbf{B}_i(\mathbf{r},t)=\nabla\times\mathbf{A}_i(\mathbf{r},t)$)

$$\begin{aligned}
H_i(t) &= H_i^{\mathrm{MC}}(t) + \frac{m_i c}{q_i}\int d\mathbf{r}\,\big(\nabla\times\big(\boldsymbol{\mu}_i^{\mathrm{S}}(t)\delta(\mathbf{r}-\mathbf{r}_i(t))\big)\big)\cdot\mathbf{v}_i(\mathbf{r},t) \quad \text{(B1)}\\
&= H_i^{\mathrm{MC}}(t) + \frac{m_i c}{q_i}\int d\mathbf{r}\,\big(\boldsymbol{\mu}_i^{\mathrm{S}}(t)\delta(\mathbf{r}-\mathbf{r}_i(t))\big)\cdot\big(\nabla\times\mathbf{v}_i(\mathbf{r},t)\big) \quad \text{(B2)}\\
&= H_i^{\mathrm{MC}}(t) - \int d\mathbf{r}\,\big(\boldsymbol{\mu}_i^{\mathrm{S}}(t)\delta(\mathbf{r}-\mathbf{r}_i(t))\big)\cdot\big(\nabla\times\mathbf{A}_i(\mathbf{r},t)\big) \quad \text{(B3)}\\
&= H_i^{\mathrm{MC}}(t) - \boldsymbol{\mu}_i^{\mathrm{S}}(t)\cdot\mathbf{B}_i(t), \quad \text{(B4)}
\end{aligned}$$

neglecting the term quadratic in the magnetization current. $H_i^{\mathrm{MC}}(t)$ is the minimal coupling Hamiltonian of Eq. (3.5). Eq. (B4) is the Pauli coupling Hamiltonian of Eq. (3.8).

C: Deriving the Schrödinger-Pauli equation

Based on Ref. [104]. Quantities $n(\mathbf{r}\mathbf{r}',t)$ and $\mathbf{S}(\mathbf{r}\mathbf{r}',t)$ are defined from the Fourier transforms $n(\mathbf{r},\mathbf{p},t)=\int d\mathbf{r}' e^{2i\mathbf{p}\cdot\mathbf{r}'/\hbar}n(\mathbf{r}\mathbf{r}',t)$ and $\mathbf{S}(\mathbf{r},t)n(\mathbf{r},\mathbf{p},t)=\int d\mathbf{r}' e^{2i\mathbf{p}\cdot\mathbf{r}'/\hbar}\mathbf{S}(\mathbf{r}\mathbf{r}',t)$,

where $\hbar$ (Planck's reduced constant) has dimension of action. Eq. (4.1) then takes the form

$$\left(i\hbar\frac{\partial}{\partial t}-\frac{\hbar^2}{2m}\frac{\partial^2}{\partial\mathbf{r}\cdot\partial\mathbf{r}'}+q\nabla\phi(\mathbf{r},t)\cdot 2\mathbf{r}'\right)n(\mathbf{r}\mathbf{r}',t)-\gamma\sum_i S_i(\mathbf{r}\mathbf{r}',t)\nabla B_i(\mathbf{r},t)\cdot 2\mathbf{r}'=0. \quad \text{(C1)}$$

If $\hbar$ is treated as small it follows that n and $\mathbf{S}$ are non-zero only for small values of $\mathbf{r}'$. The terms of the form $\nabla f(\mathbf{r})\cdot 2\mathbf{r}'$ can then be replaced by $f(\mathbf{r}_+)-f(\mathbf{r}_-)$, where $\mathbf{r}_+=\mathbf{r}+\mathbf{r}'$ and $\mathbf{r}_-=\mathbf{r}-\mathbf{r}'$. With $\frac{\partial^2}{\partial\mathbf{r}\cdot\partial\mathbf{r}'}=\frac{\partial^2}{\partial\mathbf{r}_+^2}-\frac{\partial^2}{\partial\mathbf{r}_-^2}$, it follows that

$$\begin{aligned} i\hbar\frac{\partial}{\partial t}n(\mathbf{r}\mathbf{r}',t) &= \left(\frac{\hbar^2}{2m}\frac{\partial^2}{\partial\mathbf{r}_+^2}-q\phi(\mathbf{r}_+,t)\right)n(\mathbf{r}\mathbf{r}',t)+\gamma\mathbf{B}(\mathbf{r}_+,t)\cdot\mathbf{S}(\mathbf{r}\mathbf{r}',t) \\ &\quad -\left(\frac{\hbar^2}{2m}\frac{\partial^2}{\partial\mathbf{r}_-^2}-q\phi(\mathbf{r}_-,t)\right)n(\mathbf{r}\mathbf{r}',t)-\gamma\mathbf{B}(\mathbf{r}_-,t)\cdot\mathbf{S}(\mathbf{r}\mathbf{r}',t). \end{aligned} \quad \text{(C2)}$$

Searching for solutions to Eq. (C2) of the form

$$n(\mathbf{r}\mathbf{r}',t)=\Psi^\dagger(\mathbf{r}_+,t)\Psi(\mathbf{r}_-,t), \quad \text{(C3)} \qquad \mathbf{S}(\mathbf{r}\mathbf{r}',t)=\Psi^\dagger(\mathbf{r}_+,t)\mathbf{S}\Psi(\mathbf{r}_-,t), \quad \text{(C4)}$$

where $\Psi(\mathbf{r},t)=\big(\Psi_\uparrow(\mathbf{r},t)\ \Psi_\downarrow(\mathbf{r},t)\big)^T$ is the two-component spinor wavefunction[10] and

$$\mathbf{S}=\frac{\hbar}{2}\boldsymbol{\sigma}=\frac{\hbar}{2}(\sigma^x,\sigma^y,\sigma^z)=\frac{\hbar}{2}\left(\begin{pmatrix}0&1\\1&0\end{pmatrix},\begin{pmatrix}0&-i\\i&0\end{pmatrix},\begin{pmatrix}1&0\\0&-1\end{pmatrix}\right) \quad \text{(C5)}$$

is the spin operator (σ^i are Pauli matrices), yields

$$\Psi^\dagger(\mathbf{r}_+,t)\left(i\hbar\frac{\partial}{\partial t}+\frac{\hbar^2}{2m}\frac{\partial^2}{\partial\mathbf{r}_-^2}-q\phi(\mathbf{r}_-,t)+\gamma\mathbf{S}\cdot\mathbf{B}(\mathbf{r}_-,t)\right)\Psi(\mathbf{r}_-,t)-(\mathbf{r}_+\leftrightarrow\mathbf{r}_-)^*=0. \quad \text{(C6)}$$

The non-trivial solution Ψ fulfils the Schrödinger-Pauli equation of Eq. (4.2).

D: Deriving the orbital magnetization

Heisenberg's equation of motion, exemplified by Eq. (5.15), can be applied to the position operator to define the velocity operator. In the Schrödinger picture, it then follows that

$$\hat{\mathbf{v}}=\frac{i}{\hbar}\big[\hat{H},\hat{\mathbf{r}}\big], \quad \text{(D1)}$$

where $\hat{H}$ is the Hamiltonian without external fields. For periodic systems, the one-body Bloch eigenstates $|\psi^\sigma_{\mathbf{k}n}\rangle=e^{i\mathbf{k}\cdot\hat{\mathbf{r}}}|u^\sigma_{\mathbf{k}n}\rangle$, where $u^\sigma_{\mathbf{k}n}(\mathbf{r})=\langle\mathbf{r}|u^\sigma_{\mathbf{k}n}\rangle$ is lattice-periodic, fulfil

[10] The spinor follows from Dirac's relativistic quantum mechanics, where it has four components. In the non-relativistic limit, particle-antiparticle decoupling results in an effective two-component spinor.

$\hat{H}|\psi^\sigma_{\mathbf{k}n}\rangle = \epsilon^\sigma_{\mathbf{k}n}|\psi^\sigma_{\mathbf{k}n}\rangle$ and are related to the Wannier states $|\phi^\sigma_{\mathbf{R}n}\rangle$ by Eqs. (4.14)-(4.15). The momentum-average $\frac{1}{N}\sum_{\mathbf{k}}$ is replaced by a continuous integral $\int \frac{d\mathbf{k}}{(2\pi)^3/\Omega}$, where $\Omega = V/N$ is the unit cell volume. It is also useful to introduce $|\tilde{u}^\sigma_{\mathbf{k}n}\rangle = e^{-i\mathbf{k}\cdot\hat{\mathbf{r}}}|\tilde{\psi}^\sigma_{\mathbf{k}n}\rangle$. The states are normalized to $\langle\tilde{\psi}^{\sigma_1}_{\mathbf{k}_1 n_1}|\tilde{\psi}^{\sigma_2}_{\mathbf{k}_2 n_2}\rangle = \frac{(2\pi)^3}{\Omega}\delta(\mathbf{k}_1-\mathbf{k}_2)\delta_{n_1n_2}\delta_{\sigma_1\sigma_2}$ and $\langle\phi^{\sigma_1}_{\mathbf{R}_1 n_1}|\phi^{\sigma_2}_{\mathbf{R}_2 n_2}\rangle = \delta_{\mathbf{R}_1\mathbf{R}_2}\delta_{n_1n_2}\delta_{\sigma_1\sigma_2}$. The unitary matrix $S^\sigma_{mn}(\mathbf{k})$, which is a spin-dependent generalization of that in Eq. (4.15), guarantees that the Bloch states vary smoothly at $\mathbf{k}$ points with degeneracies. It is thus crucial for obtaining exponentially localized Wannier functions, and is optimized by minimizing their spread [19]. It is here assumed that $|\tilde{\psi}^\sigma_{\mathbf{k}+\mathbf{G},n}\rangle = |\tilde{\psi}^\sigma_{\mathbf{k}n}\rangle$, where $\mathbf{G}$ is a reciprocal lattice vector, as applies to periodic solids with a vanishing Chern invariant (see Eq. (7.5)).

The cross product of Eq. (7.1) can be split into $(\hat{\mathbf{r}}-\mathbf{R}_1)\times\hat{\mathbf{v}}$ and $\mathbf{R}_1\times\hat{\mathbf{v}}$. For the diagonal components ($|\phi^\sigma_{\mathbf{R}_1 n_1}\rangle = |\phi^\sigma_{\mathbf{R}_2 n_2}\rangle$), the former describes a local contribution associated with the self-rotation of the Wannier functions and the latter an itinerant contribution stemming from the rotation of the centre-of-mass of the Wannier functions around the origin. $\mathbf{M}^{\mathrm{orb}}$ will thus be written as the sum $\mathbf{M}^{\mathrm{L}}+\mathbf{M}^{\mathrm{I}}$, where L and I denote the local and itinerant contributions, respectively. The local contribution can be written as

$$\mathbf{M}^{\mathrm{L}} = \frac{i\hbar e}{2\Omega c}\sum_{\mathbf{R}}\langle\phi^\sigma_{\mathbf{0}n_1}|\hat{\mathbf{r}}\times\hat{\mathbf{v}}|\phi^\sigma_{\mathbf{R}n_2}\rangle G^\sigma_{\mathbf{R}n_2,\mathbf{0}n_1} \tag{D2}$$

$$= \frac{-e}{2\Omega c}\sum_{\mathbf{R}}\langle\phi^\sigma_{\mathbf{0}n_1}|\hat{\mathbf{r}}\times\hat{H}\hat{\mathbf{r}}|\phi^\sigma_{\mathbf{R}n_2}\rangle G^\sigma_{\mathbf{R}n_2,\mathbf{0}n_1} \tag{D3}$$

$$= \frac{-e}{2c}\int\frac{d\mathbf{k}}{(2\pi)^3}\langle\tilde{\boldsymbol{u}}'^\sigma_{\mathbf{k}n_1}|\times\Big(\hat{H}_{\mathbf{k}}|\tilde{\boldsymbol{u}}'^\sigma_{\mathbf{k}n_2}\rangle + \tilde{\epsilon}^\sigma_{\mathbf{k}n_3n_2}|\tilde{u}^\sigma_{\mathbf{k}n_3}\rangle\nabla_{\mathbf{k}}\Big)G^\sigma_{n_2n_1}(\mathbf{k}), \tag{D4}$$

with the definitions $\tilde{\epsilon}^\sigma_{\mathbf{k}n_1n_2} = S^{\sigma\dagger}_{n_1n_3}(\mathbf{k})\epsilon^\sigma_{\mathbf{k}n_3}S^\sigma_{n_3n_2}(\mathbf{k})$, $G^\sigma_{n_2n_1}(\mathbf{k}) = \sum_{\mathbf{R}}e^{-i\mathbf{k}\cdot\mathbf{R}}G^\sigma_{\mathbf{R}n_2,\mathbf{0}n_1}$, $|\tilde{\boldsymbol{u}}'^\sigma_{\mathbf{k}n}\rangle = |\nabla_{\mathbf{k}}\tilde{u}^\sigma_{\mathbf{k}n}\rangle$ and $\hat{H}_{\mathbf{k}} = e^{-i\mathbf{k}\cdot\hat{\mathbf{r}}}\hat{H}e^{i\mathbf{k}\cdot\hat{\mathbf{r}}}$ ($\hat{H}_{\mathbf{k}}|u^\sigma_{\mathbf{k}n}\rangle = \epsilon^\sigma_{\mathbf{k}n}|u^\sigma_{\mathbf{k}n}\rangle$). Einstein summation is used for the band and spin indices. Eq. (D2) holds since the local part of Eq. (7.1) is independent of $\mathbf{R}_1$ and Eq. (D3) follows from Eq. (D1). Eq. (D4) uses the relation

$$\hat{\mathbf{r}}|\phi^\sigma_{\mathbf{R}n}\rangle = i\int\frac{d\mathbf{k}}{(2\pi)^3/\Omega}e^{i\mathbf{k}\cdot\hat{\mathbf{r}}}\nabla_{\mathbf{k}}\big(e^{-i\mathbf{k}\cdot\mathbf{R}}|\tilde{u}^\sigma_{\mathbf{k}n}\rangle\big), \tag{D5}$$

which is verified by partial integration. The itinerant contribution can be written as

$$\mathbf{M}^{\mathrm{I}} = \frac{i\hbar e}{2Vc}\sum_{\mathbf{R}_1\mathbf{R}_2}\mathbf{R}_1\times\langle\phi^\sigma_{\mathbf{R}_1n_1}|\hat{\mathbf{v}}|\phi^\sigma_{\mathbf{R}_2n_2}\rangle G^\sigma_{\mathbf{R}_2n_2,\mathbf{R}_1n_1} \tag{D6}$$

$$= \frac{-e}{2\Omega c}\sum_{\mathbf{R}_1\mathbf{R}_2}\mathbf{R}_1\times\Big(\langle\phi^\sigma_{\mathbf{R}_1n_1}|\hat{H}|\phi^\sigma_{\mathbf{0}n_3}\rangle\langle\phi^\sigma_{\mathbf{0}n_3}|\hat{\mathbf{r}}|\phi^\sigma_{\mathbf{R}_2n_2}\rangle - \hat{H}\leftrightarrow\hat{\mathbf{r}}\Big)G^\sigma_{\mathbf{R}_2n_2,\mathbf{R}_1n_1} \tag{D7}$$

$$= \frac{-e}{2c}\int\frac{d\mathbf{k}}{(2\pi)^3}\langle\tilde{\boldsymbol{u}}'^\sigma_{\mathbf{k}n_1}|\times\Big(\delta_{n_1n_4}\tilde{\epsilon}^\sigma_{\mathbf{k}n_2n_3}|\tilde{\boldsymbol{u}}'^\sigma_{\mathbf{k}n_2}\rangle - \delta_{n_1n_2}\tilde{\boldsymbol{\epsilon}}'^\sigma_{\mathbf{k}n_4n_2}|\tilde{u}^\sigma_{\mathbf{k}n_3}\rangle\Big)G^\sigma_{n_3n_4}(\mathbf{k}), \tag{D8}$$

where $\tilde{\boldsymbol{\epsilon}}'^{\sigma}_{\mathbf{k}n_1n_2} = \nabla_{\mathbf{k}}\tilde{\epsilon}^{\sigma}_{\mathbf{k}n_1n_2}$. Eq. (D7) utilizes Eq. (D1), the completeness relation and the fact that both G^+ and the matrix elements of $\hat{H}$ only depend on the difference between the lattice vectors. This first yields Eq. (D7), but with R_{1j} replaced by $R_{1j} + R_{3j}$ and $\hat{r}_k$ by $\hat{r}_k + R_{3k}$. However, since $\mathbf{R}_3 \times \mathbf{R}_3 = \mathbf{0}$, the terms containing $R_{3j}R_{3k}$ vanish, and since for each $\mathbf{R}_3$ there is an associated $-\mathbf{R}_3$, also the terms linear in either R_{3j} or R_{3k} vanish. Eq. (D8) is obtained by first making use of the relations

$$\langle \phi^{\sigma}_{\mathbf{R}_1 n_1} | \hat{\boldsymbol{r}} | \phi^{\sigma}_{\mathbf{R}_2 n_2} \rangle = \mathbf{R}_1 \, \delta_{\mathbf{R}_1\mathbf{R}_2}\delta_{n_1n_2} - i\int \frac{d\mathbf{k}}{(2\pi)^3/\Omega} e^{i\mathbf{k}\cdot(\mathbf{R}_1-\mathbf{R}_2)} \langle \tilde{\boldsymbol{u}}'^{\sigma}_{\mathbf{k}n_1} | \tilde{u}^{\sigma}_{\mathbf{k}n_2} \rangle, \tag{D9}$$

$$\langle \phi^{\sigma}_{\mathbf{R}_1 n_1} | \hat{H} | \phi^{\sigma}_{\mathbf{R}_2 n_2} \rangle = \int \frac{d\mathbf{k}}{(2\pi)^3/\Omega} e^{i\mathbf{k}\cdot(\mathbf{R}_1-\mathbf{R}_2)} \tilde{\epsilon}^{\sigma}_{n_1n_2}(\mathbf{k}), \tag{D10}$$

where Eq. (D9) follows from Eq. (D5), and performing partial integration. The boundary term vanishes since $|\tilde{\psi}^{\sigma}_{\mathbf{k}+\mathbf{G},n}\rangle = |\tilde{\psi}^{\sigma}_{\mathbf{k}n}\rangle$ is assumed.

References

[1] F. Aryasetiawan. Time-dependent exchange-correlation potential in lieu of self-energy. *Physical Review B*, 105(7):075106, 2022.

[2] L. Hedin. New method for calculating the one-particle Green's function with application to the electron-gas problem. *Physical Review*, 139(3A):A796, 1965.

[3] R. Starke and G. A. H. Schober. Functional approach to electrodynamics of media. *Photonics and Nanostructures-Fundamentals and Applications*, 14:1–34, 2015.

[4] D. C. Jiles and D. L. Atherton. Theory of ferromagnetic hysteresis. *Journal of applied physics*, 55(6):2115–2120, 1984.

[5] R. Resta. Theory of the electric polarization in crystals. *Ferroelectrics*, 136(1):51–55, 1992.

[6] R. Resta. Electrical polarization and orbital magnetization: The modern theories. *Journal of Physics: Condensed Matter*, 22(12):123201, 2010.

[7] R. B. Griffiths. Spontaneous magnetization in idealized ferromagnets. *Physical Review*, 152(1):240, 1966.

[8] J. Friedel. The distribution of electrons round impurities in monovalent metals. *The London, Edinburgh, and Dublin Philosophical Magazine and Journal of Science*, 43(337):153–189, 1952.

[9] J. C. Slonczewski. Current-driven excitation of magnetic multilayers. *Journal of Magnetism and Magnetic Materials*, 159(1-2):L1–L7, 1996.

[10] R. Resta, D. Ceresoli, T. Thonhauser, and D. Vanderbilt. Orbital magnetization in extended systems. *ChemPhysChem*, 6(9):1815–1819, 2005.

[11] A. G. Gurevich and G. A. Melkov. *Magnetization oscillations and waves*. CRC press, 2020.

[12] D. Xiao, J. Shi, and Q. Niu. Berry phase correction to electron density of states in solids. *Physical review letters*, 95(13):137204, 2005.

[13] G. Bastard. Wave mechanics applied to semiconductor heterostructures. 1990.

[14] P. Bargueño and S. Miret-Artés. The generalized Schrödinger–Langevin equation. *Annals of Physics*, 346:59–65, 2014.

[15] P. Hohenberg and W. Kohn. Inhomogeneous electron gas. *Physical review*, 136(3B):B864, 1964.

[16] W. Kohn and L. J. Sham. Self-consistent equations including exchange and correlation effects. *Physical review*, 140(4A):A1133, 1965.

[17] R. O. Jones and O. Gunnarsson. The density functional formalism, its applications and prospects. *Reviews of Modern Physics*, 61(3):689, 1989.

[18] A. D. Becke. Perspective: Fifty years of density-functional theory in chemical physics. *The Journal of chemical physics*, 140(18):18A301, 2014.

[19] N. Marzari, A. A. Mostofi, J. R. Yates, I. Souza, and D. Vanderbilt. Maximally localized Wannier functions: Theory and applications. *Reviews of Modern Physics*, 84(4):1419, 2012.

[20] T. Ayral, J. Vučičević, and O. Parcollet. Fierz convergence criterion: A controlled approach to strongly interacting systems with small embedded clusters. *Physical Review Letters*, 119(16):166401, 2017.

[21] G. D. Mahan. *Many-particle physics*. Springer Science & Business Media, 2013.

[22] T. Matsubara. A new approach to quantum-statistical mechanics. *Progress of theoretical physics*, 14(4):351–378, 1955.

[23] A. L. Fetter and J. D. Walecka. *Quantum theory of many-particle systems*. Courier Corporation, 2012.

[24] B. Holm and F. Aryasetiawan. Total energy from the Galitskii-Migdal formula using realistic spectral functions. *Physical Review B*, 62(8):4858, 2000.

[25] P. Sun and G. Kotliar. Extended dynamical mean-field theory and GW method. *Physical Review B*, 66(8):085120, 2002.

[26] S. Biermann, F. Aryasetiawan, and A. Georges. First-principles approach to the electronic structure of strongly correlated systems: Combining the GW approximation and dynamical mean-field theory. *Physical review letters*, 90(8):086402, 2003.

[27] F. Nilsson, L. Boehnke, P. Werner, and F. Aryasetiawan. Multitier self-consistent GW+ EDMFT. *Physical Review Materials*, 1(4):043803, 2017.

[28] T. N. Lan, A. Shee, J. Li, E. Gull, and D. Zgid. Testing self-energy embedding theory in combination with GW. *Physical Review B*, 96(15):155106, 2017.

[29] P. Romaniello, F. Bechstedt, and L. Reining. Beyond the GW approximation: Combining correlation channels. *Physical Review B*, 85(15):155131, 2012.

[30] G. Onida, L. Reining, and A. Rubio. Electronic excitations: Density-functional versus many-body Green's-function approaches. *Reviews of modern physics*, 74(2):601, 2002.

[31] A. L. Kutepov and G. Kotliar. One-electron spectra and susceptibilities of the three-dimensional electron gas from self-consistent solutions of Hedin's equations. *Physical Review B*, 96(3):035108, 2017.

[32] G. Baym. Field-theoretic approach to the properties of the solid state. *Annals of Physics*, 14:1–42, 1961.

[33] E. G. Maksimov. A self-consistent description of the electron-phonon system in metals and the problem of lattice stability. *Zh. Eksp. Teor. Fiz*, 69:2236–2248, 1975.

[34] L. Hedin and S. Lundqvist. Effects of electron-electron and electron-phonon interactions on the one-electron states of solids. In *Solid state physics*, volume 23, pages 43–51. Elsevier, 1970.

[35] F. Giustino. Electron-phonon interactions from first principles. *Reviews of Modern Physics*, 89(1):015003, 2017.

[36] J. Lindhard. On the properties of a gas of charged particles. *Dan. Vid. Selsk Mat.-Fys. Medd.*, 28:8, 1954.

[37] T. Miyake, F. Aryasetiawan, and M. Imada. Ab initio procedure for constructing effective models of correlated materials with entangled band structure. *Physical Review B*, 80(15):155134, 2009.

[38] F. Aryasetiawan, M. Imada, A. Georges, G. Kotliar, S. Biermann, and A. I. Lichtenstein. Frequency-dependent local interactions and low-energy effective models from electronic structure calculations. *Physical Review B*, 70(19):195104, 2004.

[39] F. Aryasetiawan, J. M. Tomczak, T. Miyake, and R. Sakuma. Downfolded self-energy of many-electron systems. *Physical review letters*, 102(17):176402, 2009.

[40] E. Şaşıoğlu, C. Friedrich, and S. Blügel. Effective Coulomb interaction in transition metals from constrained random-phase approximation. *Physical Review B*, 83(12):121101, 2011.

[41] F. Aryasetiawan and O. Gunnarsson. Product-basis method for calculating dielectric matrices. *Physical Review B*, 49(23):16214, 1994.

[42] A. K. McMahan, R. M. Martin, and S. Satpathy. Calculated effective Hamiltonian for La_2CuO_4 and solution in the impurity Anderson approximation. *Physical Review B*, 38(10):6650, 1988.

[43] S. N. Putilin, E. V. Antipov, O. Chmaissem, and M. Marezio. Superconductivity at 94 K in $HgBa_2Cu0_{4+\delta}$. *Nature*, 362(6417):226–228, 1993.

[44] V. A. Fotiev, G. V. Bazuev, and V. G. Zubkov. Synthesis and electric properties of the solid solutions $SrV_xMo_{1-x}O_3$ with the perovskite structure. *Inorg. Mater.*, 23(6):895, 1987.

[45] The FLEUR group. `https://www.flapw.de/`.

[46] C. Friedrich, S. Blügel, and A. Schindlmayr. Efficient implementation of the GW approximation within the all-electron FLAPW method. *Physical Review B*, 81(12):125102, 2010.

[47] P. W. Anderson. Spin-charge separation is the key to the high T_c cuprates. *Physica C: Superconductivity*, 341:9–10, 2000.

[48] M. Lüders, M. A. L. Marques, N. N. Lathiotakis, A. Floris, G. Profeta, L. Fast, A. Continenza, S. Massidda, and E. K. U. Gross. Ab initio theory of superconductivity. i. Density functional formalism and approximate functionals. *Physical Review B*, 72(2):024545, 2005.

[49] R. Akashi and R. Arita. Development of density-functional theory for a plasmon-assisted superconducting state: Application to lithium under high pressures. *Physical review letters*, 111(5):057006, 2013.

[50] J. L. Wagner, P. G. Radaelli, D. G. Hinks, J. D. Jorgensen, J. F. Mitchell, B. Dabrowski, G. S. Knapp, and M. A. Beno. Structure and superconductivity of $HgBa_2CuO_{4+\delta}$. *Physica C: Superconductivity*, 210(3-4):447–454, 1993.

[51] S. W. Cheong, J. D. Thompson, and Z. Fisk. Properties of La_2CuO_4 and related compounds. *Physica C: Superconductivity*, 158(1-2):109–126, 1989.

[52] F. Aryasetiawan, K. Karlsson, and T. Miyake. Green's function theory of orbital magnetic moment of interacting electrons in solids. *Physical Review B*, 93(16):161104, 2016.

[53] D. Ceresoli, T. Thonhauser, D. Vanderbilt, and R. Resta. Orbital magnetization in crystalline solids: Multi-band insulators, Chern insulators, and metals. *Physical Review B*, 74(2):024408, 2006.

[54] M. V. Berry. Quantal phase factors accompanying adiabatic changes. *Proceedings of the Royal Society of London. A. Mathematical and Physical Sciences*, 392(1802):45–57, 1984.

[55] T. Thonhauser. Theory of orbital magnetization in solids. *International Journal of Modern Physics B*, 25(11):1429–1458, 2011.

[56] T. Thonhauser, D. Ceresoli, D. Vanderbilt, and R. Resta. Orbital magnetization in periodic insulators. *Physical review letters*, 95(13):137205, 2005.

[57] T. Thonhauser and D. Vanderbilt. Insulator/Chern-insulator transition in the Haldane model. *Physical Review B*, 74(23):235111, 2006.

[58] J. Shi, G. Vignale, D. Xiao, and Q. Niu. Quantum theory of orbital magnetization and its generalization to interacting systems. *Physical review letters*, 99(19):197202, 2007.

[59] D. Xiao, M.-C. Chang, and Q. Niu. Berry phase effects on electronic properties. *Reviews of modern physics*, 82(3):1959, 2010.

[60] M. G. Lopez, D. Vanderbilt, T. Thonhauser, and I. Souza. Wannier-based calculation of the orbital magnetization in crystals. *Physical Review B*, 85(1):014435, 2012.

[61] D. Ceresoli, U. Gerstmann, A. P. Seitsonen, and F. Mauri. First-principles theory of orbital magnetization. *Physical Review B*, 81(6):060409, 2010.

[62] R. Nourafkan, G. Kotliar, and A.-M. S. Tremblay. Orbital magnetization of correlated electrons with arbitrary band topology. *Physical Review B*, 90(12):125132, 2014.

[63] K. V. Klitzing, G. Dorda, and M. Pepper. New method for high-accuracy determination of the fine-structure constant based on quantized Hall resistance. *Physical review letters*, 45(6):494, 1980.

[64] Y. Machida, S. Nakatsuji, S. Onoda, T. Tayama, and T. Sakakibara. Time-reversal symmetry breaking and spontaneous Hall effect without magnetic dipole order. *Nature*, 463(7278):210–213, 2010.

[65] F. D. M. Haldane. Model for a quantum hall effect without Landau levels: Condensed-matter realization of the "parity anomaly". *Physical review letters*, 61(18):2015, 1988.

[66] T. I. Vanhala, T. Siro, L. Liang, M. Troyer, A. Harju, and P. Törmä. Topological phase transitions in the repulsively interacting Haldane-Hubbard model. *Physical review letters*, 116(22):225305, 2016.

[67] V. S. Arun, R. Sohal, C. Hickey, and A. Paramekanti. Mean field study of the topological Haldane-Hubbard model of spin-1/2 fermions. *Physical Review B*, 93(11):115110, 2016.

[68] E. O. Kane. The $\mathbf{k} \cdot \mathbf{p}$ method. In *Semiconductors and semimetals*, volume 1, pages 75–100. Elsevier, 1966.

[69] K.-I. Uchida, H. Adachi, T. An, T. Ota, M. Toda, B. Hillebrands, S. Maekawa, and E. Saitoh. Long-range spin Seebeck effect and acoustic spin pumping. *Nature materials*, 10(10):737–741, 2011.

[70] M. Weiler, H. Huebl, F. S. Goerg, F. D. Czeschka, R. Gross, and S. T. B. Gönnenwein. Spin pumping with coherent elastic waves. *Physical Review Letters*, 108(17):176601, 2012.

[71] H. Hayashi and K. Ando. Spin pumping driven by magnon polarons. *Physical review letters*, 121(23):237202, 2018.

[72] L. Zhang and Q. Niu. Angular momentum of phonons and the Einstein–de Haas effect. *Physical Review Letters*, 112(8):085503, 2014.

[73] D. A. Garanin and E. M. Chudnovsky. Angular momentum in spin-phonon processes. *Physical Review B*, 92(2):024421, 2015.

[74] J. Holanda, D. S. Maior, A. Azevedo, and S. M. Rezende. Detecting the phonon spin in magnon–phonon conversion experiments. *Nature Physics*, 14(5):500–506, 2018.

[75] X. Zhang, Y. Zhang, S. Okamoto, and D. Xiao. Thermal Hall effect induced by magnon-phonon interactions. *Physical review letters*, 123(16):167202, 2019.

[76] R. Silberglitt. Effect of spin waves on the phonon energy spectrum of a Heisenberg ferromagnet. *Physical Review*, 188(2):786, 1969.

[77] J. Jensen and J. G. Houmann. Spin waves in terbium. II. Magnon-phonon interaction. *Physical Review B*, 12(1):320, 1975.

[78] T.-M. Cheng and L. Li. Magnon–phonon coupling in two-dimensional Heisenberg ferromagnetic system. *Journal of magnetism and magnetic materials*, 320(1-2):1–7, 2008.

[79] A. L. Chernyshev and W. Brenig. Thermal conductivity in large-J two-dimensional antiferromagnets: Role of phonon scattering. *Physical Review B*, 92(5):054409, 2015.

[80] S. F. Maehrlein, I. Radu, P. Maldonado, A. Paarmann, M. Gensch, A. M. Kalashnikova, R. V. Pisarev, M. Wolf, P. M. Oppeneer, J. Barker, et al. Dissecting spin-phonon equilibration in ferrimagnetic insulators by ultrafast lattice excitation. *Science advances*, 4(7):eaar5164, 2018.

[81] S. L. Holm, A. Kreisel, T. K. Schäffer, A. Bakke, M. Bertelsen, U. B. Hansen, M. Retuerto, J. Larsen, D. Prabhakaran, P. P. Deen, et al. Magnetic ground state and magnon-phonon interaction in multiferroic h- $YMno_3$. *Physical Review B*, 97(13):134304, 2018.

[82] S. Holm-Dahlin, A. Kreisel, T. K. Schäffer, A. Bakke, M. Bertelsen, U. B. Hansen, M. Retuerto, J. Larsen, D. Prabhakaran, P. P. Deen, et al. Erratum: Magnetic ground state and magnon-phonon interaction in multiferroic h- $YMno_3$ [Phys. Rev. B 97, 134304 (2018)]. *Physical Review B*, 98(9):099902, 2018.

[83] S. C. Guerreiro and Sergio M. Rezende. Magnon-phonon interconversion in a dynamically reconfigurable magnetic material. *Physical Review B*, 92(21):214437, 2015.

[84] R. Takahashi and N. Nagaosa. Berry curvature in magnon-phonon hybrid systems. *Physical review letters*, 117(21):217205, 2016.

[85] J. Hellsvik, D. Thonig, K. Modin, D. Iuşan, A. Bergman, O. Eriksson, L. Bergqvist, and A. Delin. General method for atomistic spin-lattice dynamics with first-principles accuracy. *Physical Review B*, 99(10):104302, 2019.

[86] S. Streib, N. Vidal-Silva, K. Shen, and G. E. W. Bauer. Magnon-phonon interactions in magnetic insulators. *Physical Review B*, 99(18):184442, 2019.

[87] E. Şaşıoğlu, A. Schindlmayr, C. Friedrich, F. Freimuth, and S. Blügel. Wannier-function approach to spin excitations in solids. *Physical Review B*, 81(5):054434, 2010.

[88] C. R. Jacob and M. Reiher. Spin in density-functional theory. *International Journal of Quantum Chemistry*, 112(23):3661–3684, 2012.

[89] G. L. Goodvin and M. Berciu. Momentum average approximation for models with electron-phonon coupling dependent on the phonon momentum. *Physical Review B*, 78(23):235120, 2008.

[90] A. Rückriegel, P. Kopietz, D. A. Bozhko, A. A. Serga, and B. Hillebrands. Magnetoelastic modes and lifetime of magnons in thin yttrium iron garnet films. *Physical Review B*, 89(18):184413, 2014.

[91] J. W. Negele. *Quantum many-particle systems*. CRC Press, 2018.

[92] B. D. E. McNiven, G. T. Andrews, and J. P. F. LeBlanc. Single particle properties of the two-dimensional Hubbard model for real frequencies at weak coupling: Breakdown of the Dyson series for partial self-energy expansions. *Physical Review B*, 104(12):125114, 2021.

[93] O. Gunnarsson and B. I. Lundqvist. Exchange and correlation in atoms, molecules, and solids by the spin-density-functional formalism. *Physical Review B*, 13(10):4274, 1976.

[94] J. C. Slater. A simplification of the Hartree-Fock method. *Physical review*, 81(3):385, 1951.

[95] T. Giamarchi. *Quantum physics in one dimension*, volume 121. Clarendon press, 2003.

[96] F. H. L. Essler, H. Frahm, F. Göhmann, A. Klümper, and V. E. Korepin. *The one-dimensional Hubbard model*. Cambridge University Press, 2005.

[97] C. Kim, A. Y. Matsuura, Z.-X. Shen, N. Motoyama, H. Eisaki, S. Uchida, T. Tohyama, and S. Maekawa. Observation of spin-charge separation in one-dimensional $SrCuO_2$. *Physical review letters*, 77(19):4054, 1996.

[98] C. Kim, Z.-X. Shen, N. Motoyama, H. Eisaki, S. Uchida, T. Tohyama, and S. Maekawa. Separation of spin and charge excitations in one-dimensional $SrCuO_2$. *Physical Review B*, 56(24):15589, 1997.

[99] H. Benthien and E. Jeckelmann. Spin and charge dynamics of the one-dimensional extended Hubbard model. *Physical Review B*, 75(20):205128, 2007.

[100] J. P. Perdew, R. G. Parr, M. Levy, and J. L. Balduz Jr. Density-functional theory for fractional particle number: Derivative discontinuities of the energy. *Physical Review Letters*, 49(23):1691, 1982.

[101] A. A. Ovchinnikov. Excitation spectrum in the one-dimensional Hubbard model. *Sov. Phys. JETP*, 30:1160, 1970.

[102] A. Georges, G. Kotliar, W. Krauth, and M. J. Rozenberg. Dynamical mean-field theory of strongly correlated fermion systems and the limit of infinite dimensions. *Reviews of Modern Physics*, 68(1):13, 1996.

[103] A. Go and G. S. Jeon. Properties of the one-dimensional Hubbard model: Cellular dynamical mean-field description. *Journal of Physics: Condensed Matter*, 21(48):485602, 2009.

[104] K. Dechoum, H. de M. França, and C. P. Malta. Classical aspects of the Pauli-Schrödinger equation. *Physics Letters A*, 248(2-4):93–102, 1998.

Part III

Scientific publications

Author contributions

I **Position representation of effective electron-electron interactions in solids**

I derived the formulas needed to obtain the spatial representations when working with a mixed product basis, wrote the necessary extension to the existing codes, produced the figures and plots and wrote most of the article.

II **Influence of correlations on the orbital magnetization of the spin-1/2 Haldane-Hubbard model**

I wrote the majority of the code, ran the calculations, produced the plots and wrote most of the article, except the introduction.

III **Magnon-phonon interaction and the underlying role of the Pauli exclusion principle**

I came up with most crucial steps for deriving the magnon-phonon interaction, like the Fierz ambiguity, to work with a crossing-symmetric extension of Hedin's W, to use an iterative scheme and to contract the four-point interaction between the reference magnons at the end. I also constructed the model, produced the results and wrote most of the article.

IV **Spectral functions of the half-filled one-dimensional Hubbard chain within the exchange-correlation potential formalism**

I contributed with initial ideas, made connections to the standard self-energy approach, performed some calculations and helped writing the article.

Printed by Media-Tryck, Lund 2022 NORDIC SWAN ECOLABEL 3041 0903

Lund University
Faculty of Science
Department of Physics

ISBN 978-91-8039-355-3